الجمهورية الجزائرية الديمقراطية الشعبية
People's Democratic Republic of Algeria
وزارة التعليم العالي والبحث العلمي
Ministry of Higher Education and Scientific Research

جامعة زيان عاشور بالجلفة
Ziane Achour University of Djelfa

كلية العلوم و التكنولوجيا
Faculty of Science and Technology

Department: Electrical Engineering

Order N°: 009 / 2020

Defense authorization N° 227/2020

DOCTORAL THESIS

3rd Cycle Doctoral (D-LMD)

Presented by

Naâs DJEDDAOUI

With a view to obtaining the doctoral diploma in 3rd Cycle Doctoral (D-LMD)

Branch: Automatic

Specialty: Industrial control

Topic

Prediction and diagnosis of solar cells properties under climatic conditions

Supported, on 28 /11 / 2020, before the jury composed of:

Last and first name	Grade	Institution of affiliation	Designation
Mr Ahmed GUEDDIM	Professor	University of Djelfa	President
Mr Larbi BOUKEZZI	Professor	University of Djelfa	Supervisor
Mr Lakhdar BESSISSA	S. Lecturer	University of Djelfa	Co-Supervisor
Mme Assia BOURAIOU	Professor	University of Djelfa	Examiner
Mr Abdelaziz RABEHI	S. Lecturer	University Centre of Tissemsilt	Examiner

Djelfa University, FST – 2020

الجمهورية الجزائرية الديمقراطية الشعبية
République Algérienne Démocratique et Populaire
وزارة التعليم العالي والبحث العلمي
Ministère de l'Enseignement Supérieur et de la Recherche Scientifique

جامعة زيان عاشور بالجلفة
Université Ziane Achour de Djelfa

كلية العلوم والتكنولوجيا
Faculté des Sciences et de la Technologie

Département : Génie Electrique

N° d'Ordre : 009 / 2020

Autorisation de Soutenance N° 227/2020

THESE DE DOCTORAT

Doctorat 3ème Cycle (D-LMD)

Présentée par

Naâs DJEDDAOUI

En vue de l'obtention du diplôme de Docteur en 3ème Cycle D-LMD

Filière : Automatique

Spécialité : Contrôle industrielle

Thème

Prediction and diagnosis of solar cells properties under climatic conditions

Soutenue publiquement, le 28 /11 /2020, devant le jury composé de :

Nom et Prénom	Grade	Etablissement de rattachement	Désignation
Mr Ahmed GUEDDIM	Professeur	Université de Djelfa	Président
Mr Larbi BOUKEZZI	Professeur	Université de Djelfa	Directeur de thèse
Mr Lakhdar BESSISSA	MCA	Université de Djelfa	Co Directeur de thèse
Mme Assia BOURAIOU	Professeur	Université de Djelfa	Examinateur
Mr Abdelaziz RABEHI	MCA	Centre Universitaire deTissemsilt	Examinateur

Dedication

I dedicate this modest work to:

My dear parents (DJEDDAOUI BENDJEDDOU & BRAHIMI BENTNAOUM)

For all their sacrifices, their love, their tenderness, their support and their prayers

Throughout my studies

For all my **brothers** especially (**FARID DJEDDAOUI**) and my **sisters**

And of course to **my wife (IKRAM BELKHIRI)** for her support throughout this project

To the late my teacher **GARBOUZ MOHAMED** may God grant rest to his soul and keep it in Paradise.

To all my friends

And to all those who have contributed directly or indirectly to make this

Project be possible, thank you

Naas DJEDDAOUI

Acknowledgements

First and foremost, I would like to thank **God** Almighty for giving me the strength, knowledge, ability and opportunity to undertake this research study and to persevere and complete it satisfactorily. Without his blessings, this achievement would not have been possible.

I would like to thank the following people for helping with this research project:

I express my gratitude to Mr. **BOUKEZZI Larbi** and **Mr.BESSISSA Lakhdar,** as supervisors of this work, by their knowledge, time, dedication, guidance, support, encouragement and invaluable advices throughout of this work to achieve the Ph.D. degree.

Furthermore, I would like to express my sincere thanks to the members of jury: **Pr. GUEDDIM Ahmed** as a president of jury, and **Pr. BOURAIOU Assia** and **Dr. RABEHI Abdelaziz** as examiners for their acceptance to evaluate and examine my works.

Our sincere thanks go to **Mr. GUEDDIM Ahmed (MSIL Laboratory director)** for having us on his laboratory and his help in the experimental work.

I would like to thank **Mr. Morten Madsen** from SDU Laboratory, University of Southern Denmark for accepting me in her group of Organic Solar Cells. I appreciate also all the help, support and knowledge. I would also like to thank **Vida Engmann** by the support during the research done in the SDU Laboratory and not forgetting all the SDU staff for their supports.

Abstract

In this study we have analyzed investigations on the aging and degradation of organic solar cells (OSCs). In the first part of this study we have conducted QUV aging on commercial samples of OSCs. The use of QUV chamber leads to study the effect of cyclic aging on the electrical and optical properties namely PCE, J_{sc}, FF, V_{oc}, UV-VIS and PL measurements under variation of UV irradiation, temperature, humidity and dark. The degradation process of the OSCs under cyclic aging fits with the earlier finding in the literature and is occurred in two phases with deferent aging rates. Furthermore, it has been found that the OSCs lose more than 60% of their initial performances, and for some properties like PCE the decrease reaches 80%. This drastic drop of the OSCs performances, associated to the formation of bubbles, indicates that samples undergo very hard bulk degradation. In the second part we have assessed the degradation behaviour of lab-scale and scalable OSCs devices employing similar non-fullerene (NFA) based active layers. It is demonstrated that the scalable NFA OSC exhibit completely reversible degradation when assessed in ISOS-O-1 outdoor conditions, which is in contrast to the lab-scale devices assessed via the indoor ISOS-L-2 protocol. Results from transient photovoltage (TPV) indicate the presence of charge trap formation, and a number of potential mechanisms are proposed. In the end of this study we have reported some results of the ANN prediction of the OSCs performances under aging. The reported results show that the accuracy of prediction is very good and the predicted values are close to the experimental values.

Keywords : Photovoltaic Solar cells, Aging, Degradation, Prediction, Recovery, Artificial Neural Network (ANN).

الملخص

في هذه الدراسة قمنا بتحليل و تحقيق حول تدهور و شيخوخة الخلايا الشمسية العضوية (OSCs). في الجزء الاول من الدراسة طبقنا الشيخوخة على عينات تجارية من الخلايا الشمسية العضوية بواسطة اختبارQUV المسرع للعوامل الجوية. يسمح استخدام اختبار QUVالمسرع للعوامل الجوية بدراسة تأثير الشيخوخة الدورية على الخصائص الكهربائية والخصائص الضوئية مثل الأشعة فوق البنفسجية واللمعان الضوئي تحت مختلف الأشعة فوق البنفسجية ودرجة الحرارة والرطوبة والظلام. تتناسب عملية تدهور الشيخوخة الدورية للخلايا الشمية العضوية مع النتائج المتحصل عليها سابقا و يتم ذلك في مرحلتين مع اختلاف في معدل الشيخوخة. علاوة على ذلك، فقد وجد أن الخلايا الشمسية العضوية تخسر أكثر من 60 ٪ من أدائها الأولي، وبالنسبة لبعض الخصائص مثل PCE يصل الانخفاض إلى 80 ٪. يشير هذا الانخفاض الحاد في أداء الخلايا الشمسية العضوية، المرتبط بتشكيل الفقاعات، إلى أن العينات تخضع لتدهور كبير جدًا. في المرحلة الثانية تطرقنا الى تقيم سلوك تحلل اجهزة الخلايا الشمسية العضوية في مقياس المختبر التي تستخدم طبقات نشطة مماثلة غير الفوليرين. ثبت أن تطور الخلايا الشمسية العضوية الغير فوليرين تظهر انحطاطًا يمكن عكسه تمامًا عند إخضاعه للظروف الخارجية ISOS-O-1 (القمة الدولية حول استقرار الخلايا الكهروضوئية العضوية)، و هذا ما يتناقض مع نتائج القياسات المختبرية عبر بروتوكول ISOS-L-2 الداخلي. تشير نتائج الجهد الكهربائي العابر (TPV) إلى وجود مصيدة شحن تم تشكيلها، مع اقتراح عدد من الآليات المحتملة. في نهاية هذه الدراسة ، قدمنا بعض النتائج عن التنبؤ باستخدام الذكاء الصناعي للشبكات العصبية (ANN) لأداء الخلايا الشمسية العضوية في حالة الشيخوخة. أظهرت النتائج المقدمة أن دقة التنبؤ جيدة جدًا وأن القيم المتنبئة قريبة من القيم التجريبية.

الكلمات المفتاحية: الخلايا الشمسية الكهروضوئية، الشيخوخة، التدهور، التنبؤ، التعافي، شبكة الاعصاب الصناعية

Résumé

Dans cette étude, nous avons analysé des travaux de recherche sur le vieillissement et la dégradation des cellules solaires organiques (CSOs). Dans la première partie de cette étude, nous avons effectué un vieillissement QUV sur des échantillons commerciaux des CSOs. L'utilisation de la chambre QUV permet d'étudier l'effet du vieillissement cyclique sur les propriétés électriques et optiques, notamment : PCE, J_{sc}, FF, V_{oc}, UV-VIS et PL sous l'effet de la variation de l'irradiation UV, de la température, de l'humidité et de l'obscurité. Le processus de dégradation des CSOs lors du vieillissement cyclique est en accord avec celui reporté dans littérature et se produit en deux phases avec des taux de vieillissement déférents. De plus, il a été constaté que les OSC perdent plus de 60% de leurs performances initiales, et pour certaines propriétés comme le PCE, la diminution atteint 80%. Cette chute drastique des performances des OSC, associée à la formation de bulles, indique que les échantillons subissent une dégradation massive très dure. Dans la deuxième partie, nous avons évalué le comportement de dégradation des dispositifs des CSOs à l'échelle du laboratoire et des dispositifs évolutifs utilisant des couches actives similaires non basées sur le fullerène. Il est démontré que les CSO NFA non évolutives présentent une dégradation totalement réversible lorsqu'elles sont évaluées dans les conditions extérieures ISOS-O-1, ce qui est le contraire avec les dispositifs à l'échelle du laboratoire évalués par le biais du protocole ISOS-L-2 en intérieur. Les résultats de la phototension transitoire (TPV) indiquent la présence d'une formation de piège à charge, et un certain nombre de mécanismes potentiels sont proposés. À la fin de cette étude, nous avons présenté certains résultats de la prédiction en utilisant les réseaux de neurones artificiels (ANN) des performances des CSOs en cours de vieillissement. Les résultats rapportés montrent que la précision de la prédiction est très bonne et que les valeurs prédites sont proches des valeurs expérimentales.

Mots clés: Cellules solaires photovoltaïques, Vieillissement, dégradations, Prédiction, Récupération, Réseau neuronal artificiel (RNA).

Contents

Chapter II: Degradation of organic solar cells

Chapter III: Degradation of organic solar cells under different climatic conditions

Chapter IV: Degradation and lifetime prediction of lab-scale and scalable non-fullerene OSCs

List of Figures

Chapter IV: Degradation and lifetime prediction of lab-scale and scalable non-fullerene OSCs

List of Tables

Notations

Abbreviations

- PV: Photovoltaic.
- ITO: Indium tin Oxide.
- OCS: Organic Solar Cells.
- AM: Air Mass.
- OPV: Organic photovoltaic.
- PCE: Power conversion efficiency.
- D: Donor.
- A: Acceptor.
- HOMO: Highest Occupied Molecular Orbital.
- LUMO: Lowest Unoccupied Molecular Orbital.
- BHJ: Bulk heterojunction.
- PFN: Polyfluorene .
- ZnO: Zinc oxide.
- J-V: Characteristic (Current-Voltage).
- J_{SC}: Short- circuit current.
- V_{OC}: Open-circuit current.
- FF: Fill Factor
- PC60/70BM: phenyl-C60/70-butyric acid methyl ester.
- NFA: Non-fullerene.
- ANN: Artificial Neural Network model.
- PET: Polyethylene terephthalate.
- TPV: Transient photovoltage.
- RBF: Radial basis function.
- ROM: Random optimization method

Scientific Publications

PUBLICATIONS

[1]. Djeddaoui Naas, Larbi Boukezzi, and Lakhdar Bessissa. "Aging and Degradation of Organic Solar Cells Using QUV Accelerated-Weathering Tester." Transactions on Electrical and Electronic Materials 20, no. 3 (2019): 189-197.

[2]. Greenbank William, Naas Djeddaoui, Elodie Destouesse, Jani Lamminaho, Michela Prete, Larbi Boukezzi, Thomas Ebel et al. "Degradation Behavior of Scalable Nonfullerene Organic Solar Cells Assessed by Outdoor and Indoor ISOS Stability Protocols." Energy Technology 8, no. 12 (2020): 2000295.

INTERNATIONAL CONFERENCES

[1]. **N. Djeddaoui**, L. Boukezzi, L. Bessissa, "Prediction of PCE Parameter of Organic Solar Cells Using Nonlinear Regression and Poisson Regression " 2nd. Inter. Conf. Electr. Engineering (ICEEB), Biskra, Algeria, 2 -3 December 2018.

[2]. **N. Djeddaoui,** L. Boukezzi, L. Bessissa, "Prediction of J-V Characteristic of Organic Solar Cells Using ANFIS Model " Inter. Symposium. Mechatronics. Renew. Energies (ISMRE), Eloud, Algeria, 10 -11 December 2018.

[3]. **N. Djeddaoui,** L. Boukezzi, L. Bessissa, "Use of MLP Artificial Neural Network in Prediction of J-V Characteristic of Organic Solar Cells" IEEE Int. Conf. Communi. Electr. Engin. (ICCEE), El-Oued, Algeria, December 17-18, 2018. https://ieeexplore.ieee.org/document/8634558

[4]. **N. Djeddaoui,** L. Boukezzi, L. Bessissa, "Prediction of Short Circuit Current under QUV aging of Organic Solar Cells Using Nonlinear Regression" The First Inter. Conf on Mate, Envi, Mech and Indu Sys (ICMEMIS'19), Djelfa, Algeria, 29-30 Jun 2019**.**

[5]. **N. Djeddaoui,** L. Boukezzi, L. Bessissa "Performance of Organic Solar Cells with Recovery" IEEE International Conference on Advanced Electrical Engineering ,(ICAEE2019)Algiers, Algeria, 19-21 November 2019. https://ieeexplore.ieee.org/document/9014758

INTERNSHIP

[1]. **Short internship** from 01/02/2018 to 12/05/2018 under the supervisor of Prof. Morten Madsen, in Nanosyd Lab, University of Southern Denmark, SDU, Mads Clausen Institute, Sønderborg, Denmark.

[2]. **Long internship** from 15/01/2020 to 30/07/2020 under the supervisor of Prof. Morten Madsen, in Nanosyd Lab, University of Southern Denmark, SDU, Mads Clausen Institute, Sønderborg, Denmark.

Introduction

Introduction

In the recent years, organic solar cells (OSCs) attracted great attention because their several advantages like the low-cost, flexibility, and lightweight. Moreover, the power conversion efficiency (PCE) can be enhanced more than 10% by using an appropriate choice of the used conjugate copolymers [1]. To get high-efficiency solar cells and converting the sunlight into electricity there are crucial parameters as the absorption range, the photon–electron conversion rate and the carrier mobility's of the light-harvesting polymers are among [2].

However, the organic solar cells present some limitations in their stability under different conditions, because the used organic materials as active layers undergo some degradation process under external factors. The resulting degradation can alter the physical properties of the photovoltaic cells, which leads to the reduction in the electrical properties of cells such as: (PCE), the open circuit voltage (Voc), the short circuit current density (Jsc), and the fill factor (FF).

In the last research, the conjugated polymer–fullerene bulk heterojunction (BHJ) solar cell takes big parts of interest in carried out work done by the scientific community interesting on the renewable energy [3–5]. Moreover, they found a great defiance to improve the efficiency, because higher value of the lowest unoccupied molecular orbital (LUMO) of the fullerene [6]. Lately it has been discovered that non-fullerene small molecules, which consider as very promising electron acceptors in OSCs and PCEs can reach 12% [7].

Historically, the studies of the stability and degradation in polymer organic photovoltaic are started since 1990s, and these studies have been included as footnotes in the followed studies [8]. In the state of the art, the stability of organic solar cells is related to their efficiency. Therefore, the most research work done in the last few years is focused on ways to improve the stability of the OSCs and consequently enhance their efficiency. A lot of techniques have been investigated in these studies and many parameters and factors have been considered (outdoor, indoor, additives,…etc). Furthermore, different protocols called ISOS specialised in the stability of organic solar cells have been used in the most carried out research works [9–11]. These protocols suggest that the degradation of the solar cells is caused by a several factors such as humidity, oxygen, UV light, and water. Indeed, the stability of OSCs can be studied in indoor or outdoor conditions. Reese et al. [9] have well explained all the considered conditions for each protocol used in the study of organic solar cells stability. A lot of papers have been published in last decade reporting interesting results on the solar cells stability using ISOS protocols. Brestow et al. [12] have conducted a diurnal analysis on the OSCs modules under outdoor conditions and they have observed that the OSCs

modules exhibit some poor performances under low light conditions such as overcast days. Angmo et al. [13] have used ISOS-D-2 and ISOS-O-1 to carry out outdoor experiments during 2 to 3 years. The almost of studies using standard protocols use for example a continuous illumination from a solar simulator which is a very common form of degradation experiment, and while it will be relevant for some degradation effects, it may miss other degradation mechanisms that arise from cycling the light on and off, as it happens in an outdoor test. Moreover, there is a risk that indoor laboratory studies, carried out in ISOS-L conditions using laboratory scale fabrication and device architectures, will be used to eliminate potential active layer materials when they may exhibit much higher stability in outdoor tests, when scalable fabrication and device designs are employed. For this purpose we have carried out a work in this thesis firstly on the degradation of OSCs under QUV aging cell to simulate the cyclic effect of the climatic conditions which happening in one day of real climatic conditions. Secondly, we have studied the degradation of lab-scale and scalable non-fullerene OSCs under laboratory and outdoor ISOS protocols to show the effect of the partial recovery when the OSC device is working under real outdoor setting.

This Thesis is organized as follows: After a general introduction, we have started with the **first chapter,** where we have firstly introduce and demonstrate of organic solar cells (OSCs), and different structure of OSCs, namely the working principle, electrical characterization of organic solar cells in the last the fabrication flexible OSCs. However, in the recent years, organic solar cells attracted great attention because several advantages like low-cost, flexibility, and lightweight. Moreover, the energy efficiency significantly increased. In the s**econd chapter** we have explored and demonstrate the phenomenon of degradation mechanisms of organic solar cells (OSCs) and explain the different consensus stability testing protocols ISOS for organic photovoltaic materials and devices. Nevertheless, with all advantage there is one hindrance prevents organic solar cells from being marketed due to unstable.

In the **third chapter** we have investigated the effect of cyclic aging on a commercial OSCs samples using QUV aging tester. Many characterization techniques have been used to highlight the degradation behavior of samples. The same samples have been used to study the recovery phenomenon under ISOS-O-1 protocol.

Finally the **fourth chapter**, applied two tests indoor ISOS-L-2, and the outdoor ISOS-O-1 using small organic solar cells (OSCs) with a recovery. We use intelligent techniques based on RBFG Artificial Neural Networks (ANN) trained with Random Optimization Method (ROM) to predict the aging of different parameters of organic solar cells (PCE, V_{oc}, J_{sc}, FF, R_s and R_{sh}) under the light

with time. The obtained results are compared with the experimental values and prediction quality is evaluated using the Root Mean Square Error (RMSE) and Mean Absolute Relative Error (MARE).

This thesis is closed by a conclusion.

References

[1] Liu, Chang, Chao Yi, Kai Wang, Yali Yang, Ram S. Bhatta, Mesfin Tsige, Shuyong Xiao, and Xiong Gong. "Single-junction polymer solar cells with over 10% efficiency by a novel two-dimensional donor–acceptor conjugated copolymer." ACS applied materials & interfaces 7, no. 8 (2015): 4928-4935.

[2] Manceau, Matthieu, Dechan Angmo, Mikkel Jørgensen, and Frederik C. Krebs. "ITO-free flexible polymer solar cells: from small model devices to roll-to-roll processed large modules." Organic Electronics 12, no. 4 (2011): 566-574.

[3] Dennler, Gilles, Markus C. Scharber, and Christoph J. Brabec. "Polymer-fullerene bulk-heterojunction solar cells." Advanced materials 21, no. 13 (2009): 1323-1338.

[4] Hleli, E., S. Alam, A. Saaidia, C. Kästner, S. Hoeppener, C. Ulbricht, S. Romdhane et al. "Improvement of polymer: fullerene bulk heterojunction morphology via temperature and anti-solvent effect." Synthetic Metals 243 (2018): 8-16.

[5] Yang, Zhenhua, Maria Moffa, Ying Liu, Hongfei Li, Luana Persano, Andrea Camposeo, Rosalba Saija et al. "Electrospun conjugated polymer/fullerene hybrid fibers: photoactive blends, conductivity through tunneling-AFM, light scattering, and perspective for their use in bulk-heterojunction organic solar cells." The Journal of Physical Chemistry C 122, no. 5 (2018): 3058-3067.

[6] Koster, L. J. A., V. D. Mihailetchi, and P. W. M. Blom. "Ultimate efficiency of polymer/fullerene bulk heterojunction solar cells." Applied Physics Letters 88, no. 9 (2006): 093511.

[7] Li, Sunsun, Long Ye, Wenchao Zhao, Shaoqing Zhang, Subhrangsu Mukherjee, Harald Ade, and Jianhui Hou. "Energy-level modulation of small-molecule electron acceptors to achieve over 12% efficiency in polymer solar cells." Advanced materials 28, no. 42 (2016): 9423-9429.

[8] Jørgensen, Mikkel, Kion Norrman, and Frederik C. Krebs. "Stability/degradation of polymer solar cells." Solar energy materials and solar cells 92, no. 7 (2008): 686-714.

[9] Reese, Matthew O., Suren A. Gevorgyan, Mikkel Jørgensen, Eva Bundgaard, Sarah R. Kurtz, David S. Ginley, Dana C. Olson et al. "Consensus stability testing protocols for organic photovoltaic materials and devices." Solar Energy Materials and Solar Cells 95, no. 5

(2011): 1253-1267.

[10] Corazza, Michael, Frederik C. Krebs, and Suren A. Gevorgyan. "Predicting, categorizing and intercomparing the lifetime of OPVs for different ageing tests." Solar energy materials and solar cells 130 (2014): 99-106.

[11] Kettle, Jeffrey, Vasil Stoichkov, Dinesh Kumar, M. Corazza, S. A. Gevorgyan, and F. C. Krebs. "Using ISOS consensus test protocols for development of quantitative life test models in ageing of organic solar cells." Solar Energy Materials and Solar Cells 167 (2017): 53-59.

[12] Bristow, N., and J. Kettle. "Outdoor performance of organic photovoltaics: Diurnal analysis, dependence on temperature, irradiance, and degradation." Journal of Renewable and Sustainable Energy 7, no. 1 (2015): 013111.

[13] Angmo, Dechan, and Frederik C. Krebs. "Over 2 Years of Outdoor Operational and Storage Stability of ITO-Free, Fully Roll-to-Roll Fabricated Polymer Solar Cell Modules." Energy Technology 3, no. 7 (2015): 774-783.

CHAPTER I

Generality about the Organic solar cells

I.1 Introduction

The solar energy is the energy was taken from of the solar radiations, as it is known the most energy sources (excluding nuclear and geothermal energy) on the earth are a converted form of solar energy. It is the most abundant renewable energy source. There are two components in the radiation received by the surface: the first depends on the distance through the atmosphere and the second component is called diffuse radiation, and this component comes from solar radiation that diffuses through clouds and dust in the atmosphere [1].

I.2 Solar Spectrum

The solar radiation wavelengths that reach the earth revolve from approximately 300 nanometers to 400 nanometers [2]. Indeed the Photovoltaic (PV) industry has defined two spectral distributions for the sun. The Air Mass AM 0 spectrum and represents the spectrum for outer space at a standard direct normal and a standard total spectral irradiance the AM 1.5G spectrums described terrestrial solar radiation. **Figure I.1** shows the distributions [3].

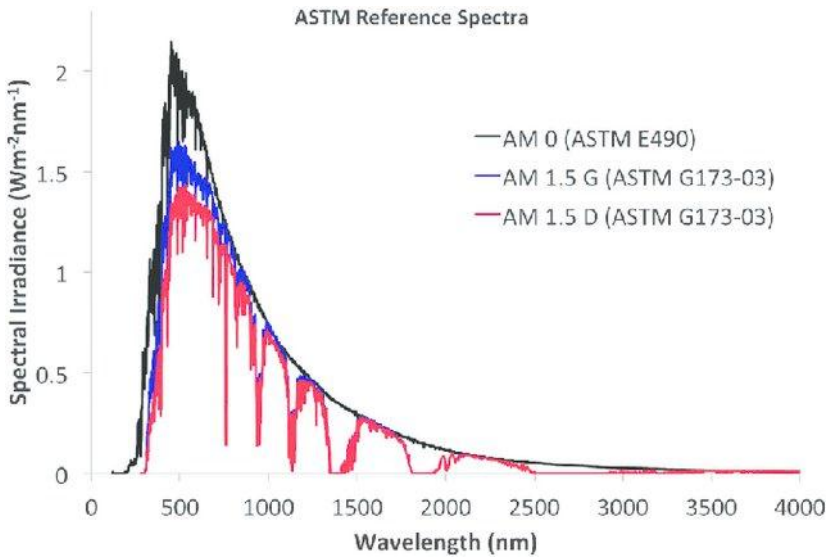

Figure I.1: AM 0 and AM 1.5G spectrums [4].

I.3 A brief history of organic solar cells

The research of organic solar cells (OSC) started between 1970 and 1975; however the right time started from 1986. The OSC take intention due to two factors: first, to minimize the pollution of CO_2 in the planet cause of the fossil fuels; and second, is that the OSC is cheaper than the silicon one [5,6].

The power conversion efficiency (PCE) of organic solar cells has increased over time [7]. It started in 1975 by 0.001% and reaches 1% in 1986. After that in 2006 the PCE jumps to 5% and exceeds 6% in 2009. In the next three years the organic solar cell PCE increases from 8.3% in 2010 to 12% in 2013. In 2019 the efficiency reaches values over than 13.45 % [8].

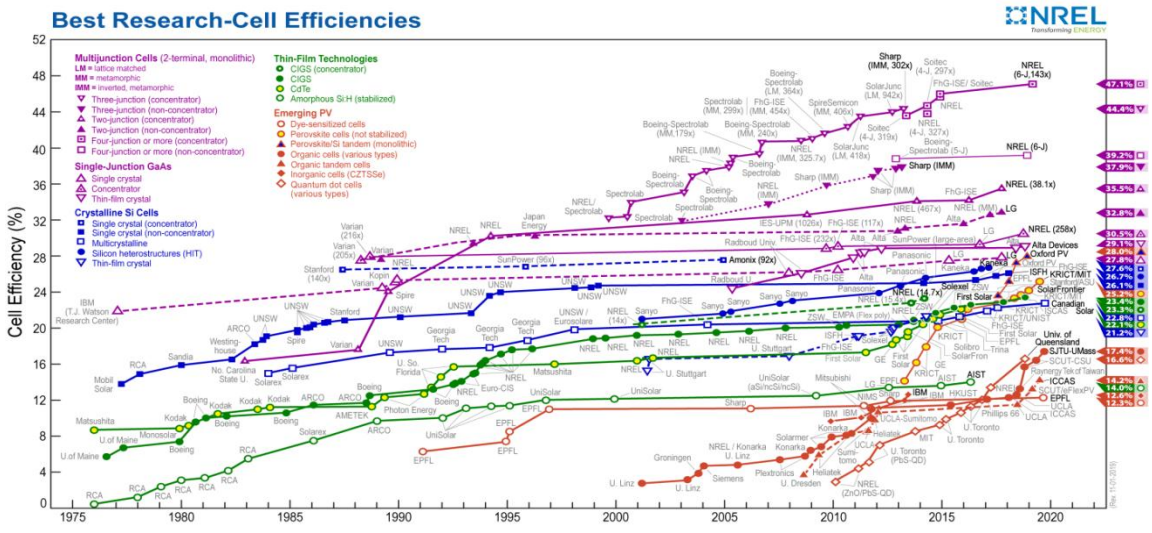

Figure I.2: Compares the efficiencies of OSC using different technologies [9].

The investigation on OCS takes the attention of researchers through the world due to considerable potential in terms of:

1. Semi-transparency.
2. Flexibility and light weight.
3. Low-cost of manufacture.
4. Manufacture at low temperatures.
5. Integration as a photovoltaic device for large areas.
6. Modulation to change properties of the organic semiconductor.
7. New structures and morphologies.

The researchers firstly concentrate to understand the physical mechanisms, the stability phenomena how they work and the most focused on the efficiency to increase how it would operate. When they overcome these obstacles, the OSC will be commercialized.

I.4 Operation principles

Further most of organic solar cells made up of one or more active layers between two electrodes of different materials. The Indium Tin Oxide (ITO) used repeatedly and the electrodes should one from them transparent or semi-transparent. In additional the electrode is a metal whose work function must be smaller to from an Ohmic contact with the n-type material of the blend prepared [7].

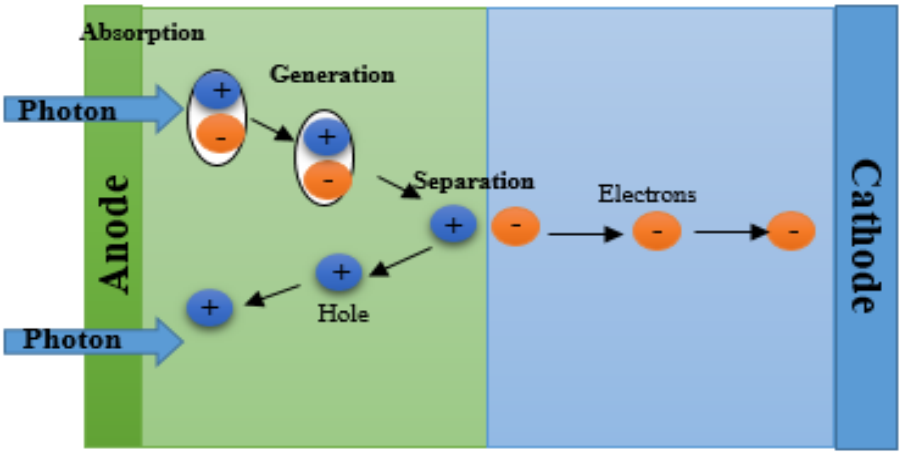

Figure I.3: A diagram representing the working mechanism of the organic solar cells [10].

The working principle of the OSC can be described in just few points as mentioned below:

1- Photons are incident on the active layer, therefore giving the photo excitation. This Organic layer, in its simplest form, consists of a single layer of semiconducting polymer, although it is most often composed of a mixture of two or more semiconducting polymers. The first of these polymers is a p-type material, which acts as an electron donor (D) and the second is an n-type material and acts as an electron acceptor (A).

2- The incident photons create excitons in the active layer, where the exciton is formed by an electron and hole polaron that are linked.

3- In order to dissociate the exciton in the electron and hole polaron (hereinafter only electron and hole), an energy of 250 meV or more is required, so the exciton must diffuse until the heterojunction is formed between the D and A materials. Generally, this process takes an ultra-short time interval of around 45 fs, and depends on the type of semiconductor polymers used. The exciton diffusion length is very short (between 10 and 20 nm).

4- Once separated into electron and hole, these charge carriers must be transported through by the n-type (acceptor) and p-type (donor) materials, respectively, until they reach the electrodes where they must be collected. If the active layer is formed by a single

semiconductor material, the separation process of the charge requires energies be provided by the asymmetry of the work functions of the electrodes.

5- The charge carriers are collected at the electrodes; the holes at the anode and electrons at the cathode.

I.4.1 Different device architectures of organic solar cell

Usually the organic solar cells are fabricated from three layers, with an active layer, located between the anode and a cathode layers. However, one of the electrodes should be transparent to light. Generally, typically in the metal electrode using Aluminum or Calcium as a cathode layer and the Indium Tin Oxide is used as a transparent anode layer. Most research recently is about how to improve the efficiency of organic solar cells [11]. In the next sections we present briefly the main categories of OSC architectures.

I.4.1.1 Single layer organic solar cell

In this structure of single-layer semiconductor solar cell is simplest of the OSCs. It is consisting of one layer of organic semiconductor between two metallic conductors. A typical layer of ITO with high work function and a metal layer of low work function are used. The difference between the functions of those two conductors is the set up of an electric field in the organic layer. After the absorbing of the light, the electrons excite the lowest unoccupied molecular orbital (LUMO) and leave holes in the highest occupied molecular orbital (HOMO) forming excitons. This potential gives rise to separate the exciton pairs, pulling electrons to the positive electrode and holes to the negative electrode [7].

I.4.1.2 Bilayer (BL) organic solar cells

Bilayer is consists from two layers of organic semiconductor, are named Donor-Acceptor shaped between two electrodes. The first one the ITO is the anode and the second the metal is the cathode. This structure is also called a planar donor-acceptor hetero-junction [7].

The ionization energy of an atom or molecule describes the amount of energy required to remove an electron from the atom or molecule in the gaseous state:

$$X + \text{energy} \rightarrow X^+ + e^-$$

The different affinities between the two layers generate a potential that can break up the excitons. As well known that exciton dissociation is efficient at the interface between materials with different electron affinity EA and ionization potential IP. The layer with higher electron affinity and ionization potential is called the acceptor, and the other layer is called the donor.

I.4.1.3 Bulk heterojunction (BHJ) solar cell

Bulk heterojunction (BHJ) organic solar cells are made up by blend of two or more polymeric materials with different electronic affinities and ionization potential. Those polymeric materials must be diluted in a mutual solvent. The resulting blend is dropped by spin coating to obtain a thin film with dominions of both materials in nanometric scale the interpenetrated regions should be keep transport the charge carriers towards electrodes as is shown in **Figure I.4**. the separation result a formation of the interpenetrated network, this caused by the conditions of the manufacturing process such as the temperature, annealing vapour, solvents, additives,…etc [7].

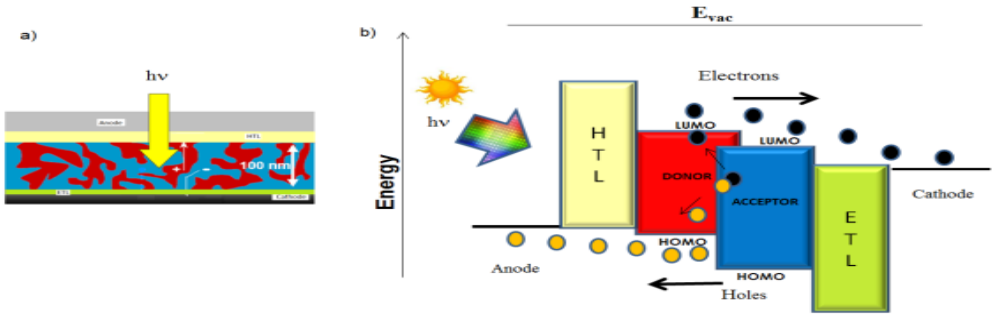

Figure I.4: (a) Structure of device; (b) Energy band diagram on BHJ organic solar cell shows the collection direction of the charge carriers. In the structure are added hole and electron transport layers (HTL and ETL) [7].

I.4.1.4 Nanostructured (NS) solar cell

The perfection of the Nanostructured photovoltaic solar cells owing to their ordered donor/acceptor interface in the nanometer measure between 10 and 20 nm, that what is equal to the diffusion length of the exciton. In the solar cell the well-defined interfaces (D/A) consider as short highways which the charge carrier can take facilely to reach their respective metal contacts. The raise of the cell efficiency backs to the solar cells with interdigitated structure which increase their interfacial area help to reduce charge carrier recombination. **Figure I.5** shows this interdigitated structure [7].

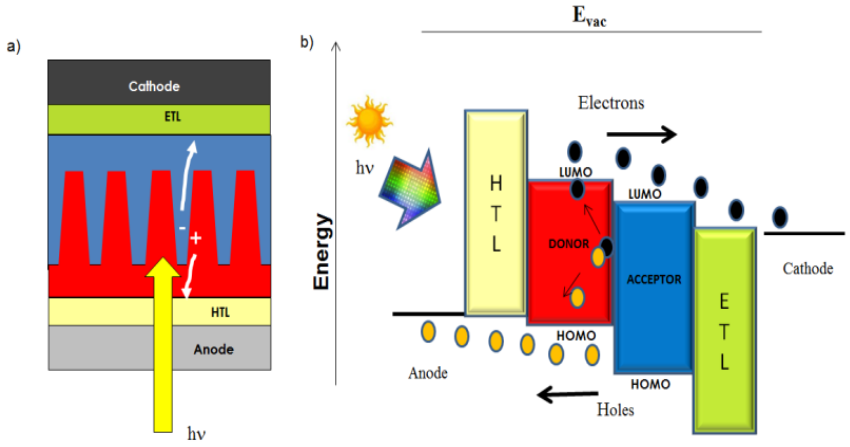

I.4 Figure I.5: (a) Nanostructured organic solar cell shows the cross section; (b) Energy band diagram of the nanostructured solar cell and shows the collection direction of the charge carriers (holes and electrons) [7].

Th

because their use leads that the lifetime in air of the solar cells increased significantly compared with the normal type solar cells. The conductor layers component for this structure are polyfluorene (PFN), titanium oxide (TiOx), zinc oxide (ZnO) and holes conductor layers are molybdenum oxide (MoO_3), vanadium oxide (V_2O_5) and tungsten oxide (WO_3) [12].

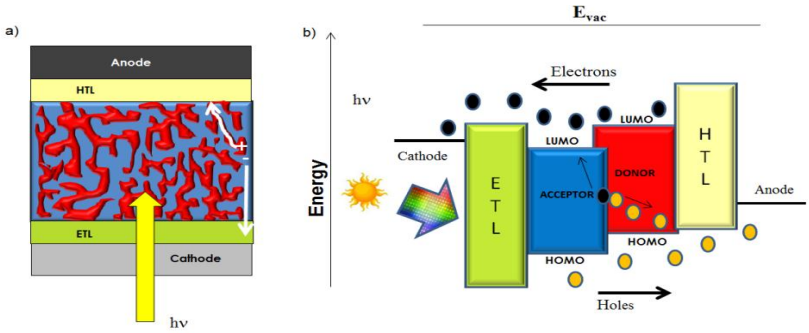

Figure I.6: (a) Inverted organic solar cell shows the structure; (b) Energy band diagram of an inverted organic solar cell which shows the collection direction of the charge carrier [7].

I.4.2 Parameters of organic solar cells

The typical J-V (Current-Voltage) characteristic for a solar cell is shown in **Figure I.7**.

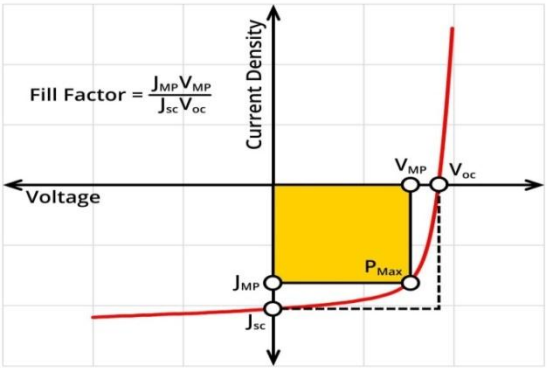

Figure I.7: The J-V characteristic (Current-Voltage) for a solar cell [13].

From this characteristic many parameters can be deduced and calculated. These parameters are:

I.4.2.1 Short- circuit current (J_{SC})

The current that flows in a PN junction under illumination is given by:

$$J = J_0 \left[exp\left(\frac{q\,V}{k\,T}\right) - 1 \right] - J_{ph} \quad (1)$$

J_{ph}: presents the density of photo generated current.

k: is the Boltzman constant.

J_0: is the current density at saturation.

$$J_0 = N_V\, N_C\, k\, T \times \exp\left(\frac{-E_g}{k\,T}\right)\left(\frac{L_n}{n\tau_n} + \frac{L_p}{p\tau_p}\right) \quad (2)$$

N_c: presents the density of states in the conduction band and N_v the density of states in valence band, Ln and L_p are the diffusion length, τ_v and τ_p are the lifetimes of electrons and holes respectively, and p and n are the density of the electrons and holes.

At V = 0 volts (the short-circuited cell), the current J_{sc} generated by the cell is: $J_{sc} = J_{ph}$.

I.4.2.2 Open circuit (V_{oc})

The open circuit voltage of a solar cell is achieved when the current flowing through the cell is zero. For photovoltaic cells based on organic materials, this origin is controversial. It depends directly on the band gap E_g.

When the current draping through the solar cell the open circuit voltage is become effectuated. For the photovoltaic cells which use as a basis the organic materials the cell is zero . This origin is dialectical and it depends directly on the band gap E_g.

The open circuit voltage of a solar cell based PN junction is given by:

$$V_{CO} = \frac{n\,k\,T}{q} \ln\left(\frac{I_{sc}}{I_S} + 1\right) \quad (3)$$

I_{sc} : is the short-current circuit density.

I_S: is the saturation current.

V_{CO}: is a function of E_g and is given by the following equation:

$$V_{CO} = \frac{n E_g}{q} - \frac{n k T}{q} \ln\left[\left(\frac{q N_C N_V}{I_{CC}}\right)\left(\frac{L_n}{n \tau_n} + \frac{L_P}{P \tau_P}\right)\right] \quad (4)$$

I.4.2.3 Fill factor

In order to improve the efficiency of organic solar cells, the most critical factor for a large impact on the different strategies depends on better fill factor FF which is given by the following relation:

$$FF = \frac{V_{max}}{V_{OC}} \frac{I_{max}}{I_{SC}} \quad (5)$$

V_{max} , I_{max}: are the voltage and current at maximum awarded by the cell extracted from the J-V characteristic of the cells.

I.4.2.4 Efficiency

The efficiency of organic solar cells is one of the factors limiting there commercialization. It is given by:

$$\eta = \frac{I_{SC} . V_{OC} . FF}{P_{in}} \quad (6)$$

P_{in} : is the power of the incident light. It is directly related at the open circuit voltage, and the short current circuit.

I.5 Fabrication processes

1.5.1 Fabrication process not compatible with upscaling

This technique has a disadvantage, not suitable for manufacturing a large number of samples. Due to several factors, for example, the time of the process for the making of any sample, through the process, there is a waste material, the energy consumption ...etc.

There are some techniques preferable used for fabricating a limited sample are spin coating (for solution processing) and evaporation (for aluminium deposition). There are other ways, like a casting, or other ones that provide more control over the deposited layer, such as organic molecular beam deposition [14,15].

I.5.1.1 Spin coating

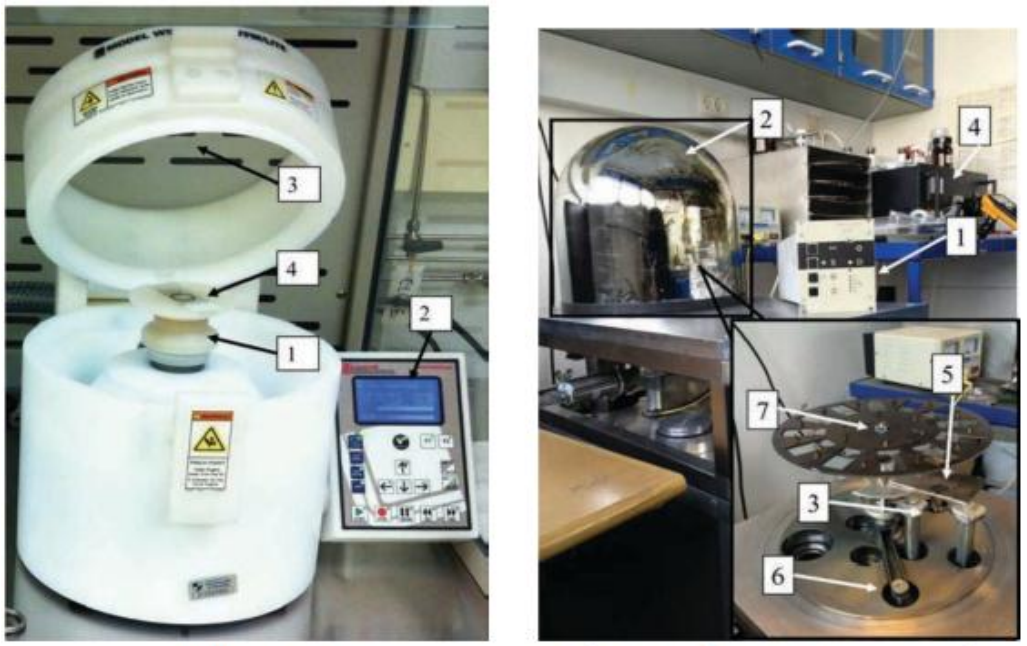

(a) Spin coater

(b) Overview of the evaporator: external view and detail of the evaporation environment, normally protected by the external bell

Figure I.8: Machinery used for layer processing using techniques not compatible with upscaling [18].

Figure I.8. Shows spin coating technique which is the common process used in lab-scale for depositing a thin layer of organic material. This device is composed of: 1) a rotating plate with adjustable rotating speed; 2) a controller which allows setting and controlling the rotating speed; 3) an opening on the spin coater top-lid that allows to drop the solution on the substrate, while protecting the user from spurts; 4) a sample holder with vacuum control to ensure a good adhesion of the sample to the holder during the rotation.

For product regular fine films of different materials with thickness varying from nanometers to micrometers, we use spin coating. For film production, the substrate is placed on the rotating plate and either covered by the solution of the material in stand still position or coated with the solution during rotation. Centrifugal force drives the dropped solution radially outward, while viscous force and surface tension lead to the formation of a thin residual film on the substrate. Finally, the residual wet film is gradually thinned depending on the evaporation of the solvents used in the solution. The thickness of the deposited layer has a square root dependence on the spin speed, so that a variation of 10 times on the speed of rotation leads to a variation of the thickness of approximately 3.2 times. Additional details on sample preparation using spin coating can be found

in the literature. The main advantage of spin coating is the easy control of the film thickness, which only requires changing the spin rotation. Other advantages are the low cost of the machinery and the fast operating system for fabricating a single sample. The main disadvantages of spin coating are the lack of material efficiency, considering that most of the solution is wasted during the thinning process, and the limited area scalability [14,16,17].

I.5.1.2 Evaporator

The evaporator is used to deposit a uniform layer in a high-vacuum environment (see **Figure I.8 (b)**). The evaporator consists of: 1) a pump needed to create the necessary vacuum; 2) a protective bell which contains the vacuum and where the evaporation takes place; 3) a metal evaporator boat (with a high melting temperature) containing the material that needs to be deposited; 4) a power supply that can provide the power required to heat the metal boat; 5) a shutter used to impede the evaporated material to reach the sample; 6) a mechanical belt connected to a motor that can rotate the stage holding the samples, guaranteeing the uniformity of the evaporated layer; 7) a stage used to hold the samples and to achieve a custom evaporation pattern. Put the material in the evaporator (inside the metal boat) for deposition this material until the vaporization process started. This process occurs in a high void that way the particles allow to go directly to the sedimentation target, without the collision with gas. Usually often is used the shutter to block the deposition of the first evaporated material together for preventing probably polluted material and also to guarantee a stabilized operation before beginning the vaporization. The stage of rotation containing the samples can start before moving the shutter. After the process has stabilized, the shutter can be moved and the deposition of the material on the sample can begin [18].

I.5.2 Fabrication process compatible with upscaling

Sundry roll-to-roll coating techniques are available for depositing functional layers, such as slot-die coating, gravure coating, slide coating, curtain coating, multilayer slot coating, spray coating,…etc. The interested reader can find comprehensive reviews on printing and coating methods elsewhere [19-28].

I.5.2.1 Machinery

In this section, we present the machinery used for processing of layers with techniques compatible with upscaling. Will be chosen the machinery depending on if compatible or not with a lab-scale approach. The lab-scale shows the possibility of manufacture different samples to test for a new kind of devices, to minimize the material [18].

I.5.2.2 Laboratory scale processing with upscalable techniques

The manufacturing processing Lab-scale showed a big advantage and very helpful for testing the modern material or new structure. The purpose of this technique it is gains the time and material. Lab-scale processing with upscalable techniques is essential to assess quality. After that can be transfer it directly to large-scale production. [18]

I.5.2.2.1 Mini roll coater

The mini roll coater is used for fabricating of entire devices utilize slot die coating and flexographic printing while keeping a lab-scale approach [29]. This method leads to develop the solar device using new materials in a simple and fast way, and with low cost. Truthfully, can't transfer the optimization in lab-scale using a spin coater directly to R2R production, that's what requests a repeat an optimization, so squandering material and time. The **Figure I.9** showed the Mini Roll Coater. It is based on an aluminum drum with built in heating elements, and having a diameter of 320 mm (1). The drum can rotate with a speed between 0 to 2 m/min, while an ink flows from the coating head (2), defining the coated layer. The coating head can be adjusted on both lateral and vertical direction, allowing the optimization of both the position of the coated layer in respect to previously deposited layers, and also to optimize the ink flow (3 and 4). Different heads can be mounted, with different widths. A syringe pump Aladdin NE-1000X is used to provide a constant flow of ink (5). The combination of rotation speed, ink flow and ink concentration determines the final thickness of the layer. Other parameters such as temperature of the drum and solvent type can influence the layer morphology and the device efficiency [30].

(a) MRC with a syringe pump on the side (b) The flexographic head mounted on the MRC

Figure I.9: The mini roll coater. Credits to Henrik F. Dam [18].

The printing of the back silver electrode is done using a flexographic printing head, mounted instead of the coating head (6). The flexo printing head consists of a block having two axes which are used to mount a 100 mm diameter coating roller. The roller is then equipped with a patterned rubber flexo roller which allows for printing a 2D pattern on the substrate, defining the solar cell final area. **Figure I.9 (b)** shows the flexo printing head mounted on the MRC.

I.5.2.3 Large scale manufacturing

Figure I.10 explains the printing setup employed for the large scale fabrication of OSC and modules with R2R coating. The R2R machinery, shown in **Figure I.10**, does not allow the processing of all the techniques, but flexographic printing, slot-die coating and rotary screen printing are possible.

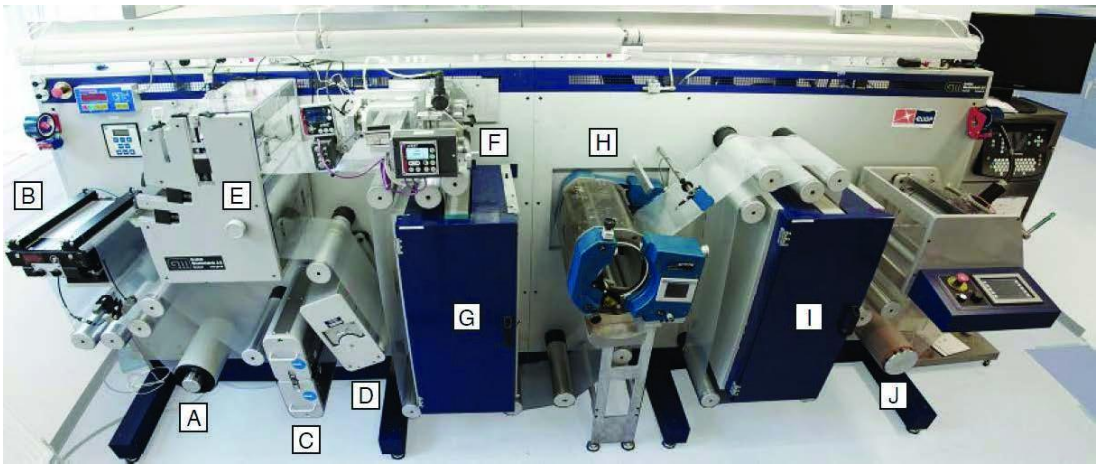

Figure I.10: Photograph of a R2R machinery for large scale manufacture. The main components in direction of web movement are: (A) unwinder, (B) edge guide, (C) web cleaner, (D) corona treatment, (E) flexo printing, (F) slot-die coating, (G) dryer, (H) rotary screen printing, (I) dryer, (J) rewinder [18].

I.5.3 Techniques

I.5.3.1 Coating techniques

I.5.3.1.1 Slot-die coating (SD)

Slot-die coating is a contact-less technique in which an ink flows through a coating head forming a uniform coated layer along the direction of a moving web (see **Figure I.11)**. The ink is fed to the coating head using a pump. The coating head is made from stainless steel and contains an ink

distribution chamber, a feed slot, and an up- and downstream lip. The thickness of the layer depends on the speed of the web, the supplied ink and the width of the coated layer. Moreover, the thickness is defined by the following equation:

$$d = \frac{f}{S \cdot w} \cdot \frac{c}{p} \tag{7}$$

where d is the thickness in cm of the coated layer, f is the flow rate in $cm^3\ min^{-1}$, S is the web speed in cm min^{-1}, w is the coated layer width in cm, c is the solid content in the ink in g cm^{-3}, ρ is the density of the dried ink material in g cm^{-3} [18].

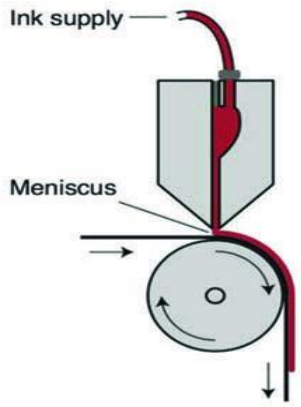

Figure I.11: Schematic representation of slot die coating [31].

I.5.3.2 Printing techniques

Mostly, the printing techniques depending on the contacts and they allow for two-dimensional patterning because of the possibility of designing a customizable printing.

I.5.3.2.1 Flexographic printing (FP)

Figure I.12 (a) shows the description of the schematically of the process. The anilox roller is filled with ink by the fountain roller, The doctor blade used to remove the excess ink, The anilox roller is full with surface of small dimples, the ink bath is contact of the fountain roller, The printing plate captures the ink from the anilox roller, the rotation makes them contact, and transfers the ink onto the substrate guided by an impression cylinder. Either the the printing plate material can be rubber or a photopolymer of different harshness, then the plate is fixed on the printing cylinder, the other optimization parameters have the ink surface tension , nilox cell geometries, nip pressure and printing speed. The flexographic printing is applied in this work to print the silver grid in the Flextrode, to allow an operational speed of 25 m min-1. [32]

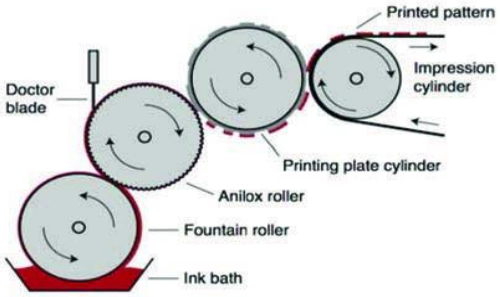

(a) Flexographic printing (FP)

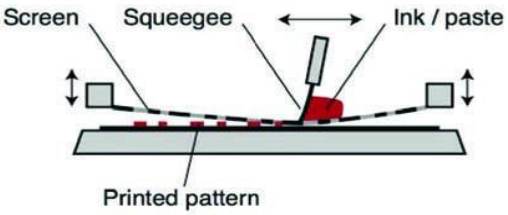

(b) Flatbed screen printing (SP)

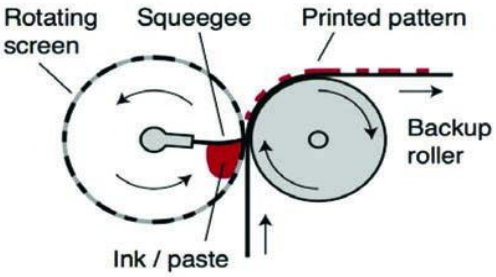

(c) Rotary screen printing (RSP)

Figure I.12: Schematic representation of the printing techniques compatible with upscaling [31].

I.6 Conclusion

This chapter has dealt in general with the presentation of an overview on the organic solar cells. In particular, we have given a brief history on the organic solar cells. After that the different device architectures of OSC were detailed. In the next section we have given the principal parameters that characterize the typical OSC. To give a good picture on the OSC manufacturing, we have presented different process of fabrication regarding their compatibility or no with upscaling. In the end of this chapter we have given the used machinery and techniques in the fabrication process.

Despite the highlighted advantages, the lifetime of OSC is the problem which hampering their application so far. The next chapter will be focused on the presentation of the degradation mechanisms of OSC under different used protocols of tests.

I.7 References

[1] Castaner, Luis, and Santiago Silvestre. Modelling photovoltaic systems using PSpice. John Wiley and Sons, 2002.

[2] Meftah, Mustapha, David Bolsée, Luc Damé, Alain Hauchecorne, Nuno Pereira, Abdanour Irbah, Slimane Bekki, Gaël Cessateur, Thomas Foujols, and Rémi Thiéblemont. "Solar irradiance from 165 to 400 nm in 2008 and UV variations in three spectral bands during solar cycle 24." Solar Physics 291, no. 12 (2016): 3527-3547.

[3] Center, Renewable Resource Data. "Reference Solar Spectral Irradiance: Air Mass 1.5." National Renewable Energy Laboratory,[Online]. Available: http://rredc. nrel. gov/solar/spectra/am1 5 (2020).

[4] Mazzio, Katherine A., and Christine K. Luscombe. "Correction: The future of organic photovoltaics." Chemical Society Reviews 44.15 (2015): 5744-5744.

[5] Aydil, Eray S. "Nanomaterials for solar cells." Nanotech. L. & Bus. 4 (2007): 275.

[6] Brabec, Christoph J., et al. "Polymer–fullerene bulk- heterojunction solar cells." Advanced Materials 22.34 (2010): 3839-3856.

[7] Balderrama Vázquez, Victor Samuel. "Fabrication of bulk and interdigitated organic solar cells and analysis of degradation mechanisms. " Diss. Universitat Rovira i Virgili, 2014.

[8] Green, Martin A., et al. "Solar cell efficiency tables (version 54)." Progress in photovoltaics: research and applications 27.7 (2019): 565-575.

[9] http://www.nrel.gov/ncpv/images/efficiency_chart.jpg 06/12/2020.

[10] Taha. Qamar. "Encapsulation of Small Molecule Organic Solar Cells for Improved Stability and Lifetime. " Diss. NanoSYD center, Mads Clausen Institute, University of Southern Denmark, Sønderborg, 2016.

[11] Sahare, Swapnil Ashok. "Enhancing the Photovoltaic Efficiency of a Bulk Heterojunction Organic Solar Cell." Diss. The Faculty of the Department of Chemistry, Western Kentucky University, Green, 2016.

[12] Kuwabara, Takayuki, et al. "Highly durable inverted-type organic solar cell using amorphous titanium oxide as electron collection electrode inserted between ITO and organic layer." Solar Energy Materials and Solar Cells 92.11 (2008): 1476-1482.

[13] Solar Cells: A Guide to Theory and Measurement https://www.ossila.com/pages/solar-cells-theory 06/12/2020

[14] Krebs, Frederik C. "Fabrication and processing of polymer solar cells: A review of printing and coating techniques." Solar energy materials and solar cells 93.4 (2009): 394-412.

[15] Kish, E. R., et al. "When the sequence of thin film deposition matters: Examination of organic-on-organic heterostructure formation using molecular beam techniques and in situ real time x-ray synchrotron radiation." The Journal of Physical Chemistry C 120.11 (2016): 6165-6179.

[16] Krebs, Frederik C., Suren A. Gevorgyan, and Jan Alstrup. "A roll-to-roll process to flexible polymer solar cells: model studies, manufacture and operational stability studies." Journal of Materials Chemistry 19.30 (2009): 5442-5451.

[17] Spin Coating: A Guide to Theory and Techniques – Ossila.http://www.ossila.com/pages/spin-coating 06/12/2020.

[18] Corazza, Michael. Characterization of Organic Solar Cell Devices and their Interfaces under Degradation: Imaging, Electrical and Mechanical Methods. Department of Energy Conversion and Storage, Technical University of Denmark, 2016. 275pp.

[19] Sahu, Niranjan, B. Parija, and S. Panigrahi. "Fundamental understanding and modeling of spin coating process: A review." Indian Journal of Physics 83.4 (2009): 493-502.

[20] Tracton, Arthur A., ed. Coatings technology handbook. CRC press, 2005.

[21] Kipphan, Helmut, ed. Handbook of print media: technologies and production methods. Springer Science & Business Media, 2001.

[22] Schunk, P. R., et al. "Liquid film coating." Free-Meniscus Coating Processes. Springer; Netherland (1997): 673-708.

[23] Shlomo, Magdassi, ed. The chemistry of inkjet inks. World Scientific, 2009.

[24] Osman A. Basaran, Haijing Gao, and Pradeep P. Bhat. “Nonstandard Inkjets”. en. In: Annual Review of Fluid Mechanics 45.1 (January 2013), pages 85–113. issn: 0066-4189.

[25] Pond, Stephen F. "Inkjet technology and product development strategies." (2000).

[26] Wengeler, Lukas, Marcel Schmitt, Katharina Peters, Philip Scharfer, and Wilhelm Schabel. "Comparison of large scale coating techniques for organic and hybrid films in polymer based

solar cells." Chemical Engineering and Processing: Process Intensification 68 (2013): 38-44.

[27] Derby, Brian. "Inkjet printing of functional and structural materials: fluid property requirements, feature stability, and resolution." Annual Review of Materials Research 40 (2010): 395-414.

[28] Riemer, Dietrich E. "The theoretical fundamentals of the screen printing process." Microelectronics International (1989): 8-17.

[29] Dam, Henrik F., and Frederik C. Krebs. "Simple roll coater with variable coating and temperature control for printed polymer solar cells." Solar Energy Materials and Solar Cells 97 (2012): 191-196.

[30] Bundgaard, Eva, Francesco Livi, Ole Hagemann, Jon E. Carlé, Martin Helgesen, Ilona M. Heckler, Natalia K. Zawacka et al. "Matrix organization and merit factor evaluation as a method to address the challenge of finding a polymer material for roll coated polymer solar cells." Advanced Energy Materials 5, no. 10 (2015): 1402186.

[31] Søndergaard, Roar R., Markus Hösel, and Frederik C. Krebs. "Roll- to- Roll fabrication of large area functional organic materials." Journal of Polymer Science Part B: Polymer Physics 51, no. 1 (2013): 16-34.

[32] Krebs, Frederik C., Thomas Tromholt, and Mikkel Jørgensen. "Upscaling of polymer solar cell fabrication using full roll-to-roll processing." Nanoscale 2, no. 6 (2010): 873-886.

CHAPTER II

Degradation of Organic Solar Cells

II.1 Introduction

The aging or degradation of organic solar cells it could happen under different affection of exterior factors such as “light, heat, oxygen and humidity" these factors effect on a different stage of photocurrent generation. In fact, to achieve good results on the stability of organic solar cells OSCs it takes more time. Including, the mechanism of degradation of organic solar cells has been studied extensively [1].

The phenomenon of degradation of organic solar cells took attention of researchers in the past years. **Figure II.1** shows those studies or publications on stability have followed an increasing trend in the last years. However, the new researches studies have been of good on stability [1].

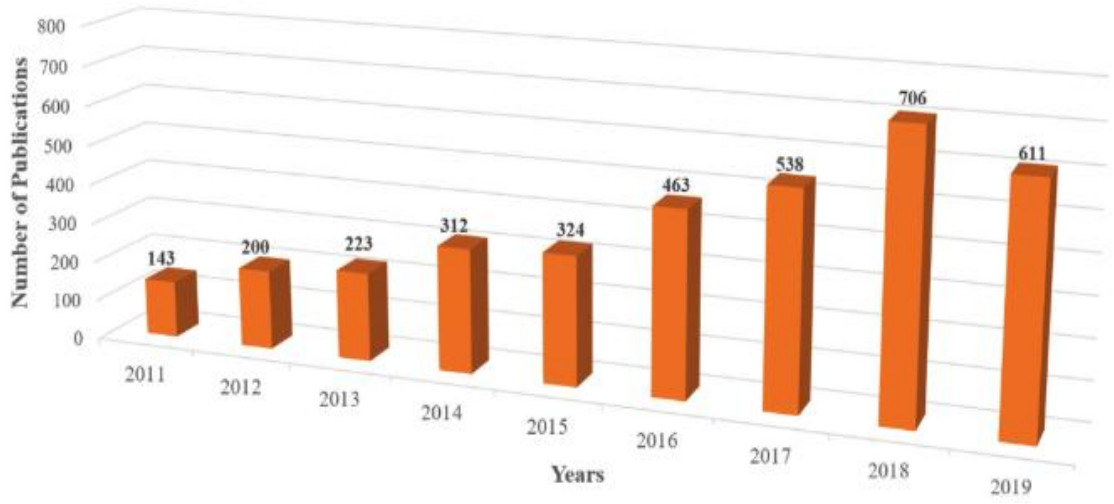

Figure II. 1: Publication trend in the stability of organic solar cells from 2011 to 2019 [1].

In contrast, when the non-fullerene acceptor (NFA) was used in the OSC, a great stability has been gained. According to the researchers, this kind of acceptor can improve the lifetime of the OSC and can reach approximately 10 years [2]. Hence, the existence relation between the use of the NFA and stability has been extensively studied in the literature [3-5].

Mechanism of degradation in organic solar cells can caused by the photo- and water-induced chemical reactions within the active layer, the degradation of device electrodes, the instability of hole and electron transport layers and a failure of device encapsulation. For more details of device degradation mechanisms there are a number of comprehensive review [6-8]. In recent years, consensus stability testing protocols have been used to study the degradation mechanisms of OSCs

[9]. Khenkin et al. [10] has explained that the degradation of cells is due to falls in short circuit current density (J_{sc}) and fill factor (FF) using outdoor test for long-term of encapsulated organic solar cells with glass and aluminum. In other hand they reported that the reversible degradation mechanisms explain the recovery between light-dark [11].

II.2 Aging of organic solar cells

Current research on organic solar cells is focused on aging due to disadvantage the operating of the lifetime of this device, because of the weak stability under different exteriors conditions such as (humidity, oxygen, etc...).

The lifetime of solar cells is given by the time taken by the device under continuous illumination for the efficiency value to reach half of its initial value.

There are different mechanisms of degradation of solar cells [12]:

1- Intrinsic ageing of materials: this type of ageing of the material under lighting, but without exposure to water and oxygen.

2- Extrinsic aging of materials: In this type, the ageing mechanism is photo-oxidation. This means the influence of two external factors (oxygen O_2 and water H_2O) on organic material and metals from the electrodes.

3- Cell aging: Occurs this type of degradation when the diffusion of impurities on both sides of the interface, it is taken into account the degradation of the interfaces following the bringing into contact of different materials (active layer-electrode for example). This kind of degradation is generally accelerated in the presence of water, oxygen, and lighting.

II.3 Mechanisms of degradation

The degradation of organic solar cells has a lot of mechanisms that can be explained in the **Figure II.2** below. The goal of this format to a clarification that the degradation issue is a little complicated, although the list is not exhaustive.

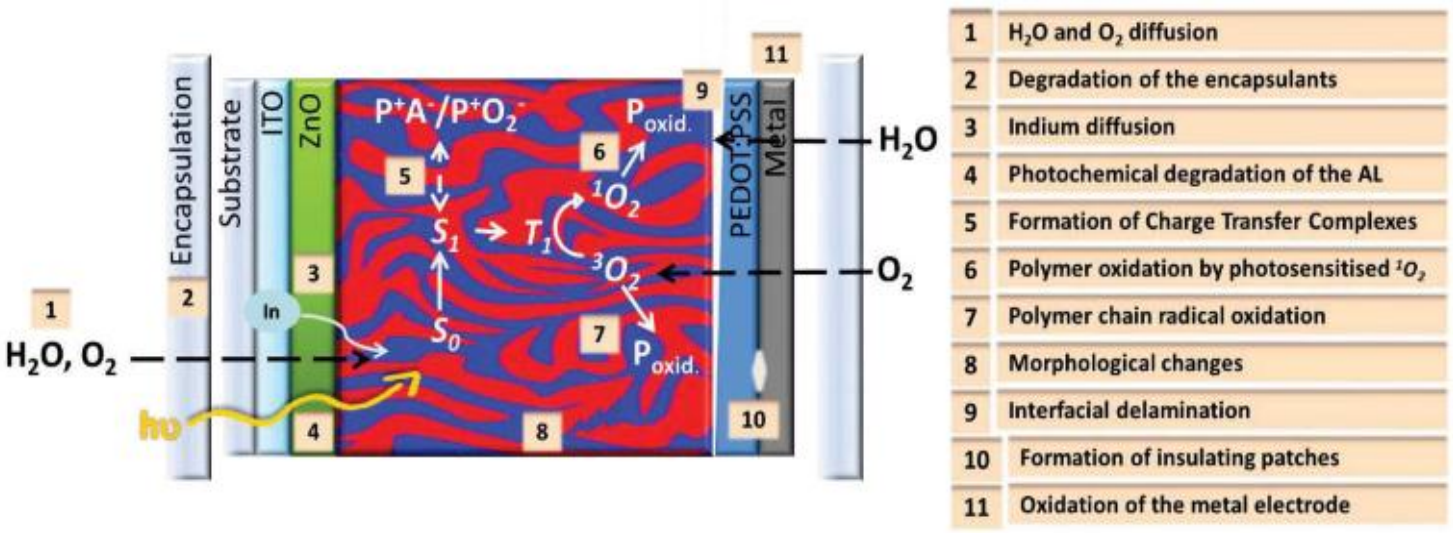

Figure II.2: commonly reported degradation mechanisms in OSCs[13].

II.3.1 Mechanical stress, delamination and interfaces

Encapsulation degradation studies should be taken and require careful investigation. However, encapsulation preserves mechanical safety in a system collected with different layers. Most importantly, save the flexibility property in the devices [14-16]. The sticking between layers shows the instability of flexible devices; because of the flex in the devices occur delamination problems over time, therefore affecting the extraction of charges. Brand *et al*, has explained the thermo mechanical characteristics of OSCs, the PEDOT: PSS with the active layer, they proposed it a dot of failing in inverted devices [14].

II.3.2 The spread of water and oxygen, deterioration of encapsulation materials

It is mostly admitted that the attendance of water and oxygen in the device is a agent limiting the corresponding service life of the device [17, 18]. The blend PEDOT: PSS and the active layer or electrodes of metal affected by external factors such as water and oxygen or we can say react with cellular components to accelerate significant processes. In fact, they have the ability to add both of this water and oxygen factors in the stack during the handling of OSCs, especially if they are industrially produced. Norrman et al, they used the roll to roll processes, demonstrate that after the handling of the full stack, major portal to the device for oxygen and water is breakthrough through

the encapsulating material [19]. Moreover, the diffusion of oxygen and water could be passing to the outer electrode with various ways such as amongst metal grains of the electrode or microscopic pinholes [20].

So, there are therefore two important components which must be prevented from entering the apparatus by improving the quality of the encapsulating materials. At last, the encapsulation depends on using a barrier film of alternating organic and inorganic layers [21, 22]. Must be preserved different properties such characteristics of the barrier and other important properties transparency or flexibility, consequently, the stack of results, it must be resistant to different stress cases is exposed to it.

II.3.3 Decay of the electrodes

The different external factors or condition climatic such as radiation, oxygen, humidity and heat, these factors effecting on the polymer or organic components, so the degradation mechanisms related materials of the barrier. Previous several investigations of chemical degradation proofed the material is a cause in decay and change the different properties this can be seen such as yellowing and cracking, eventually these type of decay leads to change the absorption of light by active materials in the heart of the device.

Mainly, the use of ITO such as a lower electrode, in the different recent studies proves the weak material. Sarkar, *et al*. Prove that they could apply by directly modifying the polar characteristics of ITO using the humidification of the active organic layer [23]. However, the humidification creates a problem on level of charge transport and boost delamination, all these problems because of adhesion between layers [24, 25]. In another hand, use layers PEDOT: PSS like a buffer layer, the PSS has a disadvantage, is deforming the ITO due the acidic [26- 28]. Moreover, the researchers prove that can use semitransparent contacts, usage allowance ITO [29, 30].

II.3.4 Decay active layer

This Decay takes the attention of researchers; due to the unstable structure such as Bulk heterojunction can develop with time. So stopping the exciton dissociation and charge transport, this influence must be enhanced with a high temperature. Moreover, the acceptor such as PCBM has a due to degradation of the device performance [31, 32]. The morphology stability of the active layer was monitored using various strategies. For example the use of a chemically functional donor

and acceptor, capable of crosslinking on heat or photochemical treatment or adding third ingredients or additives that stabilize the shape over time. [33-36].

Figure II.2. It demonstrates the effects that can happen with a polymer in the active layer. Moreover, the active layer components of organic solar cells are sensitive when exposed to solar radiation, this effect is named photochemical [37, 38].

II.4 Performance of OSCs devices with Degradation

The recent research showed how degradation mechanisms happen in all devices with different factors climatic (Indoor, Outdoor).

The degradation of power efficiency takes the exponential curve. This curve divided to three parts. All those divided parts it is depend to T 80. First part named Burn-in. Second part named linear regime. In the last part called it failure. The OSCs devices take the same curve of lifetime.

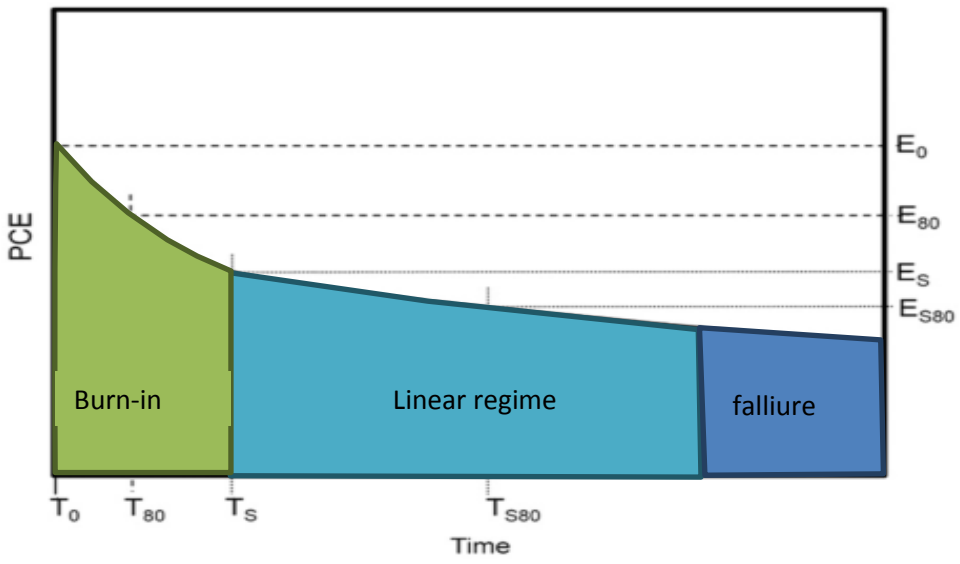

Figure II.3 curve of an OPV device shows the parameters of lifetime with the key stages of degradation [40, 41]

a) Burn-in

Burn-in takes as important stage in the degradation of OSCs, demonstrated that decay the half-life time of the cell can be determined from it [41- 45]. Nevertheless, the aging in the OSCs device shows a variable time to burn-in, it can be trapped between 100 to 150 hours form time aging [45-47]. In other studies the researcher confirmed that the decay in the efficiency results of from descending in V_{oc}, FF [48].

This degradation only happens on the presence of the light [44, 46] and it depends of his intensity [42, 49]. The mechanisms which cause the break-in of the device they consider as a photo-degradation in the device.

The V_{OC} component of burn-in it seems interfacial because of the interlayers [45] and the extension of layers is affected on the degree [50].The mechanism of this degradation it is reversible [51].

b) Linear degradation regime

The Figure II.3 shows the second regime of OSC device is characterized by a direct decrease in effectiveness with time. Frequently the linear regime used to characterize lifetime by means of the TS80 (vide supra). In reality it is the lifetime of the devices. The specific start of the linear regime is hard to characterize, as the as the burn-in is exponential and consequently doesn't have a severe end. Much of the time, The researchers used the semi-arbitrarily to decide the end of the burn-in picking where the degradation curve seems to have acquired direct character [41].In fact by the calculation of T80 lifetime estimates it is can proved. Some researches explained how use the multi-exponential fit of the degradation curve [52]. In other hand the researchers propose a method to estimating the end of burn-in with using the following bi-exponential model [53].

The degradation it can be given by a mix of intrinsic mechanisms that are an outcome of the typical operation of the device and outward instruments that are a result of the device's current

circumstance and openness to ageing stimuli and accordingly can somewhat be eliminated. And consequently the design of the device and the picked of materials are the key factors in extending lifetime whereas the lifetime of device mostly confined by intrinsic degradation mechanisms [42].

The lifetimes of direct and reverse OSC devices override 8000 hours. However, the studying of the devices display there is no degradation after the break-in. About the degradation's extrinsic sources the aging occurred under the same weather conditions but with a radiation source that does not have a UV component. This type of active layer PCDTBT: PC71BM BHJ is more stable than P3HT: PC61BM even of the high glass temperature (Tg) of the PCDTBT also encourage of further stabilization under brightening by crosslinking [54]. The elimination of the UV light or any change of materials for the active layer brings the acidic PEDOT:PSS which is more stable.

c) Catastrophic failure

To examine the failure of the device it is feasible to pick a point on a degradation curve and name it as the device's life end [53] even the uses of the TS80 to review how the failure of device happened it does not enough it may the end of lifetime of device it is caused by a different degradation mechanism which named catastrophic failure [53].

The catastrophic failure on ITO / PEDOT: PSS / P3HT: PCBM / Yb / Al shows above 300 hours of aging under AM 1.5 lighting a big losses of FF which presented in curve IV by a in S [44]. This S it means the death of the device. The accumulation of a space charge it is caused by the development a charge extraction barrier in the working area of the device [44, 55]. The researchers managed to significantly delay or even prevent catastrophic failure by the change of the materials utilized as charge extraction layers [44, 56].

However. It is possible to delayed or potentially completely the catastrophic failure caused by the intrinsic mechanisms with a smart device. the changes of the environmental conditions it might cause the degradation of the encapsulation materials and corrode electrical contacts which make

the device valueless [53].The electrode delamination is caused in the first place by the mechanical stresses and this back to metal electrodes adhere to the organic layers [53,25].

II.5 Strategies to minimize device degradation

As we know in this chapter the intrinsic and extrinsic mechanisms this is the reason for the degradation of OSC devices. in this part we will examine some strategies that increase the lifespan of a device on both aspects of degradation

- integrating longer photo-stable and morphologically stable donor types;
- Connection the donor and acceptor types so that is photolysis is reduced and stabilized the BHJ morphology [57];
- Interlocking the donor and acceptor types to stabilize the BHJ morphology [54];
- Add a chemicals hard interlayers and electrodes [34];
- Add more stable inverted device architecture [44, 58]

To ensure the stability of the device it has to be there some form of encapsulation whereas The least stable device required a good encapsulation which it expensive [59]. Due the encapsulation addresses a huge segment of conclusive gadget cost, this has suggestions for the monetary reasonability and energy time of the device [60.61].there are a several of encapsulation methods it may be used in OSC devices one of those is the glass-on-glass method.in this model the device is manufactured on a glass substrate and an extra piece of glass is gotten on top of the sample with an adhesive [62]. This method it is the best way f encapsulation in which the lone compelling course of water and oxygen entrance is around the edges of the typified device. But it still has abuses especially its incapability for roll-to-roll processing and flexible devices.

There is the method thin-film polymer materials [60].But it is not affective as the glass and this up to thin-film polymer materials [60].This laminate films it can be substrates and encapsulation

barriers [59,63,60,64]. The researchers found strategies for the design and fabrication of encapsulation materials [65, 66].

II.6 The ISOS protocols

The researches about the stability and degradation of organic solar cells take more attention to researchers, in this part different laboratories around the world take a step to collaboration for study and create different protocols demonstrate everything from lab-scale ageing under simulated sunlight to outdoor testing under operational conditions (see **Table II.1**) [17,41]

The major principle of the protocols, is not only related to the testing practices or the equipment, but also aims at limiting the environmental conditions of the test (such as temperature, relative humidity, etc.) to only certain levels. Some ISOS tests are mild and do not hint an accelerated test, while others are hard, and encourage a fast degradation (**Figure II.3** and **Table II.2**) shows the parameter power conversion efficiency (PCE), including E_0 and T_0, E_S and T_S, E_{80} and T_{80}, and E_{S80} and $T_{S80.}$ $_T$hose four (4) parameters explain the carefully depict of the degradation [41].

In other factors such as FF, V_{oc}, J_{sc}, etc. can also be included using the same established protocol.

E_0: present the first point at the measurement it is mean after fabrication should be test the OSC device immediately and the most accurate device, at time t = 0, T_0.

E_S at T_S, show as the second measurement of the OSC device, the operator designates this time T_S, arbitrarily after the fabrication of a device. E_S shows to us if the device stabilized and capable of moving to another stage of aging conditions.

The two last parameters, E_{80} and E_{S80}, clarify the performance of organic photovoltaic cells at time T_{80} or T_{S80}, respectively. Where those parameters shows the degradation the device from initial or

second testing measurement when this device get 20% after decay. It is also necessary to report the J-V curve for each of the four time points highlighted in the decay curve.

Three levels

Basic (level 1): "Handheld" measurement using the simplest equipment and few conditions.

Intermediate (level 2): Fixed conditions and protocols suited for most labs.

Advanced (level 3) Standardized tests applied in certified labs. Extended range of parameters to monitor etc.

Type	Dark			Outdoor		
Test ID	ISOS-D-1 shelf	ISOS-D-2 high temp. storage	ISOS-D-3 damp. heat	ISOS-O-1 outdoor	ISOS-O-2 outdoor	ISOS-O-3 outdoor
Light source	None	None	None	Sunlight	Sunlight	Sunlight
Temps a)	Ambient	65/85 °C	65/85 °C	Ambient	Ambient	Ambient
Relative humidity (RH) a)	Ambient	Ambient (low)	85%	Ambient	Ambient	Ambient
Environment a)	Ambient	Oven	env. chamber	outdoor	Outdoor	Outdoor
Characterization light source	Solar simulator or sunlight	Solar simulator	Solar simulator	Solar simulator	Sunlight	Sunlight and Solar simulator
Load b)	Open circuit	Open circuit	Open circuit	MPP or Open circuit	MPP or Open circuit	MPP
Type	Laboratory weathering testing			Thermal cycling		
Test ID	ISOS-L-1 Laboratory weathering	ISOS-L-2 Laboratory weathering	ISOS-L-3 Laboratory weathering	ISOS-T-1 Thermal cycling	ISOS-T-2 Thermal cycling	ISOS-T-3 Thermal cycling
Light source	Simulator	Simulator	Simulator	None	None	None
Temps a)	Ambient	65/85 °C	65/85 °C	Between room temp. and 65/85 °C	Between room temp. and 65/85 °C	-40 to +85% °C
Relative humidity (RH) a)	Ambient	Ambient	Near 50%	Ambient	Ambient	Near 50%
Environment /setup	Light only	Light and temp	Light temp., RH	Hot plate/oven	Oven / env. chamber	env. chamber
Characterization light source	Solar simulator	Solar simulator	Solar simulator	Solar simulator or sunlight	Solar simulator	Solar simulator
Load b)	MPP or Open circuit	MPP or Open circuit	MPP	Open circuit	Open circuit	Open circuit

Table II.1 Consensus stability testing protocols for organic photovoltaic [41]

a) The ambient conditions are defined as 23 °C 50% RH in general. And 27 °C accepted in tropical countries according to ISO291 (2008): plastics— standard atmo- spheres for conditioning and testing b) open circuit refers to simply disconnected device or device connected a source meter set to 0 current.

TABLE II.2 The Paramters of stability

	Initial burn-instage		***Stabilized Stage***	
PV Paramters	E_0	E_{80}	E_S	E_{S80}
Time	T_0	T_{80}	T_S	T_{S80}

II.7 Stability measurement protocols

In the test protocols divided to different classes: outdoor, dark, simulated light, stress testing and thermal cycling. There are three levels for each test: Basic (Level 1), Intermediate (Level 2) and Advanced (Level 3). In these protocols there are different factors should be taken into consideration (temperature, humidity, environment, light and electrical load) [41].

For more demonstration those different categories of protocols: Outdoor testing (type O) test the device under different real condition climatic with open circuit or maximum power. The Dark testing (type D) is performed to test the shelf life of the devices and their resistance to high temperatures and humidity. Laboratory weathering testing (type L) is made to imitate the real weather with accelerating aging of a device using a well-calibrated solar simulator and a controlled atmosphere. Eventually, the thermal cycling test (type T) puts the device under accelerated variation temperature, to tests the lifetime and decay the device. As we mentioned earlier, there are three levels for monitoring different parameters. For example L1 in this level must be monitored those cell parameters the V_{oc} and J_{sc} with provide a source of constant light. But in level three (L3) requires monitoring of am parameters (V_{oc}, J_{sc}, FF and PCE) with a filter AM 1.5 solar simulator environmental chamber.

The organic solar cells OSCs contain different structure with the use of different material for design. Recent studies have shown a variation in lifespan between devices. This is due to the different designs. Nevertheless, the lifetime of OSCs can be divided into three stages generally: running-in, linear disintegration and device failure.

II.8 Conclusion

In this chapter we have presented an overview on the degradation process and mechanisms of organic solar cells. It is found from the literature that the degradation process can be affected by several intrinsic and extrinsic factors. UV Light, temperature, humidity, dark and oxygen are the main preponderant factors in the degradation mechanism. It is highlighted also that degradation mechanisms can undergo mechanical stress, delamination and interfaces, water and oxygen diffusion, degradation of the encapsulation materials, chemical degradation of the electrodes and finally the photochemical and morphological degradation of the active layer. In the end of the chapter different ISOS protocols which used in the OSC stability and lifetime analysis are summarized.

II.9 References

[1] Duan, Leiping, and Ashraf Uddin. "Progress in Stability of Organic Solar Cells." Advanced Science 7.11 (2020): 1903259.

[2] Du, Xiaoyan, et al. "Efficient polymer solar cells based on non-fullerene acceptors with potential device lifetime approaching 10 years." Joule 3.1 (2019): 215-226.

[3] Gasparini, Nicola, et al. "Burn- in Free Nonfullerene- Based Organic Solar Cells." Advanced Energy Materials 7.19 (2017): 1700770.

[4] He, Yakun, et al. "Evidencing Excellent Thermal- and Photostability for Single- Component Organic Solar Cells with Inherently Built- In Microstructure." Advanced Energy Materials 9.21 (2019): 1900409.

[5] Zhang, Chaohong, et al. "A top-down strategy identifying molecular phase stabilizers to overcome microstructure instabilities in organic solar cells." Energy & Environmental Science 12.3 (2019): 1078-1087.

[6] Mateker, William R., and Michael D. McGehee. "Progress in understanding degradation mechanisms and improving stability in organic photovoltaics." Advanced materials 29, no. 10 (2017): 1603940.

[7] Cheng, Pei, and Xiaowei Zhan. "Stability of organic solar cells: challenges and strategies." Chemical Society Reviews 45, no. 9 (2016): 2544-2582.

[8] Lee, Jea Uk, et al. "Degradation and stability of polymer-based solar cells." Journal of Materials Chemistry 22.46 (2012): 24265-24283.

[9] Reese, Matthew O., et al. "Consensus stability testing protocols for organic photovoltaic materials and devices." Solar Energy Materials and Solar Cells 95.5 (2011): 1253-1267.

[10] Katz, E. A., et al. "Out-door testing and long-term stability of plastic solar cells." The

European Physical Journal-Applied Physics 36.3 (2006): 307-311.

[11] Khenkin, Mark V., et al. "Dynamics of photoinduced degradation of perovskite photovoltaics: from reversible to irreversible processes." ACS Applied Energy Materials 1.2 (2018): 799-806.

[12] Esselink, F. J., and G. Hadziioannou. "Transmission electron microscopy study of the indium/P3OT and aluminium/P3OT interfaces (P3OT is poly (3-octylthiophene))." Synthetic metals 75.3 (1995): 209-212.

[13] Dupont, Stephanie R., Mark Oliver, Frederik C. Krebs, and Reinhold H. Dauskardt. "Interlayer adhesion in roll-to-roll processed flexible inverted polymer solar cells." Solar Energy Materials and Solar Cells 97 (2012): 171-175.

[14] Brand, Vitali, Christopher Bruner, and Reinhold H. Dauskardt. "Cohesion and device reliability in organic bulk heterojunction photovoltaic cells." Solar energy materials and solar cells 99 (2012): 182-189.

[15] Brand, Vitali, Kemal Levi, Michae D. McGehee, and Reinhold H. Dauskardt. "Film stresses and electrode buckling in organic solar cells." Solar energy materials and solar cells 103 (2012): 80-85.

[18] Jørgensen, Mikkel, Kion Norrman, Suren A. Gevorgyan, Thomas Tromholt, Birgitta Andreasen, and Frederik C. Krebs. "Stability of polymer solar cells." Advanced materials 24, no. 5 (2012): 580-612.

[19] Norrman, Kion, Morten V. Madsen, Suren A. Gevorgyan, and Frederik C. Krebs. "Degradation patterns in water and oxygen of an inverted polymer solar cell." Journal of the American Chemical Society 132, no. 47 (2010): 16883-16892.

[20] Grossiord, Nadia, Jan M. Kroon, Ronn Andriessen, and Paul WM Blom. "Degradation

mechanisms in organic photovoltaic devices." Organic Electronics 13, no. 3 (2012): 432-456.

[21] Norrman, K.; Larsen, N. B.; Krebs, F. C., Lifetimes of Organic Photovoltaics: Combining Chemical and Physical Characterisation Techniques to Study Degradation Mechanisms. Solar Energy Materials and Solar Cells 2006, 90, 2793-2814.

[22] Dennler, Gilles, Christoph Lungenschmied, Helmut Neugebauer, Niyazi S. Sariciftci, Mohamed Latreche, Grzegorz Czeremuszkin, and Michael R. Wertheimer. "A new encapsulation solution for flexible organic solar cells." Thin Solid Films 511 (2006): 349-353.

[23] Sarkar, Smita, Jason H. Culp, Jon T. Whyland, Margret Garvan, and Veena Misra. "Encapsulation of organic solar cells with ultrathin barrier layers deposited by ozone-based atomic layer deposition." Organic Electronics 11, no. 12 (2010): 1896-1900.

[24] Wang, Guang-Feng, Xiao-Ming Tao, and Rong-Xin Wang. "Flexible organic light-emitting diodes with a polymeric nanocomposite anode." Nanotechnology 19, no. 14 (2008): 145201.

[25] Kim, J. S., R. H. Friend, and F. Cacialli. "Improved operational stability of polyfluorene-based organic light-emitting diodes with plasma-treated indium–tin–oxide anodes." Applied Physics Letters 74, no. 21 (1999): 3084-3086.

[26] Dupont, Stephanie R., Mark Oliver, Frederik C. Krebs, and Reinhold H. Dauskardt. "Interlayer adhesion in roll-to-roll processed flexible inverted polymer solar cells." Solar Energy Materials and Solar Cells 97 (2012): 171-175.

[27] Shrotriya, Vishal, Gang Li, Yan Yao, Chih-Wei Chu, and Yang Yang. "Transition metal oxides as the buffer layer for polymer photovoltaic cells." Applied Physics Letters 88, no. 7 (2006): 073508.

[28] De Jong, M. P., L. J. Van Ijzendoorn, and M. J. A. De Voigt. "Stability of the interface

between indium-tin-oxide and poly (3, 4-ethylenedioxythiophene)/poly (styrenesulfonate) in polymer light-emitting diodes." Applied Physics Letters 77, no. 14 (2000): 2255-2257.

[29] Chen, Ming-Chung, Yi-Shiang Chiou, Jian-Ming Chiu, Abebe Tedla, and Yian Tai. "Marked improvement in the stability of small molecule organic photovoltaics by interfacial modification using self-assembled monolayers to prevent indium diffusion into the active layer." Journal of Materials Chemistry A 1, no. 11 (2013): 3680-3687.

[30] Wilken, Sebastian, Thomas Hoffmann, Elizabeth Von Hauff, Holger Borchert, and Jürgen Parisi. "ITO-free inverted polymer/fullerene solar cells: interface effects and comparison of different semi-transparent front contacts." Solar energy materials and solar cells 96 (2012): 141-147.

[31] Carlé, Jon E., Martin Helgesen, Morten V. Madsen, Eva Bundgaard, and Frederik C. Krebs. "Upscaling from single cells to modules–fabrication of vacuum-and ITO-free polymer solar cells on flexible substrates with long lifetime." Journal of Materials Chemistry C 2, no. 7 (2014): 1290-1297.

[32] Klimov, E., W. Li, X. Yang, G. G. Hoffmann, and J. Loos. "Scanning near-field and confocal Raman microscopic investigation of P3HT− PCBM systems for solar cell applications." Macromolecules 39, no. 13 (2006): 4493-4496.

[33] Swinnen, Ann, Ilse Haeldermans, Martin vande Ven, Jan D'Haen, Geert Vanhoyland, Stefano Aresu, Marc D'Olieslaeger, and Jean Manca. "Tuning the dimensions of C60- based needlelike crystals in blended thin films." Advanced Functional Materials 16, no. 6 (2006): 760-765.

[34] Nam, Chang-Yong, Yang Qin, Young S. Park, Htay Hlaing, Xinhui Lu, Benjamin M. Ocko, Charles T. Black, and Robert B. Grubbs. "Photo-cross-linkable azide-functionalized polythiophene for thermally stable bulk heterojunction solar cells." Macromolecules 45, no. 5

(2012): 2338-2347.

[35] Wantz, Guillaume, Lionel Derue, Olivier Dautel, Agnès Rivaton, Piétrick Hudhomme, and Christine Dagron- Lartigau. "Stabilizing polymer- based bulk heterojunction solar cells via crosslinking." Polymer international 63, no. 8 (2014): 1346-1361.

[36] Derue, Lionel, C. Lecourtier, T. Gorisse, Lionel Hirsch, Olivier Dautel, and Guillaume Wantz. "A solvent additive to enhance the efficiency and the thermal stability of polymer: fullerene solar cells." RSC Advances 5, no. 5 (2015): 3840-3843.

[37] Goubard, Fabrice, and Guillaume Wantz. "Ternary blends for polymer bulk heterojunction solar cells." Polymer international 63, no. 8 (2014): 1362-1367.

[38] Rivaton, Agnes, Aurélien Tournebize, Julien Gaume, Pierre- Olivier Bussière, Jean- Luc Gardette, and Sandrine Therias. "Photostability of organic materials used in polymer solar cells." Polymer international 63, no. 8 (2014): 1335-1345.

[39] Gardette, Jean-Luc. "Fundamental and technical aspects of the photooxidation of polymers." In Handbook of polymer degradation, pp. 697-702. CRC Press, 2000.

[40] Schafferhans, Julia, Andreas Baumann, Alexander Wagenpfahl, Carsten Deibel, and Vladimir Dyakonov. "*Oxygen doping of P3HT: PCBM blends: Influence on trap states, charge carrier mobility and solar cell performance*." Organic Electronics 11, no. 10 (2010): 1693-1700.

[41] William, Greenbank. "*Interfacial stability and degradation in organic photovoltaic solar cells*. " 2016. University of Bordeaux, PhD dissertation.

[42] Reese, Matthew O., Suren A. Gevorgyan, Mikkel Jørgensen, Eva Bundgaard, Sarah R. Kurtz, David S. Ginley, Dana C. Olson et al. "Consensus stability testing protocols for organic photovoltaic materials and devices." Solar Energy Materials and Solar Cells 95, no. 5 (2011): 1253-1267.

[43] Mateker, William R., I. T. Sachs-Quintana, George F. Burkhard, Rongrong Cheacharoen, and Michael D. McGehee. "Minimal long-term intrinsic degradation observed in a polymer solar cell illuminated in an oxygen-free environment." Chemistry of Materials 27, no. 2 (2015): 404-407.

[44] Peters, Craig H., I. T. Sachs- Quintana, John P. Kastrop, Serge Beaupre, Mario Leclerc, and Michael D. McGehee. "High efficiency polymer solar cells with long operating lifetimes." Advanced Energy Materials 1, no. 4 (2011): 491-494.

[45] Voroshazi, Eszter, Bregt Verreet, Tom Aernouts, and Paul Heremans. "Long-term operational lifetime and degradation analysis of P3HT: PCBM photovoltaic cells." Solar Energy Materials and Solar Cells 95, no. 5 (2011): 1303-1307.

[46] Voroshazi, Eszter, Ilaria Cardinaletti, Thierry Conard, and Barry P. Rand. "Light- Induced Degradation of Polymer: Fullerene Photovoltaic Devices: An Intrinsic or Material- Dependent Failure Mechanism?." Advanced Energy Materials 4, no. 18 (2014): 1400848.

[47] Peters, Craig H., I. T. Sachs- Quintana, William R. Mateker, Thomas Heumueller, Jonathan Rivnay, Rodigo Noriega, Zach M. Beiley, Eric T. Hoke, Alberto Salleo, and Michael D. McGehee. "The mechanism of burn- in loss in a high efficiency polymer solar cell." Advanced Materials 24, no. 5 (2012): 663-668.

[48] Rösch, Roland, David M. Tanenbaum, Mikkel Jørgensen, Marco Seeland, Maik Bärenklau, Martin Hermenau, Eszter Voroshazi et al. "Investigation of the degradation mechanisms of a variety of organic photovoltaic devices by combination of imaging techniques—the ISOS-3 inter-laboratory collaboration." Energy & Environmental Science 5, no. 4 (2012): 6521-6540.

[49] Tong, Xiaoran, Nana Wang, Michael Slootsky, Junsheng Yu, and Stephen R. Forrest. "Intrinsic burn-in efficiency loss of small-molecule organic photovoltaic cells due to exciton-

induced trap formation." Solar energy materials and solar cells 118 (2013): 116-123.

[50] Reese, Matthew O., Anthony J. Morfa, Matthew S. White, Nikos Kopidakis, Sean E. Shaheen, Garry Rumbles, and David S. Ginley. "Pathways for the degradation of organic photovoltaic P3HT: PCBM based devices." Solar Energy Materials and Solar Cells 92, no. 7 (2008): 746-752.

[51] Kawano, Kenji, and Chihaya Adachi. "Reduced initial degradation of bulk heterojunction organic solar cells by incorporation of stacked fullerene and lithium fluoride interlayers." Applied Physics Letters 96, no. 5 (2010): 23.

[52] Kawano, Kenji, and Chihaya Adachi. "Evaluating carrier accumulation in degraded bulk heterojunction organic solar cells by a thermally stimulated current technique." Advanced Functional Materials 19, no. 24 (2009): 3934-3940.

[53] Krebs, Frederik C., Jon E. Carlé, Nicolaj Cruys-Bagger, Morten Andersen, Mathilde R. Lilliedal, Mark A. Hammond, and Søren Hvidt. "Lifetimes of organic photovoltaics: photochemistry, atmosphere effects and barrier layers in ITO-MEHPPV: PCBM-aluminium devices." Solar Energy Materials and Solar Cells 86, no. 4 (2005): 499-516.

[54] Roesch, Roland, Tobias Faber, Elizabeth Von Hauff, Thomas M. Brown, Monica Lira- Cantu, and Harald Hoppe. "Procedures and Practices for Evaluating Thin- Film Solar Cell Stability." Advanced Energy Materials 5, no. 20 (2015): 1501407.

[55] Tournebize, Aurélien, Agnès Rivaton, Jean- Luc Gardette, Christian Lombard, Brigitte Pépin- Donat, Serge Beaupré, and Mario Leclerc. "How Photoinduced Crosslinking Under Operating Conditions Can Reduce PCDTBT- Based Solar Cell Efficiency and then Stabilize It." Advanced Energy Materials 4, no. 10 (2014): 1301530.

[56] Züfle, Simon, Martin T. Neukom, Stéphane Altazin, Marc Zinggeler, Marek Chrapa, Ton Offermans, and Beat Ruhstaller. "An effective area approach to model lateral degradation in organic solar cells." Advanced Energy Materials 5, no. 20 (2015): 1500835.

[57] Gevorgyan, Suren A., Morten V. Madsen, Henrik F. Dam, Mikkel Jørgensen, Christopher J. Fell, Kenrick F. Anderson, Benjamin C. Duck et al. "Interlaboratory outdoor stability studies of flexible roll-to-roll coated organic photovoltaic modules: Stability over 10,000 h." Solar Energy Materials and Solar Cells 116 (2013): 187-196.

[58] Johnson, K. "Oil Prices Have Hit a 10-Year Low. They're Not Going to Stay There, With demand still growing and output finally shrinking, today's cheap oil could nearly triple in price in coming years." Foreign Policy 6 (2016).

[59] Şahin, Yücel, Salima Alem, Rémi de Bettignies, and Jean-Michel Nunzi. "Development of air stable polymer solar cells using an inverted gold on top anode structure." Thin Solid Films 476, no. 2 (2005): 340-343.

[60] Cros, S., R. De Bettignies, S. Berson, S. Bailly, P. Maisse, N. Lemaitre, and S. Guillerez. "Definition of encapsulation barrier requirements: A method applied to organic solar cells." Solar Energy Materials and Solar Cells 95 (2011): S65-S69.

[61] Hösel, Markus, Roar R. Søndergaard, Mikkel Jørgensen, and Frederik C. Krebs. "Comparison of UV- Curing, Hotmelt, and Pressure Sensitive Adhesive as Roll- to- R oll Encapsulation Methods for Polymer Solar Cells." Advanced Engineering Materials 15, no. 11 (2013): 1068-1075.

[62] Lin, Yuze, and Xiaowei Zhan. "Non-fullerene acceptors for organic photovoltaics: an emerging horizon." Materials Horizons 1, no. 5 (2014): 470-488.

[63] Tipnis, Ritesh, Jan Bernkopf, Shijun Jia, John Krieg, Sergey Li, Mark Storch, and Darin Laird.

"Large-area organic photovoltaic module—fabrication and performance." Solar Energy Materials and Solar Cells 93, no. 4 (2009): 442-446.

[64] Park, Jin-Seong, Heeyeop Chae, Ho Kyoon Chung, and Sang In Lee. "Thin film encapsulation for flexible AM-OLED: a review." Semiconductor science and technology 26, no. 3 (2011): 034001.

[65] Tanenbaum, David M., Henrik Friis Dam, Roland Rösch, Mikkel Jørgensen, Harald Hoppe, and Frederik C. Krebs. "Edge sealing for low cost stability enhancement of roll-to-roll processed flexible polymer solar cell modules." Solar Energy Materials and Solar Cells 97 (2012): 157-163.

[66] Ahmad, Jakaria, Kateryna Bazaka, Liam J. Anderson, Ronald D. White, and Mohan V. Jacob. "Materials and methods for encapsulation of OPV: A review." Renewable and Sustainable Energy Reviews 27 (2013): 104-117.

CHAPTER III

Degradation of organic solar cells under different climatic conditions

III.1 Introduction

The amount of solar energy that reaches the surface of the earth is by far enough to meet the world's increasing energy demand, and thus explains the increased focus on photovoltaic (PV) technologies in the past decades [1]. This has resulted in a growing number of PV research and development groups, institutions and companies around the world. In recent years, several types of thin-film PV devices have been investigated, which also includes a strong rise in research and development within organic and hybrid photovoltaics [2–5]. Organic solar cells (OSCs) possess intriguing advantages [6] such as light weight [7], mechanical flexibility, semi-transparency and color tuning [8], making it a highly promising PV technology for the rapidly growing energy market. However, as we have evoked in the previous chapter the stability and degradation of the OSC devices present the main issues for researchers through the world and many test protocols have been developed and normalized in their operation procedure to ensure the good interpretation of the results. In This chapter we have carried out an experimental work on the effect of different climatic conditions on the OSC behavior. The idea of this work is based on application of a new protocol using a QUV aging tester. It is well known that in the standard ISOS protocols the used aging process is continuous and each factor has been applied in permanent way on the OSC sample, and in our new aging protocol we have applied a cyclic aging. The aim of this new protocol is to simulate the cyclic repetition of the climatic conditions in one operation day of OSC operation.

Obviously, in one day of real climatic conditions, the organic solar cells can be submitted to the sunlight, temperature, rain and dark of the night successively. The cyclic repetition of these climatic conditions can present harmful effects on the OSCs performances leading to the reducing of the lifetime of the photovoltaic devices. To simulate the cyclic effect of the climatic conditions on the OSCs, we have investigated, in this first part of this third chapter, an accelerated long-term aging in the accelerated-weathering tester (QUV cell). QUV cell has a possibility to simulate all the climatic conditions (see section experimental setup). To simulate the sunlight, the QUV tester is occupied with UVA-340 lamps characterized by wavelength of 340 nm. The UVA-340 lamp permits us to generate different concentration of UV irradiance. To highlight the degradation of the OCSs caused by the cyclic climatic conditions, the usual electrical parameters (PCE, V_{oc}, J_{sc} and FF) calculated from *J-V* characteristics and optical properties (UV-VIS and Photoluminescence measurement) have been studied according the aging time.

In the second part of the chapter, the same samples have been subjected to an ISOS protocol which is the outdoor test ISOS-O-1 (see Table II.1) to study the recovery phenomenon caused by the light/dark effect on the OSC behaviour.

III.2 Experimental setup

III.2.1 Materials

In this study we have used encapsulated samples of commercial organic solar cells (80×110 mm^2 in dimension) (**Figure III.1a**) supplied by Infinity OPV manufacturer. These samples were prepared at ambient roll-to-roll (R2R) printing and coating techniques. The provided parameters of the used OSCs are listed in **Table 1**.

Table III.1: Different parameters the samples

Parameters	Values
Dimension	(8*110)mm, this cutting using laser in OPV infinity
Voc	Around 6 Mv
Isc	60-70 mA under full sun
FF	50%
PCE	1,5%

III.2.2 Accelerated climatic aging tester QUV

The accelerated-weathering tester QUV was designed to make a real weather with different climatic conditions like UV irradiation, temperature, humidity, dark and spray. It has been monitored by many standard aging program having specific climatic conditions. Moreover, it had a simple interface to put our own aging program. In our work, we have used the QUV cell for long-term aging experiments of 1080 h under various aging conditions. The samples are put in the sample holder as presented in **Figures III.1b** and **III.1c** (two faces of the sample holder) and then irradiated with UVA-340 lamp. This lamp represents characteristics close to the real sunlight. The spectral power distribution of UVA-340 fluorescent lamps, represented in **Figure III.2**, shall comply with the requirements specified in [9].

III.2.3 Indoor test aging in QUV

The OSC samples were placed in a QUV cell for 1080 h representing 45 aging cycles of a combined effect of UV irradiation, temperature, spray, condensation and dark. The weathering

cycle duration is 24 h divided as follow: in the first step, the samples were irradiated by UV light for 8 h maintaining the temperature of the chamber at 50 °C. Then, the samples were sprayed for 5 min and followed by 4 h of condensation at 50 °C (humidity generation). Finally the samples were kept in dark (the temperature of the chamber is decreased to 30 °C) for 12 h.

The irradiation of the samples is controlled and the aging process was done for three levels of the UV irradiance (0.83 W/m^2, 1.20 W/m^2 and 1.30 W/m^2) at 50 °C. The aging time is 1080 h for each case. The samples were taken after each 15 cycles and submitted to the different characterization techniques to study the effect of climatic aging time on the different performances of OSC.

Figure III.1. (a) the organic solar cell before degradation, (b) the cells in support of QUV on face, (c) the support of QUV in front.

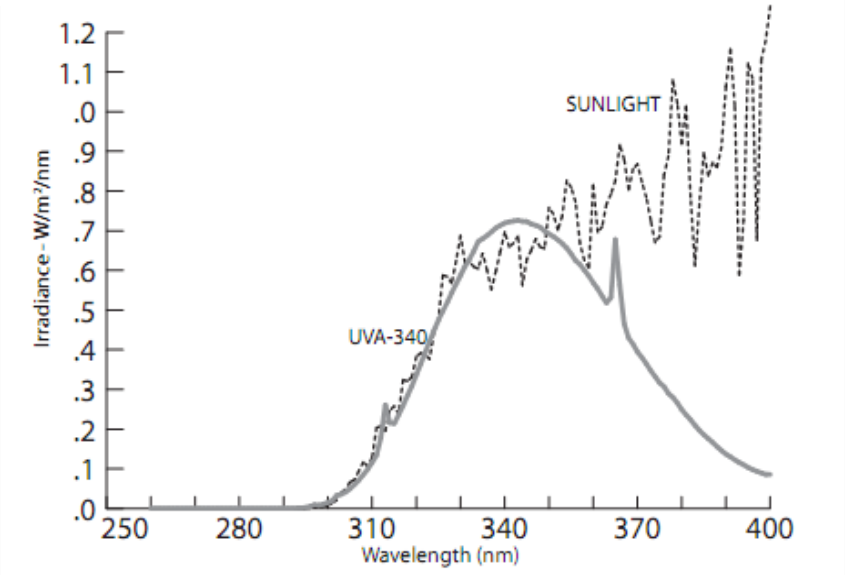

Figure III.2. UVA-340 lamps vs sunlight.

III.2.4 ISOS-O-1 outdoor test

This test is done in Sonderborg, Denmark (latitude 54.91°N; longitude, 9.79217 °E; altitude, 24 m). The cell is fixed on the roof in angle 30° from morning to evening (10:00 AM to 16:00 PM) with using ISOS-O-1 protocol [10]. The duration of the test in outdoor takes 5 days the remainders 9 days are preserved to the second part of the experience. In this part we put the samples in the glove box for the whole day. Sometimes we keep them two days in the glove box without measuring to understand what happened exactly. The period of test is limited from 20 February 2018 to 04 March 2018.

III.2.5 Measuring devices

The *J–V* characteristics of OSCs before and after each aging period were recorded using Keithley 2400 source meter unit. The samples were exposed to illumination of 1000 W/m^2 as per air mass (AM) 1.5 G in a solar simulator (Abet Technologies Sun 3000 Solar Simulator) inside the glove box (**Figure III.3a**). The devices were illuminated through a calibrated mask to avoid the parasitic photocurrent arising from the areas outside the electrodes. The results shown in this work are an average of 3 measurements. In **Figures III.3b** and **III.3c** we have shown a photograph of the used materials for the UV-VIS and PL measurements.

a 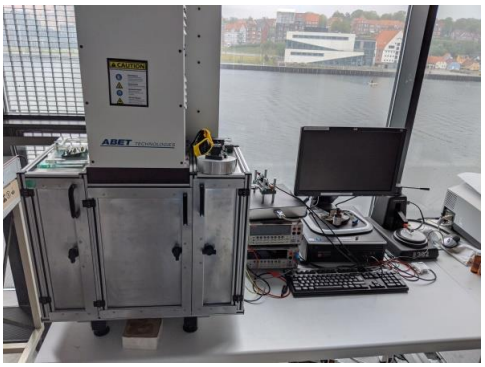  b

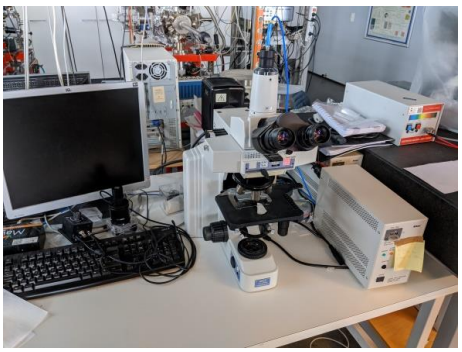 c

Figure III.3: The equipment of measurement: a) solar simulator with ketheliy; b) UV-VIS; c) PL measurement.

III.3 Results and discussion for the indoor test (QUV)

III.3.1 Electrical Properties Degradation

The carried out QUV aging protocol undergoes the effect of the simultaneous existent climatic conditions. It can be considered more harmful than the harsh ISOS protocol (ISOS-L-3). The degradation of the samples occurs in fast way. After each 15 cycles (practically 360 h) the *J–V* characteristics of the OSCs are recorded and presented in **Figures III. 4a** to **III.4c** for different UV irradiation doses. Before aging the *J–V* characteristic presents the typical characteristic of the OSC with its different parameters mainly the maximum power point (MPP). After aging at different irradiation doses, the shape of the curves is deformed and the rectifying properties of the samples are fully lost. It is possible also to observe a neat decrease in V_{oc}, J_{sc} and FF which means that aging under QUV conditions undergoes serious bulk degradation in the different parts of the OSC mainly in the active layer. The same behavior has been observed by Benatto et al. [11] on the PEDOT:PSS back electrode samples under ISOS-D-3 and ISOS-L-3 aging, and by Tromholt et al. [12] on the PEDOT:PSS/Ag-grid back electrode when they studied the effect of temperature and sunlight concentration on the organic photovoltaic solar cells. Furthermore, it is well known that the degradation in the OSCs can be monitored with both extrinsic factors such as water and oxygen, and intrinsic factors related to the high temperature. This latter is named thermal diffusion at the interfaces of the OSCs layers and can cause morphological evolution inside the BHJ structure. The photo-degradation caused by UV light can also accelerate the intrinsic degradation with using the heat of UV light.

To well highlight the effect of the QUV aging on the performances of the OSCs, we have plotted the commonly used parameters (PCE, J_{sc}, FF and V_{oc}) deduced from the *J–V* characteristic against the aging time. All the plotted values are normalized and the obtained results are presented in **Figures III. 5, 6, 7 and 8**. As PCE presents the most important characteristic of an OSC, so its evolution with aging time gives a good picture on the OSC quality.

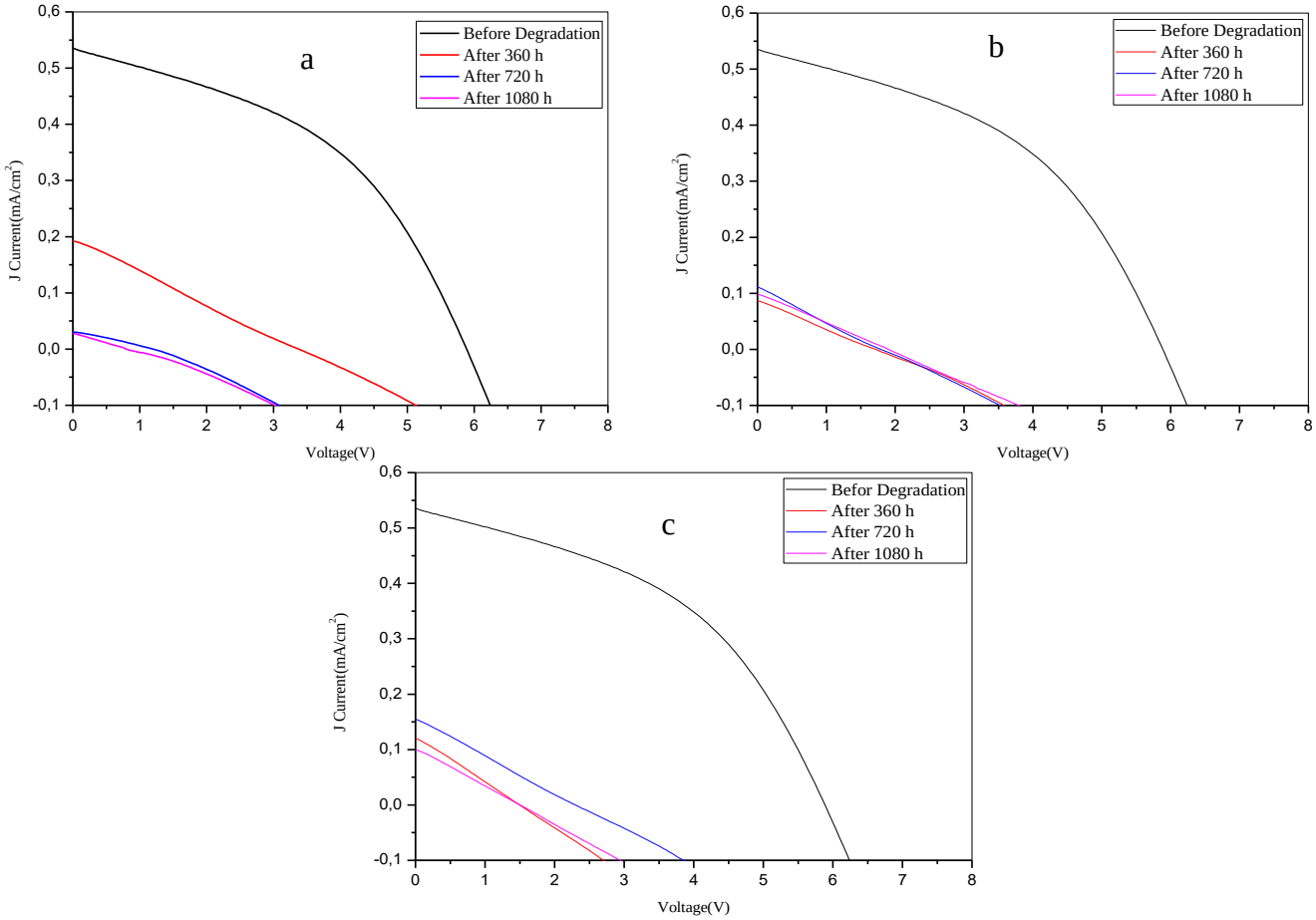

Figure III.4 *J-V* caractersitics for different aging period, (a) aging at 0.83 W/m², (b) aging at 1.2 W/m², (c) aging at 1.3 W/m².

The normalized values of PCE according to the aging time for different UV irradiation concentration are plotted in **Figure III. 5**. It is very clear that, for all UV irradiation concentrations, PCE decreases with aging time. The decrease of PCE obeys to the typical OSCs degradation profile often experiences initial rapid aging (burn in) followed by a more stabilized phase [13,14].

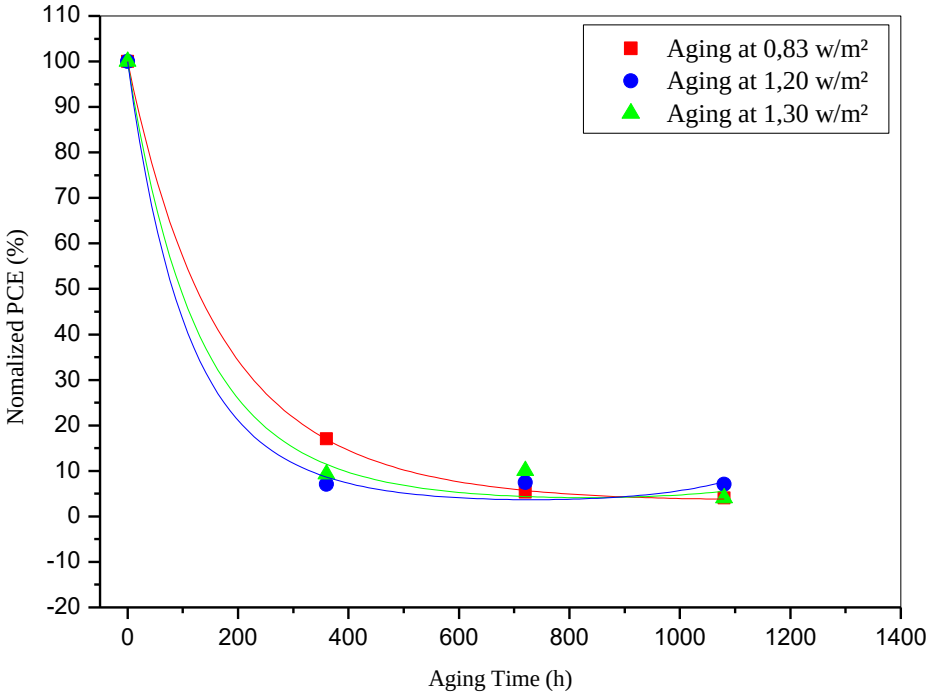

Figure III.5 Normalised PCE variation according to the aging time.

Furthermore, the fast decrease of PCE due to the rapid aging speed at the beginning is done in the first 15 cycles of aging (first 360 h of aging). In this phase, the OSCs lost the almost of their PCE values. In fact, in the case of QUV aging at 0.83 W/m^2, the PCE decreases from 100 to 16% (i.e. it loses 84% of its initial value), and in the case of aging at 1.2 W/m^2 and 1.30 W/m^2 it loses practically 93% of its initial value. This fast degradation of the OSCs performance is due to the effect of cyclic climatic conditions (UV irradiation, spray, humidity and dark) that has experienced each sample during the aging period. The followed 30 cycles (the remain 720 h of aging) are characterized by the stabilized phase in the PCE variations. In this phase, PCE decreases slightly with only 12.3% during 720 h of aging at 0.83 W/m^2. However, in the case of aging at 1.2 W/m^2 the PCE values remain constant, and present a slight decrease of 3.7% in the case of aging at 1.3 W/m^2 during all this aging period. In the other hand, PCE variations with aging time can be modeled by a first exponential fitting as given in equation (1):

$$\frac{PCE(t)}{PCE(0)} = Ae^{-t/\tau} \qquad (1)$$

Where PCE (0) is the initial value of the power conversion efficiency (at t = 0 h), A is a weighing or degradation power factor and τ is the time constant of the degradation. A and τ are obtained with mean square fit. This fitting equation seems to be different to those proposed in the literature [14,15] where they use series of exponential functions with two weighing (A_1, A_2) and two times constant (τ_1, τ_2) to simulate different degradation mechanisms. In our equation, if we put $A_1 = A_2 = A/2$ and $\tau_1 = \tau_2 = \tau$, the equation (1) becomes:

$$\frac{PCE(t)}{PCE(0)} = A_1 e^{-t/\tau 1} + A_2 e^{-t/\tau 2} \qquad (2)$$

Equation (2) is matched to that fond in literature and our results can be analyzed in the same way. The calculated parameters for different aging conditions are listed in **Table III.2**.

Table III.2: Numerical decay parameters according to the general equation 2

Aging conditions	$A_1=A_2=A/2$	$\tau_1=\tau_{2=}\tau$ **(h)**
0.83 W/m²	50	169.9
1.20 W/m²	49.97	111.1
1.30 W/m²	49.96	130.2

It is well known that light, temperature and humidity are the main causes of the OSCs degradation process. In **Figure III.5** we can well observe that there is no significant difference in the decrease of the PCE for different UV irradiation and all the curves decay practically in the same way. This result suggests that the predominance effects in the OSCs degradation are fast variation of both heat and humidity. These two factors are characterized by (A_1, A_2) and (τ_1,τ_2) in the equation (2). The same values taken by τ_1 and τ_2, and by A_1 and A_2 suggest that the temperature and the humidity take parts in the degradation process in the same way and their effects are very predominant.

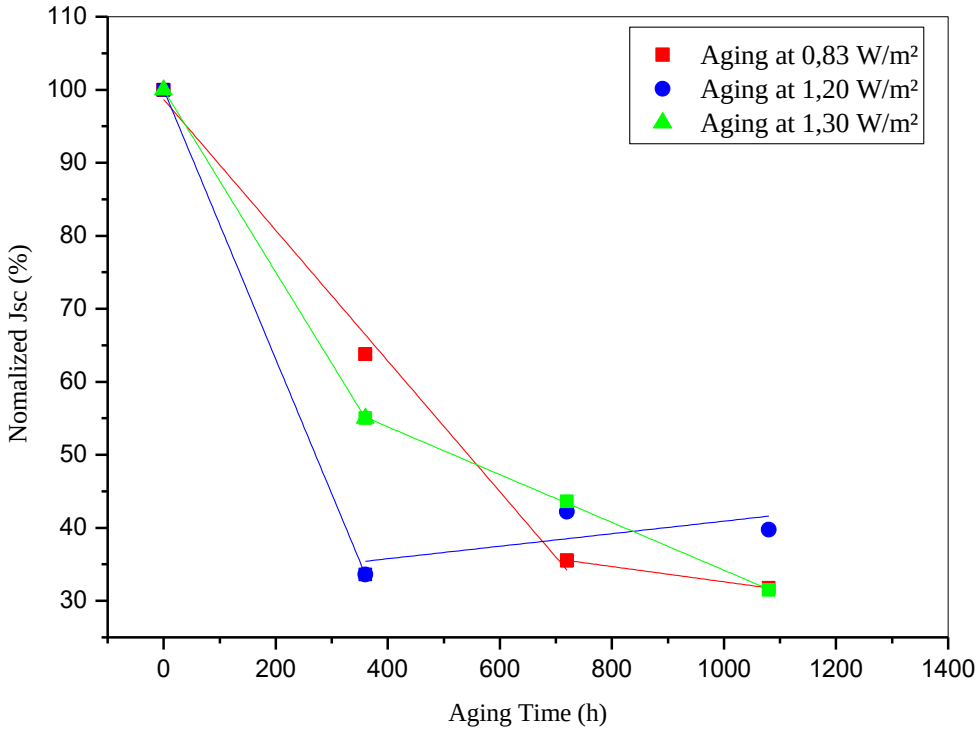

Figure III.6 Normalised J_{sc} variation according to the aging time.

To better analyze the trend of OSCs degradation, the normalized values of J_{sc} versus aging time (**Figure III.6**) will be analyzed as the PCE characteristic but with different manner. Moreover, the degradation of OCSs device is characterized by the so-called degradation constant K_{deg} that is obtained by the fitting of considered decaying characteristic (J_{sc} in our case). The variation of J_{sc} can be fitted with either a linear equation (equation (3)) or a first order exponential function (equation (4)) [16]. In our analysis we have chosen the linear fit as presented in some earlier literature [16,17]. Furthermore, the degradation constant K_{deg} was found depends on the temperature T. This dependence is given by an Arrhenius type presented in equation (5) [16]. An acceleration factor K and an activation energy E_a can be deduced from equation (5) by plotting Log (K_{deg}) according to 1/T.

$$\frac{J_{sc}(t)}{J_{sc}(0)} = \left(1 - K_{deg}t\right) \quad (3)$$

$$\frac{J_{sc}(t)}{J_{sc}(0)} = exp\left(-K_{deg}t\right) \quad (4)$$

$$K_{deg} = exp\left(\frac{-E_a}{K_B T}\right) \quad (5)$$

The curves of J_{sc} presented in **Figure III.6** have the same trends of variation as the PCE showing a fast decay at the first 360 h of aging, except in the case of aging under UV irradiation of 0.83 W/m² where the fast decay is enlarged until 720 h. After that, the decay of J_{sc} curves present, in the second region, more stabilized trends. The fast degradation leads to the lost of the conductive character of the OSCs. After 720 h of aging at 0.83W/m² the current J_{sc} loses 64% of its initial value and more than 67% of the J_{sc} initial performance was lost after only 360 h at 1.20W/m². However, in the case of aging at 1.30W/m² the OSCs, lose rapidly about 45% of its conductive character in the first region (after 360 h of aging) and about 24% in the second region (slowly decay). Meanwhile, in the stabilized phase J_{sc} drops with only 4% during 360 h of aging under 0.83 W/m² UV irradiation, even, some small improvements (increase of the J_{sc}) have been observed in the case of aging at 1.2 W/m² UV irradiation.

Using the equation (3), the degradation constant K_{deg} was deduced for both fast and slow degradation phases for each UV irradiation concentration and the obtained results are listed in **Table III.3**. Nevertheless, one limitation of our investigated work that the acceleration factor and the activation energy could not be deduced here because the variation of K_{deg} according the inverse of the temperature is not possible (the investigated temperature is constant and equal to 50°C).
The general degradation of the OSCs under QUV aging is not limited to the decrease of the PCE and J_{sc}, but also extended to the FF and V_{oc}. The evolution of these parameters according to the aging time is presented in **Figure III.7** and **Figure III.8**.

Table III.3: Rates of degradation for different phases of aging

Aging conditions	**Phase 1**		**Phase 2**	
	Period (h)	K_{deg}	Period (h)	K_{deg}
0.83 W/m²	0-720	0,08954	720-1080	0,01045
1.2 W/m²	0-360	0,1845	360-1080	-0,00858
1.3 W/m²	0-360	0,12495	360-1080	0,03271

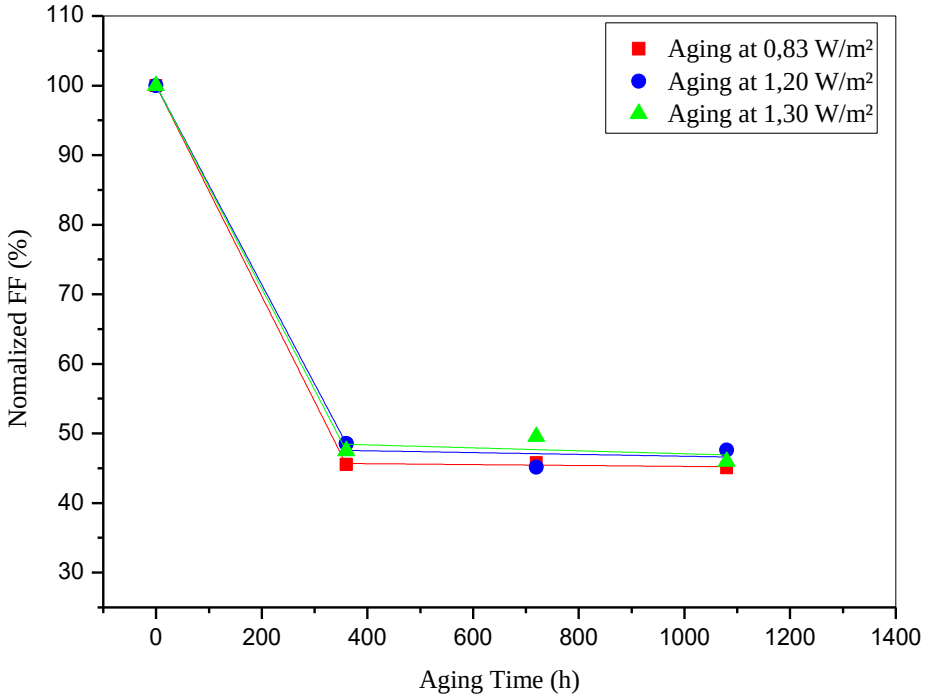

Figure III.7 Normalised FF variation according to the aging time.

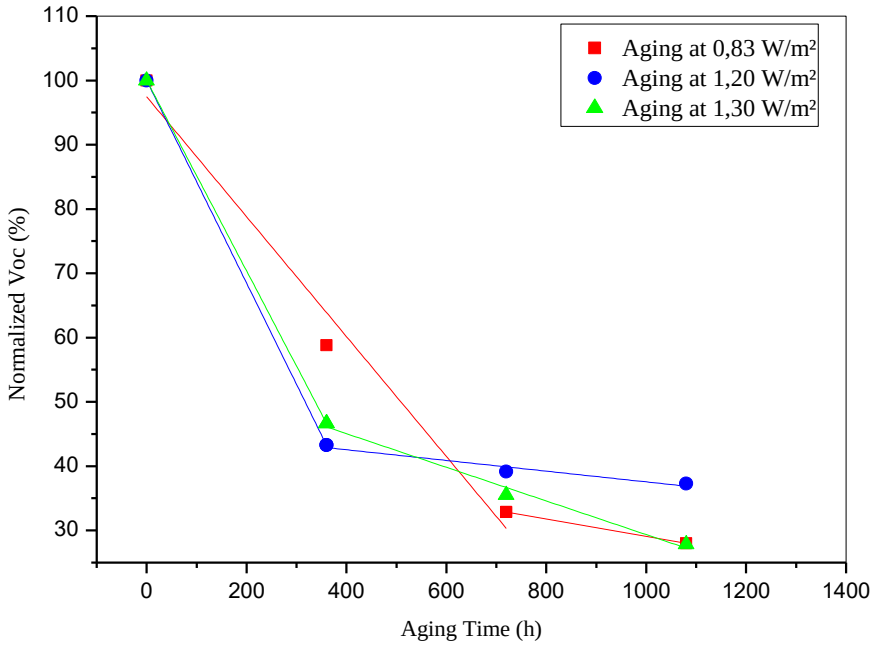

Figure III.8 Normalised V_{oc} variation according to the aging time.

Both characteristics decrease as the aging time goes on. The fast degradation process at the beginning of aging followed by more stabilized phase is also well observed in the evolution of both properties. At the end of the fast decay phase (after 360h of aging) the FF drops to 45% of its initial value for different aging conditions and remains after that constant in the followed stabilized phase. However, the evolution of V_{oc} is quite similar to the one observed in J_{sc} where the fast degradation process in the case of aging at 0.83 W/m² UV irradiation is extended to 720 h. In this phase V_{oc} loses more than 70% of its initial value, and then continuous in decreasing slowly in the followed stabilized phase to reach a low value (25% of its initial value).

In the other cases of aging, V_{oc} drops speedily with more than 55% of its initial value after 360 h of aging and continuous slowly with linear decrease to lose more than 60% and 70% of its initial value for second and third cases of aging respectively.

Overall, we can ascertain that under the carried out experimental protocol, the aged OSCs undergo a serious degradation process resulting in the fast alteration in the main electrical properties of the cells. The carried out cyclic aging process in the QUV chamber can be considered very harsh combining different protocols similar to commonly used ISOS protocols in the same time. In one cycle of aging, the samples were performed initially, for 8 hours, to a protocol similar to ISOS-L-2 (UV radiation (light), temperature and ambient humidity), followed by one similar to ISOS-D-3 for 4 hours (temperature and controlled humidity). Finally the samples are subjected to the last one similar to ISOS-D-2 for 12 hours (temperature less than ISOS-D-3, ambient humidity). The cyclic aging includes the simultaneous effect of rapid variation of temperature, humidity, light and water on the OSCs performances. As a result, overall electrical properties decrease drastically and lose more than 60%, and even more than 80% for certain properties (PCE), of their initial values in the first stage of aging after only 360 h of aging. The following interpretation can be useful to analyze the fast decrease of the OSCs properties: The fast reduction of the J_{sc} is probably due to morphological changes of the bulk hetero Junction (BHJ) blend [18-20] that can affect the charge mobility and the generation of a charge transfer [21]. Furthermore, the rapid variation of different aging conditions can generate different phase segregation of donor: acceptor pairs and increase of defect states which controls the recombination leading to the variation of the V_{oc} [22, 23]. In the other hand, the FF can be affected by those phenomena by a limitation of the charge transport and increase in the series resistance [21]. It has been reported also [11] that the almost decrease in the J_{sc} along with the drop in the FF further confirms the reduction of the conductivity of the PEDOT:PSS blend when exposed to high level of humidity. Moreover, it seems that all the properties behaves in the same way and present two phases of degradation, the fast degradation at the beginning followed by the stabilized one. This behavior suggests that some correlation must be made between deferent

OSCs properties. The stabilization phase at the end of aging process suggests that no bleaching of the semiconductor layer over time occurs in this phase [24].

III.3.2 Formation of bubble defects and color change

Another aspect of degradation which can be inspected visually is the gradually formation, as the aging time goes on, of bubble-like defects and color change of OSCs under QUV aging (**Figure III.9**). Our results confirm some earlier finding of Binatto et al. [11] investigating the effect of different aging protocols on the Ag-grid back electrode modules. They have found that the formation of bubbles occurs only under ISOS-L-2 and ISOS-L-3 protocols. On the contrary of other aging protocols, these two protocols present the effect of light, humidity and temperature (as in our aging case) indicating that the presence these three parameters are the main cause of the bubbles formation. It is clear from Fig. 9 that bubbles formation has been occurred after first 15 cycles of aging (first 360 h) for all UV irradiation doses with a little concentration in the case of aging at 0.83 W/m² and more important concentration in the case of the other aging conditions. As the aging time goes on, the bubbles become more intense in number, bigger in size and deeper. Moreover it has been remarked also that the formation of bubbles starts around the Ag-grid after 15 cycles of aging and spread on all the surface of the samples after 1080 h of aging, especially under UV irradiation dose of 1.30 W/m². The area around the bubbles became inactive resulting in partial decrease of the photocurrent as it is confirmed by Binatto et al. [11] with light beam induced current (LBIC) imaging. In the same published paper, it has been confirmed with microscope imaging of the areas with and without bubbles that cracks are formed in the active layer and in the AgNW/ZnO layer in the neighboring areas where the bubbles are formed. The cracks are locked to be initiated from the printed Ag-bus-bar. The porous character of back Ag-grid permits gas and solvents to be trapped. Cyclic variation of temperature leads to the expansion or contraction of gasses, hence, possibility of bubble formation. Furthermore, it has been reported by Rolston et al. [25] that the presence of heat, UV irradiation and moisture have a significant effect on the decohesion kinetics of OSCs. These environmental factors can undergo mechanical degradation leading to delamination of layers and consequently big probability of bubbles formation. In order to put in evidence the chemistry changes in the P3HT:PCBM active layer under the combination effect of light, humidity and temperature, Corazza et al. [26] have used atomic force microscopy (AFM) topography images. The obtained images prove that the created cracks are very close to the inner interface within P3HT:PCBM caused by the variation of the material structure. The presence of temperature and humidity together were then responsible for the creation of a weak layer on the surface of the active

layer. Furthermore, more physic-chemical characterization techniques will be required for better understanding the nature of the observed phenomenon.

The second degradation consequence is the color changes of the sample under different aging conditions. Some color changes were noticed at the end of aging (after 1080 h) at 1.2 W/m² and 1.3 W/m². The samples present some yellowness area on their surface and cracks on the encapsulation.

III.3.3 Optical properties degradation

To give more insight on the cyclic QUV aging effect on the organic solar cells, we have also investigated the optical properties degradation. Furthermore, the strategy of blending two or more materials, bringing about synergistic and surprising properties in structure, electronics, dielectrics, optics, thermodynamics, mechanics, and texture, contributes much to the development of organic solar cells. The bulk heterojunction (BHJ) polymer solar cells (PSCs), the miscibility between electron-donating polymers and electron-accepting molecules in the photoactive layers plays an important role in the morphology formation [27-31]. In polymer solar cells, amorphous miscibility between the donor and the acceptor is important for device performance for several reasons. First, molecular mixing governs phase behavior and morphology formation and, consequently, affects charge recombination and charge collection efficiency, which will directly influence device performance [27-28]. **Figures III.10a** to **III.10c** shows the spectra of absorption using UV-VIS. As shown in these figures the absorption spectrum shows a broad absorbance ranging from 250 nm more than 800 nm. There are two sets of absorption with peaks maximum between (250 nm and 380 nm) and 650 nm. Those results of absorption confirm the results in electrical properties the samples after 360 h it burn in, due to the samples they don't have a reaction. In other hand **Figures III.10d** to **III.10f** show the intensity measured using PL measurement, there is a pig one peaks at 500 nm, from this conclude the polymer in the organic solar cells, the thickness of our samples is damages and the links inside the samples are broken. All those optical results prove the lifetime of organic solar cells depend on the type of encapsulation. There are several types of encapsulation using a different materials and methods. So that takes into consideration the (WVTR) Water Vapour Transmission Rate to check the quality of encapsulation [32].

In other hand, we have presented in **Figure III.11** the intensity with aging time in different cycles. The first cycle showed a stable fit in all point aging time. The second cycle and third cycle shows an instable fit, this is due to the change in the irradiance in the cycles the second cycle (1.20W/m^2) and in the third cycle (1.30 W/m^2).

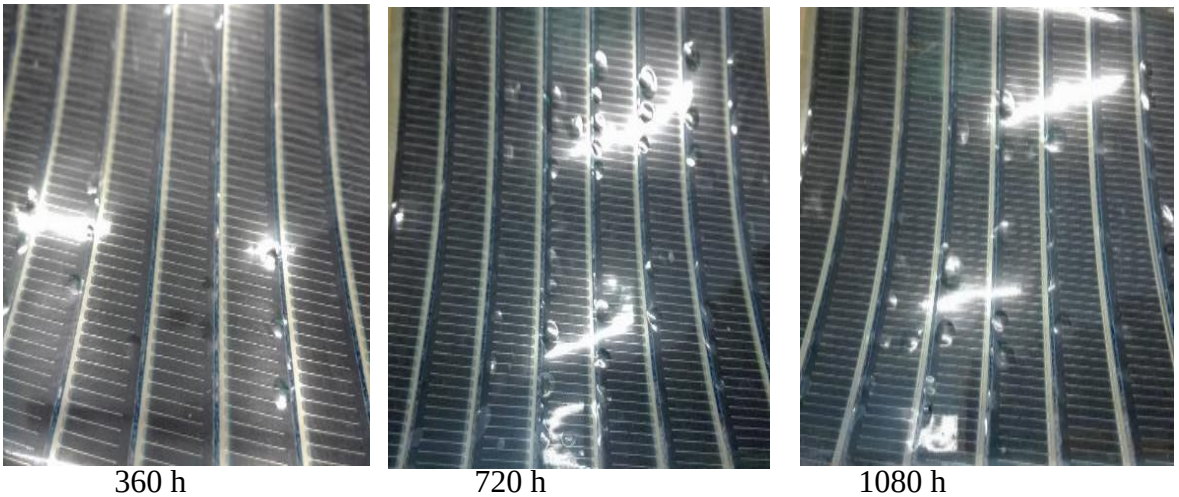

(a)

360 h 720 h 1080 h

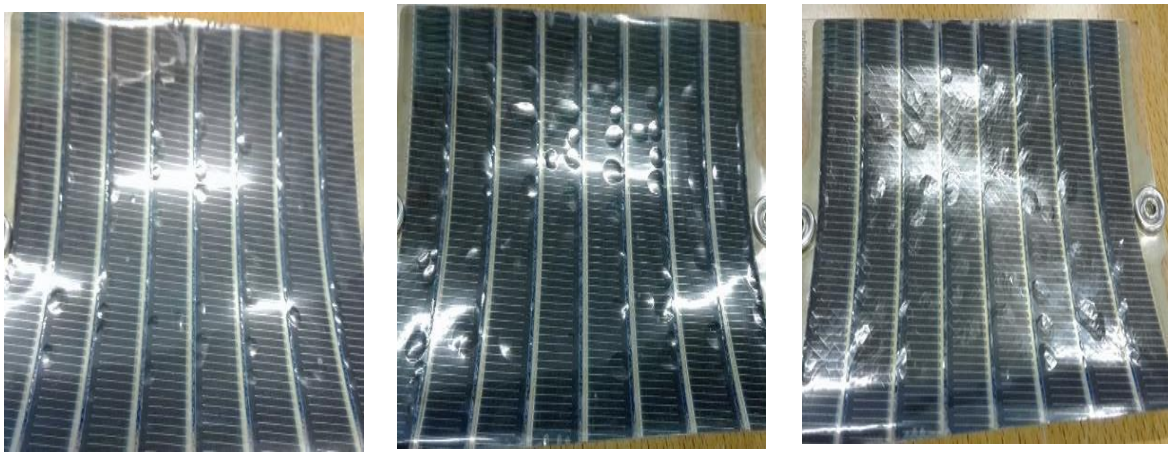

(b)

360 h 720 h 1080 h

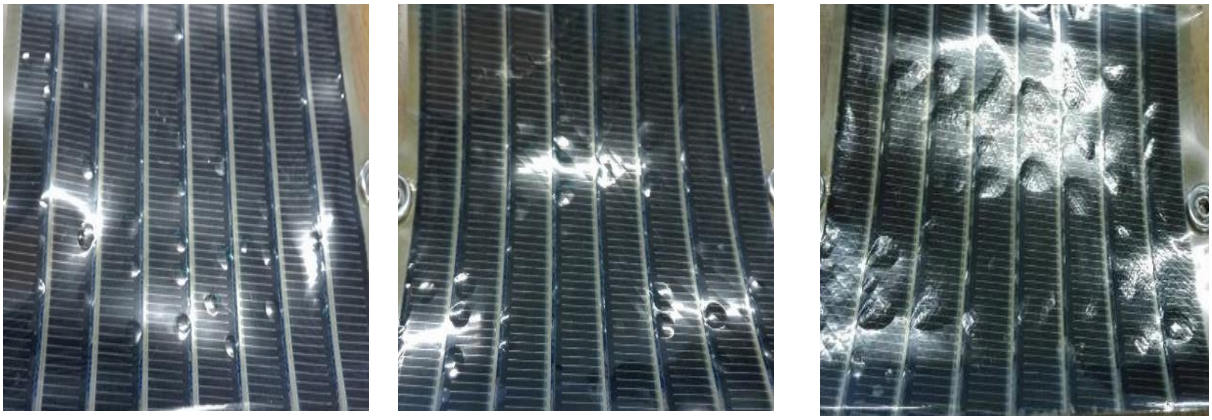

(c)

360 h 720 h 1080 h

Figure III.9 Photographs of samples for different aging period, (a) aging at 0.83 W/m², (b) aging at 1.2 W/m², (c) aging at 1.3 W/m²

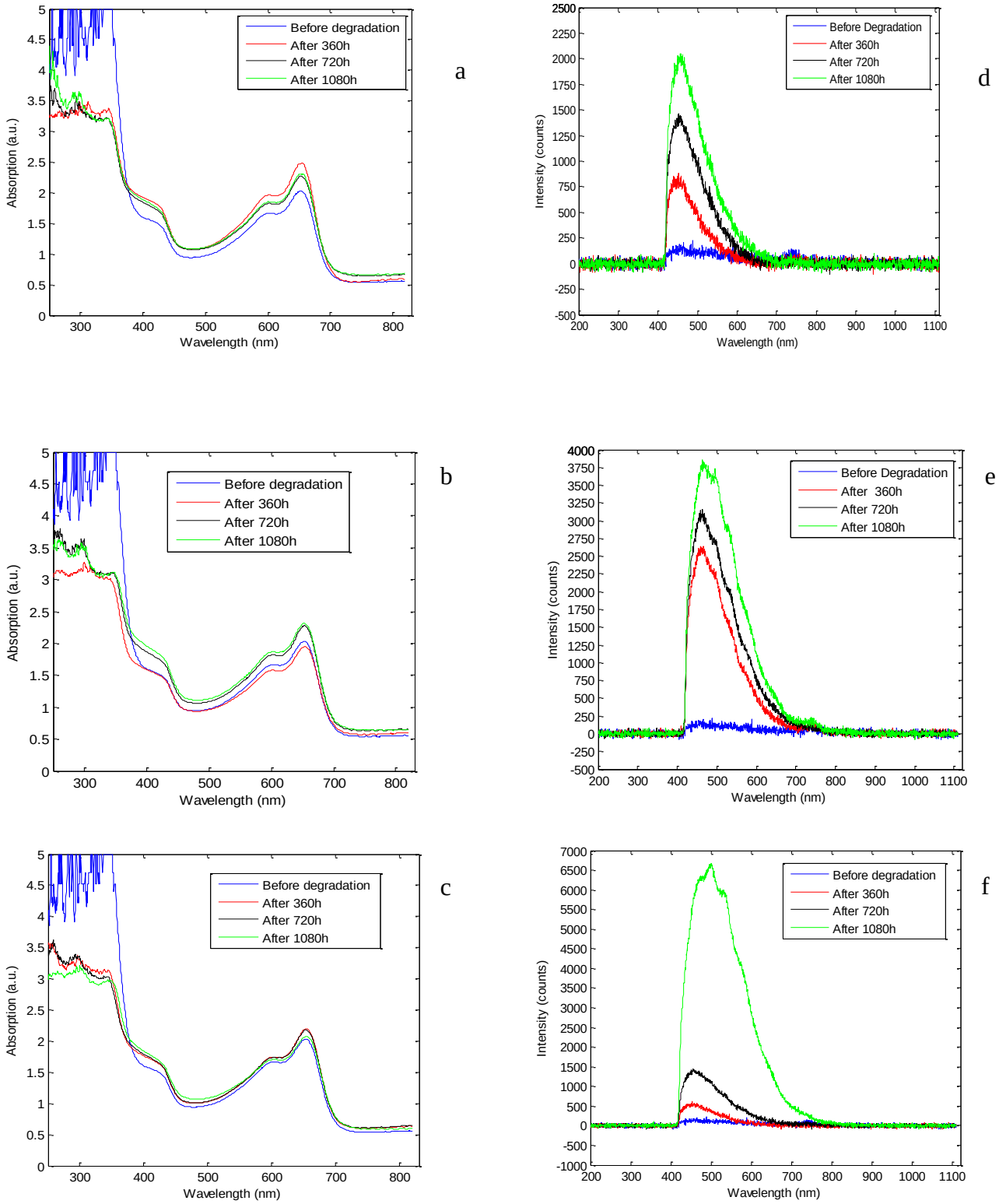

Figure III.10. Absorption UV/VIS spectra and the Intensity PL measurment. a,d) First cycle (after 360h); b,e) Second cycle (after 720h); c,f) Third cycle (after 1080h).

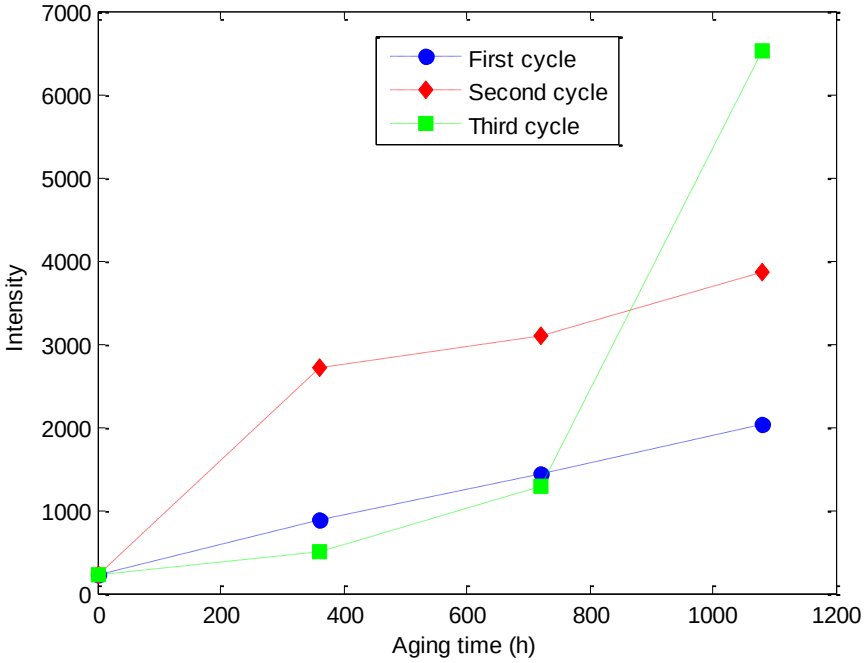

Figure III.11. Pl measurement properties with aging time

III.4 Results and discussion of outdoor test with recovery

Those results show the reaction of samples under air exposure (sun rays, rain, and temperature.....). And confirm the other studies about the recovery and degradation. The evolution of the parameters PCE, J_{sc}, V_{oc} and FF explain the reaction of cells. The test was divided into two parts. In the first part the samples were kept at the outdoor protocol for 6 hours and in the second part the samples were put in the dark (glove box) to allow the recovery phenomenon to be appeared. Meanwhile the test the samples subjected to simulated 1-sun illumination undergo reduction in efficiency value of 80%, 60%, or 50% of the initial value corresponding to the time T_{80}, T_{60}, orT_{50} respectively.

In the first part of the test, (**Figure III.12a**) showed a full degradation to 80% of the initial value PCE under illumination after 4 days of tests where we have observed a fast degradation without recovery. In the second part (the black area at the figures) in the 10 days, the PCE decreases with two environment air exposure and recovery in the glove-box. There are different mechanisms were formerly suggested for reversible degradation in Polymer Solar Cells (PSCs). Domanski et al. demonstrated that the reversible 10−15% PCE loss [33]. Nie et al. impute the light-induced reversible J_{sc} degradation in inverted planar PSCs to the formation of metastable deep traps in the perovskite layer [34]. Hoke et al. showed photoinduced changes in the PL spectra of on perovskite films give them a full reversible [35].

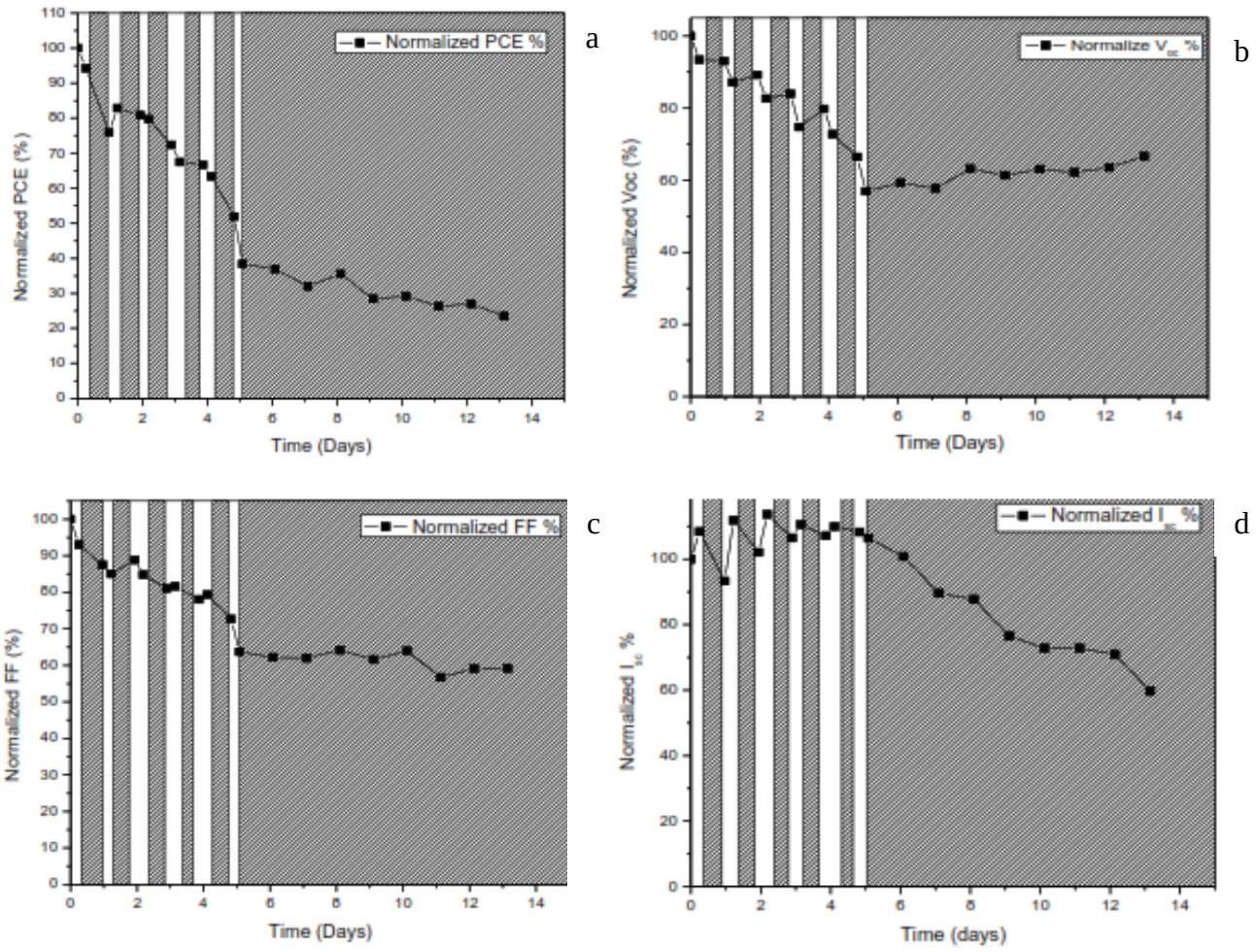

Figure III.12 . Degradation and recovery of differenat paramters of the sollar cell: a) power conversion efficiency (PCE) , b) Open-circuit voltage V_{oc}, c)Fill factor FF, d) short circuit current J_{sc}

The degradation at this stage was mostly determined by the decrease in open-circuit voltage (V_{oc}) and fill factor (FF) (**Figure III.12b and III.12c**) with the minor contribution of a short-circuit current (J_{sc}) decrease as shown in **Figure III.12d**.

The performance of samples in the dark (black area) following degradation under illumination under 40% of the PCE (**Figure III.12a**) was found to be dramatically different from that after degradation in outdoor test. In special, we observed a rapid drop in V_{oc} and FF on the first day of the test outdoor and stabilization in the dark storage. As a result, the PCE further decreased from 60% to ~40% in the first test and from 40% to 30% in the second part of the test.

We have observed a drop in the PCE at the beginning of the dark test was followed slow recovery process; the black area presents at the (**Figure III.12a**) this stage did not reach saturation over 5 days of measurement.

It is clear to find a difference between the first part and the second part from the test; the difference is qualitative and finds the time of scale in the recovery take more time. In this experiment, we not observed a full restoration to the initial PCE.

Further insights into the observed dynamics related to the PCE drop after one day of the outdoor test and the test using solar simulator 1-sun illumination we found a fast drop it is gone under 75% from the initial value.

However, 1-sun illumination of the samples whose PCE recovery in the dark did not saturate (as in **Figure III.12a** black area) resulted in a rapid PCE improvement, mostly due to increases in V_{oc} and FF, (**Figures III.12b and 12c** respectively).

As shown in **Figures III.12b and 12c**, the V_{oc} and FF show a decrease in the first part of the test from 100 % to ≈ 60% after 5 days in the outdoor test and show a recovery using solar simulator (1-sun illumination).

In the other hand, notably, the commonly observed the be affected the exposure air a fast drop at different parameters such as PCE, FF, V_{oc} and in the dark observed relative a stable status. In the case of J_{sc} (**Figure III.12d**) we have observed a vacillate between air exposure and recovery (dark black area) in the first part of the test in the outdoor, and in the second part the recovery test (black area) the sample shows a fast drop from >100% to 50% this drop took 10 days.

In accordance with our recent publication [36], this behavior of degradation under accelerated conditions constant it takes time to degraded (from 100% to 20%) 200 hours (8 days), and in the short-term degradation in the exposure air with recovery from (100% to 30%) takes 8 days.

III.5 Conclusion

In this chapter an experimental work has been carried out investigating the effect of cyclic QUV aging on the electrical properties of OSCs. The effect of cyclic variation of UV irradiation, temperature and humidity on the PCE, J_{sc}, FF and V_{oc} were studied. The main conclusions derived from this investigated work are:

- The studied OSCs characteristics decrease with aging time for different aging conditions. The degradation is done in two steps : first step is done in the first 15 cycles of aging (360 h) and characterized by a fast degradation rate and the second steps (30 cycles of aging) represents the stabilization phase and characterized with the slow degradation rate, which is in agreement with the earlier finding in the literature.
- From the obtained results, it is highlighted that PCE evolution can be approximated by the sum of two decaying exponentials with time constants τ_1 and τ_2 having the same values. The deduced values show that environment conditions can have the same predominant

degradation mechanism. Furthermore, J_{sc} has been fitted with linear model and degradation constant has been calculated for each aging step.

- After 360 h of aging under the carried out protocol, the OSCs lose more than 60%, and even more than 80% for some properties like PCE, of their initial performances. This result shows that the carried out protocol presents harsh aging conditions.
- The carried out cyclic aging process in the QUV chamber can be considered very harsh combining different protocols similar to commonly used ISOS protocols in the same time. In one cycle of aging, the samples were performed to a protocol similar to ISOS-L-2 (UV radiation (light), temperature and ambient humidity), followed by one similar to ISOS-D-3 (temperature and controlled humidity) and finally to the last one similar to ISOS-D-2 (temperature less than ISOS-D-3, ambient humidity).
- The formation of bubble defects was observed and their concentration and size increase with aging time. The probable cause of these bubbles is the expansion or contraction of gasses with exposure to the light and high temperature cycling.

In the second study the stability of OSCs with the encapsulation. The carried out experiments include two parts, one has use the ISOS-O-1 protocol and the second undergoes the recovery phenomenon where the samples are put in dark and tracking the recovery at different parameters. Fully reversible degradation was observed at the early stage ($t \leq T_{80}$).

A missing recovery at different parameters PCE, FF, V_{oc} and J_{sc} is observed after $t \geq T_{80}$. It has been observed a rapid decrease in PCE and in the V_{oc}. However the FF presents a slow decrease, which was followed by a slow incomplete recovery.

In the carried out test the recovery doesn't reach the saturation in the case of PCE, FF and V_{oc} and showed rapid increases under further illumination. In the case of J_{sc} we have found some oscillation.

III.6 References

[1] Kaushika, N. D., Anuradha Mishra, and Anil K. Rai. "Fundamentals of Photovoltaic Generation: A Review." In Solar Photovoltaics, pp. 27-41. Springer, Cham, 2018.

[2] Green, Martin A., Anita Ho-Baillie, and Henry J. Snaith. "The emergence of perovskite solar cells." Nature photonics 8, no. 7 (2014): 506-514.

[3] Green, Martin A. "Thin-film solar cells: review of materials, technologies and commercial status." Journal of Materials Science: Materials in Electronics 18, no. 1 (2007): 15-19.

[4] Lu, Luyao, Tianyue Zheng, Qinghe Wu, Alexander M. Schneider, Donglin Zhao, and Luping Yu. "Recent advances in bulk heterojunction polymer solar cells." Chemical reviews 115, no. 23 (2015): 12666-12731.

[5] Al-Alwani, Mahmoud AM, Abu Bakar Mohamad, Norasikin A. Ludin, Abd Amir H. Kadhum, and Kamaruzzaman Sopian. "Dye-sensitised solar cells: development, structure, operation principles, electron kinetics, characterisation, synthesis materials and natural photosensitisers." Renewable and Sustainable Energy Reviews 65 (2016): 183-213.

[6] Rafique, Saqib, Shahino Mah Abdullah, Khaulah Sulaiman, and Mitsumasa Iwamoto. "Fundamentals of bulk heterojunction organic solar cells: An overview of stability/degradation issues and strategies for improvement." Renewable and Sustainable Energy Reviews 84 (2018): 43-53.

[7] Kaltenbrunner, Martin, Matthew S. White, Eric D. Głowacki, Tsuyoshi Sekitani, Takao Someya, Niyazi Serdar Sariciftci, and Siegfried Bauer. "Ultrathin and lightweight organic solar cells with high flexibility." Nature communications 3, no. 1 (2012): 1-7.

[8] Amb, Chad M., Michael R. Craig, Unsal Koldemir, Jegadesan Subbiah, Kaushik Roy Choudhury, Suren A. Gevorgyan, Mikkel Jørgensen, Frederik C. Krebs, Franky So, and John R. Reynolds. "Aesthetically pleasing conjugated polymer: fullerene blends for blue-green solar cells via roll-to-roll processing." ACS Applied Materials & Interfaces 4, no. 3 (2012): 1847-1853.

[9] G154-06, Standard Practice for Operating Fluorescent Light Apparatus for UV Exposure of Nonmetallic Materials. https://www.astm.org/Standards/G154 Accessed 18 April 2018

[10] Reese, Matthew O., Suren A. Gevorgyan, Mikkel Jørgensen, Eva Bundgaard, Sarah R. Kurtz, David S. Ginley, Dana C. Olson et al. "Consensus stability testing protocols for organic

photovoltaic materials and devices." Solar Energy Materials and Solar Cells 95, no. 5 (2011): 1253-1267.

[11] dos Reis Benatto, Gisele A., Bérenger Roth, Michael Corazza, Roar R. Søndergaard, Suren A. Gevorgyan, Mikkel Jørgensen, and Frederik C. Krebs. "Roll-to-roll printed silver nanowires for increased stability of flexible ITO-free organic solar cell modules." Nanoscale 8, no. 1 (2016): 318-326.

[12] Xue, Jiangeng, Soichi Uchida, Barry P. Rand, and Stephen R. Forrest. "4.2% efficient organic photovoltaic cells with low series resistances." Applied Physics Letters 84, no. 16 (2004): 3013-3015.

[13] Tessarolo, Marta, Antonio Guerrero, Desta Gedefaw, Margherita Bolognesi, Mario Prosa, Xiaofeng Xu, Mahdi Mansour et al. "Predicting thermal stability of organic solar cells through an easy and fast capacitance measurement." Solar Energy Materials and Solar Cells 141 (2015): 240-247.

[14] Yang, Hong Bin, Qun Lian Song, Cheng Gong, and Chang Ming Li. "The degradation of indium tin oxide/pentacene/fullerene/tris-8-hydroxy-quinolinato aluminum/aluminum heterojunction organic solar cells: By oxygen or moisture?." Solar energy materials and solar cells 94, no. 5 (2010): 846-849.

[15] Yang, Hong Bin, Qun Lian Song, Cheng Gong, and Chang Ming Li. "The degradation of indium tin oxide/pentacene/fullerene/tris-8-hydroxy-quinolinato aluminum/aluminum heterojunction organic solar cells: By oxygen or moisture?." Solar Energy Materials and Solar Cells 94, no. 5 (2010): 846-849.

[16] Gevorgyan, Suren A., Mikkel Jørgensen, and Frederik C. Krebs. "A setup for studying stability and degradation of polymer solar cells." Solar Energy Materials and Solar Cells 92, no. 7 (2008): 736-745.

[17] Cao, Can, and Yongzhi Cheng. "A broadband plasmonic light absorber based on a tungsten meander-ring-resonator in visible region." Applied Physics A 125, no. 1 (2019): 15.

[18] Conings, Bert, Sabine Bertho, Koen Vandewal, Alessia Senes, Jan D'Haen, Jean Manca, and René AJ Janssen. "Modeling the temperature induced degradation kinetics of the short circuit current in organic bulk heterojunction solar cells." Applied Physics Letters 96, no. 16 (2010): 81.

[19] Wang, Tao, Andrew J. Pearson, Alan DF Dunbar, Paul A. Staniec, Darren C. Watters, Hunan Yi, Anthony J. Ryan, Richard AL Jones, Ahmed Iraqi, and David G. Lidzey. "Correlating structure with function in thermally annealed PCDTBT: PC70BM photovoltaic blends." Advanced Functional Materials 22, no. 7 (2012): 1399-1408.

[20] Cardinaletti, Ilaria, Jurgen Kesters, Sabine Bertho, Bert Conings, Fortunato Piersimoni, Jan D'Haen, Laurence Lutsen et al. "Toward bulk heterojunction polymer solar cells with thermally stable active layer morphology." Journal of Photonics for Energy 4, no. 1 (2014): 040997.

[21] Guerrero, Antonio, Hamed Heidari, Teresa S. Ripolles, Alexander Kovalenko, Martin Pfannmöller, Sara Bals, Louis-Dominique Kauffmann, Juan Bisquert, and Germà Garcia-Belmonte. "Shelf life degradation of bulk heterojunction solar cells: Intrinsic evolution of charge transfer complex." Advanced Energy Materials 5, no. 7 (2015): 1401997.

[24] Ripolles, Teresa S., Antonio Guerrero, and Germà Garcia-Belmonte. "Polymer defect states modulate open-circuit voltage in bulk-heterojunction solar cells." Applied Physics Letters 103, no. 24 (2013): 236_1.

[23] Vandewal, Koen, Scott Himmelberger, and Alberto Salleo. "Structural factors that affect the performance of organic bulk heterojunction solar cells." Macromolecules 46, no. 16 (2013): 6379-6387.

[24] Hauch, Jens A., Pavel Schilinsky, Stelios A. Choulis, Richard Childers, Markus Biele, and Christoph J. Brabec. "Flexible organic P3HT: PCBM bulk-heterojunction modules with more than 1 year outdoor lifetime." Solar Energy Materials and Solar Cells 92, no. 7 (2008): 727-731.

[25] Rolston, Nicholas, Adam D. Printz, Stephanie R. Dupont, Eszter Voroshazi, and Reinhold H. Dauskardt. "Effect of heat, UV radiation, and moisture on the decohesion kinetics of inverted organic solar cells." Solar Energy Materials and Solar Cells 170 (2017): 239-245.

[26] Corazza, Michael, Nicholas Rolston, Reinhold H. Dauskardt, MichailJ Beliatis, Frederik C. Krebs, and Suren A. Gevorgyan. "Role of stress factors on the adhesion of interfaces in R2R fabricated organic photovoltaics." Advanced Energy Materials 6, no. 11 (2016): 1501927.

[27] Collins, Brian A., Eliot Gann, Lewis Guignard, Xiaoxi He, Christopher R. McNeill, and Harald Ade. "Molecular miscibility of polymer− fullerene blends." The Journal of Physical Chemistry Letters 1, no. 21 (2010): 3160-3166.

[28] Treat, Neil D., Alessandro Varotto, Christopher J. Takacs, Nicolas Batara, Mohammed Al-Hashimi, Martin J. Heeney, Alan J. Heeger, Fred Wudl, Craig J. Hawker, and Michael L. Chabinyc. "Polymer-fullerene miscibility: a metric for screening new materials for high-performance organic solar cells." Journal of the American Chemical Society 134, no. 38 (2012): 15869-15879.

[29] Bartelt, Jonathan A., Zach M. Beiley, Eric T. Hoke, William R. Mateker, Jessica D. Douglas, Brian A. Collins, John R. Tumbleston et al. "The importance of fullerene percolation in the mixed regions of polymer–fullerene bulk heterojunction solar cells." Advanced Energy Materials 3, no. 3 (2013): 364-374.

[30] Ye, Long, Wenchao Zhao, Sunsun Li, Subhrangsu Mukherjee, Joshua H. Carpenter, Omar Awartani, Xuechen Jiao, Jianhui Hou, and Harald Ade. "High-efficiency nonfullerene organic solar cells: critical factors that affect complex multi-length scale morphology and device performance." Advanced Energy Materials 7, no. 7 (2017): 1602000.

[31] Bin, Haijun, Yankang Yang, Zhi-Guo Zhang, Long Ye, Masoud Ghasemi, Shanshan Chen, Yindong Zhang et al. "9.73% efficiency nonfullerene all organic small molecule solar cells with absorption-complementary donor and acceptor." Journal of the American Chemical Society 139, no. 14 (2017): 5085-5094.

[32] Vasileios M Drakonakis et al. “Investigating electrodes degradation in organic photovoltaics through reverse engineering under accelerated humidity lifetime conditions”. In: Solar Energy Materials and Solar Cells 130 (2014): 544–550.

[33] Domanski, K. et al., “Migration of Cations Induces Reversible Performance Losses over Day/Night Cycling in Perovskite Solar Cells,” Energy Environ. Sci., vol. 10, (2017): 604−613.

[34] Nie, Wanyi, Jean-Christophe Blancon, Amanda J. Neukirch, Kannatassen Appavoo, Hsinhan Tsai, Manish Chhowalla, Muhammad A. Alam et al. "Light-activated photocurrent degradation and self-healing in perovskite solar cells." Nature communications 7, no. 1 (2016): 1-9.

[35] Hoke, Eric T., Daniel J. Slotcavage, Emma R. Dohner, Andrea R. Bowring, Hemamala I. Karunadasa, and Michael D. McGehee. "Reversible photo-induced trap formation in mixed-halide hybrid perovskites for photovoltaics." Chemical Science 6, no. 1 (2015): 613-617.

[36] Djeddaoui, Naas, Larbi Boukezzi, and Lakhdar Bessissa. "Aging and Degradation of Organic Solar Cells Using QUV Accelerated-Weathering Tester." Transactions on Electrical and Electronic Materials 20, no. 3 (2019): 189-197.

CHAPTER IV

Degradation and lifetime prediction of lab-scale and scalable non-fullerene OSCs

IV.1 Introduction

A key factor in the future commercial success of OSCs technology is device lifetime. Device degradation can be thought of as either intrinsic or extrinsic in nature. Extrinsic mechanisms, such as oxygen, water, UV exposure, and mechanical stress can be largely controlled through the engineering of encapsulation barriers and use of device additives [1-5]. Intrinsic mechanisms include the effects of heat and light on the device structure and electronic properties, [6-8] which can only be mitigated by altering the materials or structure of the device itself. In addition, the device processing, or purity of material, may also introduce oxygen or other defects into the device structure prior to encapsulation. Understanding the effects of these degradation stimuli is therefore a critical component of device design, materials selection, and ultimately in the industrial viability of the technology.

Much of the recent rapid growth in reported OSC device performances has been due to the use of non-fullerene acceptors (NFAs), instead of the previously common phenyl-$C_{60/70}$-butyric acid methyl ester ($PC_{60/70}BM$) acceptors. While this shift has had clear and dramatic effects on initial device efficiency, it is less clear what effects on device stability could be expected. While fullerenes can act as radical scavengers that inhibit the propagation of free radicals forming due to the action of oxygen and UV radiation, they are also implicated in a number of degradation mechanisms. However, NFAs are not without their own stability issues. While some NFA-based devices have been shown to exhibit excellent thermal stability, [9] they are often fabricated using processing additives that can be detrimental to device lifetime.

As OSCs can be applied in a wide variety of settings and applications, and as multiple different degradation mechanisms can occur, it is important that their durability is tested using a range of standardized testing protocols. These were codified in 2011 with the ISOS protocols. In addition to promoting comparability between laboratories and industry confidence in research, the ISOS protocols can provide different insights into degradation mechanisms depending on which one is followed. For example, laboratory testing under continuous illumination from a solar simulator is a very common form of degradation experiment, and while it will be relevant for some degradation effects, it may miss other degradation mechanisms that arise from cycling the light on and off, as it happens in an outdoor test. Despite this, the majority of OSC degradation studies reported in the literature focus on continuous illumination at 1 sun in a laboratory setting – the ISOS-L standards. An example of the importance of having diversity in testing conditions comes from recent perovskite solar cell research. Partial recovery of performance during a dark rest period (night in an

outdoor experiment) is a significant effect in perovskite solar cells, [10] and is attributed to either metastable defect formation or reversible ion migration at grain boundaries in the active layer. [11] This partial recovery of efficiency is occasionally reported in OSC device studies too, and is either attributed to p-type doping by adsorbed oxygen, [12]or desorption of O_2 from electron transport layers (ETLs) such as ZnO, causing a breakdown in the layer's diode properties. [13] Neither explanation appears to have received much further analysis, and dark recovery is not an effect that is very commonly examined in the OSC degradation literature. For this the carried out work in this chapter is give more insight on this point. In this part of study, we have compared the degradation of scalable OSC in an outdoor setting, in accordance with the ISOS-O-1 protocol to the similar lab-scale devices aged in laboratory ISOS-L-2 conditions, with recovery periods in the dark under full 1 Sun (1 kW m^{-2}) illumination and under 0.1 Sun (100 W m^{-2}).

In another hand, some of the obtained results will be used to build up an Artificial Neural Network model (ANN) to predict the behavior of OSC under aging process. In field of OSC prediction, we have found a limited number of published work. We can cite here the work of Tessarallo *et al.* [14] using an easy and fast capacity measurement to predict the thermal stability of OSCs and the work of Dong *et al.* [15] introducing the ANN in prediction of solar cells.

IV.2 Experimental Section

IV.2.1 Sample fabrication

The cells for outdoor testing were prepared entirely by scalable methods, namely R2R sputter and S2S slot-die coating [16]. The structure of the devices is detailed in **Figure IV.1(a & c)**.

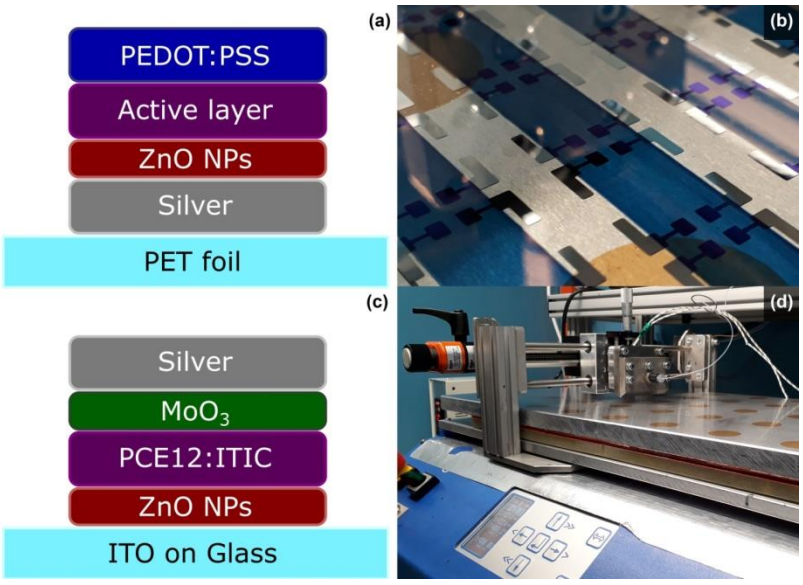

Figure IV.1:
The sample structures for (a) the outdoor degradation experiments and (c) the laboratory degradation experiments (both 1 Sun and 0.1 Sun); and (b) The electrode layout of the slot-die-coated samples and (d) the sheet-to-sheet slot-die coater used to fabricate the samples for the outdoor degradation experiments. The active layers used for the outdoor experiments were either PCE11:PCBM or PCE12:ITIC. Both device types were encapsulated via glass-on-glass encapsulation with a UV-curable epoxy. Each of the devices shown has an active area of 5.4 mm^2.

The samples used for the outdoor degradation experiments were prepared entirely by scalable fabrication techniques under ambient conditions. 100 nm thick silver electrodes were deposited on a polyethylene terephthalate (PET) foil (Melinex ST505 - DuPont Teijin Films) using a R2R sputter coater. These were then coated with a commercial ZnO nanoparticle solution (Genes'ink - H-SZ01034) via sheet-to-sheet slot-die coating (slot die head height 200 µm, speed 12 mm s^{-1}, pumping speed 50 µL min^{-1}, temperature 60°C) and annealed in a vacuum oven at 100°C for 10 minutes. This was followed by slot-die coating (**Figure IV.1(b & d)**) of the active layer (materials obtained from Brilliant Matters Inc.) from a solution with either a mixture of poly[(5,6-difluoro-2,1,3-benzothiadiazol-4,7-diyl)-alt-(3,3'''-di(2-octyldodecyl)-2,2';5',2'';5'',2'''-quaterthiophen-5,5'''-diyl)] (PCE11) and pheyl-$C_{60/70}$-butyric acid methyl ester ($PC_{60/70}BM$) (PCE11:PCBM 1:1.2 m/m, C_{60}:C_{70} = 19:1 m/m, 12 mg mL^{-1} PCE11 in 2.0% v/v p-anisaldehyde/o-xylene), or Poly[(2,6-(4,8-bis(5-(2-ethylhexyl)thiophen-2-yl)-benzo[1,2-b:4,5-b']dithiophene))-alt-(5,5-(1',3'-di-2-thienyl-5',7'-bis(2-ethylhexyl)benzo[1',2'-c:4',5'-c']dithiophene-4,8-dione)] (PCE12) and 3,9-bis(2-methylene-(3-(1,1-dicyanomethylene)-indanone))-5,5,11,11-tetrakis(4-hexylphenyl)-dithieno[2,3-d:2',3'-d']-s-indaceno[1,2-b:5,6-b']dithiophene (ITIC) (1:1 m/m, 20 mg mL^{-1} PCE12 in 0.5% v/v diiodooctane/chlorobenzene) [16]. The PCE11:PCBM mixture was deposited at 60°C with a slot die head height of 350 µm, a speed of 12.5 mm s^{-1}, pumping speed 90 µL min^{-1}. The PCE12:ITIC mixture was deposited at 70°C with a slot die head height of 200 µm, a speed of 6.3 mm s^{-1}, pumping speed 35 µL min^{-1}[16]. The PEDOT:PSS electrode was deposited via sequential slot-die coating of Heraeus Clevios HTL Solar (slot die head height of 200 µm, speed of 7.0 mm s^{-1}, pumping speed 60 µL min^{-1}) and Heraeus Clevios CPP (slot die head height of 250 µm, speed of 7.0 mm s^{-1}, pumping speed 50 µL min^{-1}). The samples were then stuck to a glass substrate and encapsulated with a glass cover slip and Delo KATIOBOND LP655 UV-active epoxy which was cured under a UV lamp (365 nm) for 15 minutes.

The samples for the laboratory degradation experiments were fabricated using laboratory-scale techniques in a glovebox with an inert nitrogen atmosphere (<0.1 ppm O_2, H_2O). ITO-coated glass substrates (Kintec) were spin-coated with the ZnO NP suspension at 2000 RPM for 60 s then annealed on a hot plate at 130°C for 15 minutes. The PCE12:ITIC active layer was then spin-coated from a 1:1 m/m solution (8.5 mg mL^{-1} of each PCE12 and ITIC in 0.5% v/v DIO in chlorobenzene) at 2400 RPM giving an active layer that is 110 nm thick. The MoO_3 hole transport layer (HTL) and silver electrode were deposited by thermal evaporation (10 nm and 100 nm respectively). Finally, encapsulation was carried out in the same way as with the outdoor degradation samples. All of the devices used in this study have active areas of 5.4 mm^2.

IV.2.2 Outdoor degradation experiments

The outdoor degradation studies were carried out in Sønderborg, Denmark (altitude, 54.913811°N; longitude, 9.79217 °E; altitude, 24 m). The devices were fixed on the SDU campus roof at an angle of 30° from morning to evening (10:00 to 16:00 CEST) in accordance with the ISOS-O-1 protocol,[17] and then stored overnight in the dark in a nitrogen-filled glovebox (<0.1 ppm O_2, H_2O). The day/night cycles were continued for five days (with the exception of one interruption on day 3), following which the samples were transferred to the glovebox where they were stored in the dark for 13 days. The experiment was conducted between 19 April 2018 and 7 May 2018.

J-V characterization was carried out at the start and end of each period in the light, and then periodically while the devices were stored in the dark for 13 days. The samples were measured in the dark and light using a KEITHLEY 2400 source-measurement unit and under an ABET technologies SUN 3000 Solar Simulator calibrated to a radiation intensity of 1000 W m^{-2}.

IV.2.3 Indoor (laboratory) degradation experiments

The indoor degradation experiments were carried out in accordance with the ISOS-L-2 protocol [17]. Samples were exposed to a simulated AM1.5G spectrum from an InfinityPV ISOSun solar simulator (HMI bulb) for around 6 hours at an elevated temperature of 65°C (either directly exposed or underneath a neutral density OD1 filter as in the 0.1 Sun experiments). The control samples were placed under the lamp alongside the aging samples – wrapped in aluminum foil to prevent radiation exposure but ensure identical thermal conditions through thermal conduction to the metallic base plate. Following the aging, the samples were stored in darkness for approximately 18 hours before aging was repeated. This cycle was repeated four times before resting the samples in the dark for 70 hours. The samples were characterized before and after each aging/dark storage step via IV analysis (using the same procedure as the outdoor samples) and TPV measurements (see below).

IV.2.4 Transient photovoltage (TPV) measurements

TPV measurements were carried out on the 1 Sun ISOS-L-2 degraded samples using a transient measurement unit (TMU) from Automatic Research GMBH, with the configuration shown in **Figure IV.2.** TPV lifetime values were determined using customized LabVIEW software by fitting the following equation to the decay curve via the sum of least squares method:

$$V_{OC}(t) = Ae^{-\frac{t}{\tau}} + C \qquad (1)$$

Where *A* and *C* are arbitrary fitting constants, *t* is the time following the end of the laser pulse, and τ is the TPV lifetime.

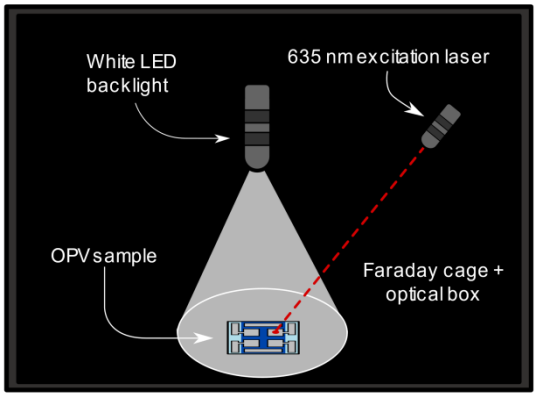

Figure IV.2. A schematic of the optical component of the TMU apparatus during a TPV lifetime measurement. Note that the intensity of the LED backlight was varied throughout the experiment to test different illumination conditions, while the laser pulse intensity and duration were varied to produce a 10 mV excitation in the OSC device.

IV.3 Prediction Method

IV.3.1 Prediction with supervised neural network

To predict the electrical properties of OSCs under indoor aging, we have used artificial neural network. This neural network is based on radial basis function (RBF) (**Figure IV. 3**) and contains an input layer with n units (aging data), a hidden layer with m units (m equal to 5 in our case) and an output layer with a single node (predicted value of property).

The use of Gaussian function allows its local characteristics to facilitate the training and improve generalization. The main idea of the RBF networks [18] is that any function *f(x)* can be approximated by an interpolation composed by the sum of *p* core functions:

$$f(x) = \sum_{i=1}^{p} w_j \, \emptyset(|x - \xi_i|) \qquad (2)$$

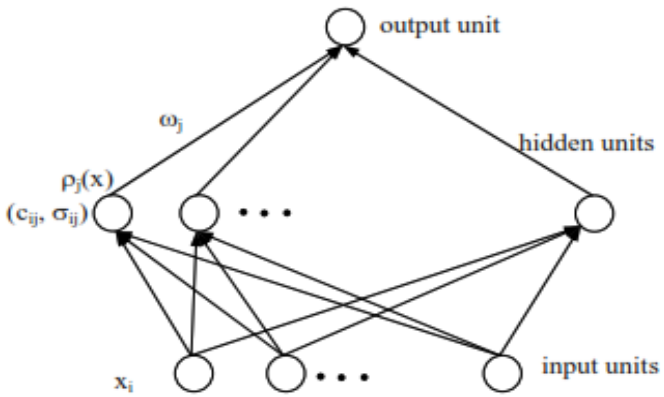

Figure IV.3. A feed-forward network with a single hidden layer and a single

Where ξ_i are the nodes of interpolation for i=1,n and are called centers and w_j are the synaptic weights that interconnect neurons to the output. $\emptyset$ is the core function, it ensures the continuity in the nodes. Each node in the hidden layer has a radial symmetric response around a node parameter vector which is called center. The output layer is a linear combiner with connection weights [19]. Giving a set of input and output data (x_i, y_i)i=1,n,

$$\rho_j(x_i)exp\left(-\frac{1}{2}\sum_{i=1}^{n}\frac{(x_i-c_{ij})^2}{\sigma_{ij}^2}\right) \qquad (3)$$

Where c_{ij} i=1,n and j=1,m are the RBFG centers,σ_{ij} define the width of Gaussians.

The chosen network in our investigation is trained by Random Optimization Method (ROM).

IV.3.1.1 RBFG trained by ROM

The RBFG centers are vectors of n dimensions; they can be selected from the trained data by some mechanisms cited in [18]. In the training by ROM proposed in this work, the used technique consists of an arrangement of centers in a regular trellis in order to cover uniformly the data input space.

The prediction process is based on two main phases: the training and the prediction

IV.3.1.2 Training phase

The used technique to train the ROM network is the FFN Pattern (data adaptive learning). In this case, the training is done on a set of samples having the form (y_i , y_{i+1}) , where y_i is a property value corresponding to aging time t_i, and y_{i+1} is the predicted value.

IV.3.1.3 Prediction phase

In order to predict a future value y_{i+1} of a set of measured data y_i, i=1,n, the algorithm will be trained on a set of samples having form (y_i , y_{i+1}) $_{i=1,n-1}$. After this training, the weights of the network are updated so that when the network receives the value y_i, its response will be y_{i+1} . Then, a new set of data is obtained with n+ 1 value. The training is repeated from the beginning in order to predict the value y_{i+2} , the new set of data will contain n+2 values, and this procedure is repeated until the prediction of the property for the entire required aging interval. In order to improve the prediction quality, after each future value prediction (n+1), the first value (1) is omitted from the set of data. In this way, the network is trained by the same number of input data.

IV.4 Results & discussion

IV.4.1 Outdoor aging studies

The results from the outdoor degradation experiments for the slot-die coated devices are shown in **Figure IV.4**. It is evident that both the PCE12:ITIC and PCE11:PCBM devices (**Figure IV.1.(a)**) experience degrees of recovery in performance when stored in the dark, but that this is more significant in the NFA based devices than in the PCBM based devices. The PCE11:PCBM devices also experience a significant degree of irreversible degradation throughout the duration of the experiment – the efficiency having dropped to 40% of its starting value by the end of the experiment with little recovery in the dark. While the PCE11:PCBM devices also use a different donor than the PCE12:ITIC devices, this behavior is most consistent with the early burn-in behavior of fullerene-containing devices that has been previously reported, [3,20,21,22] although the mechanisms behind it have not been studied further in this work. The irreversible efficiency loss is driven by short-circuit current density (J_{SC}) and fill factor (FF) loss (**Figure (b,d)**), which could be a consequence of photo-induced fullerene dimerization, as previously reported by Heumueller *et al.* noted [21]. Also singlet-oxygen based degradation has recently been pointed on for specific PCBM based systems [1-3].

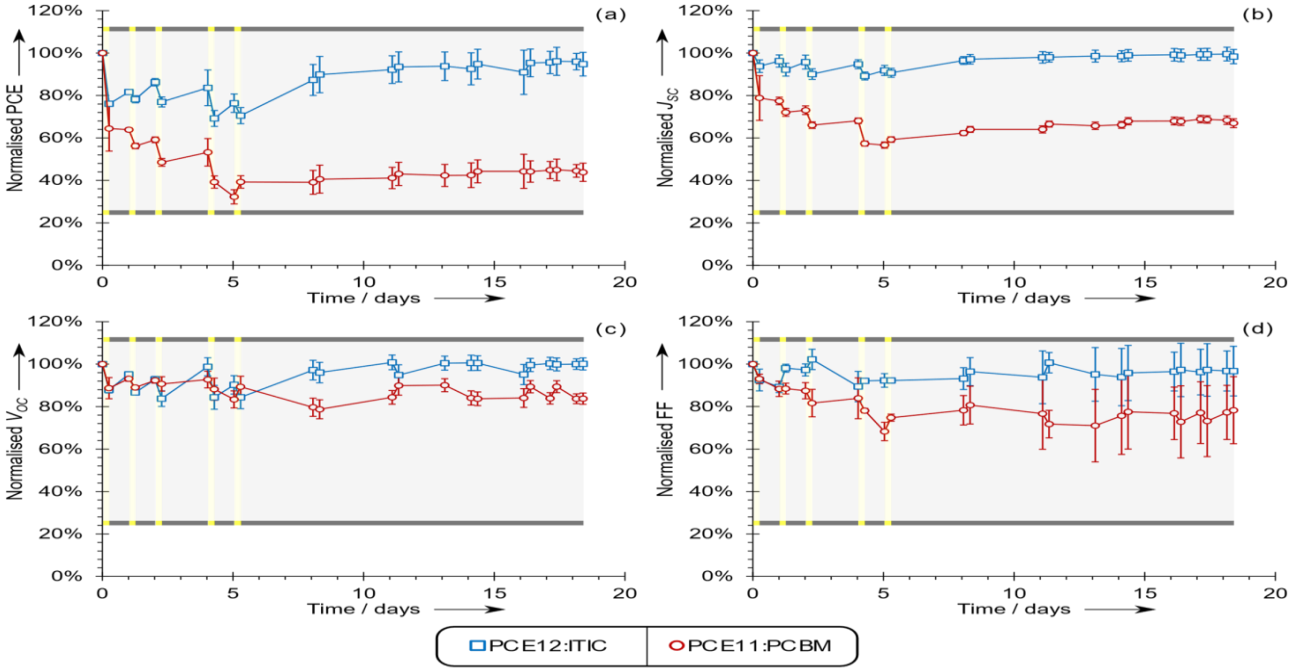

Figure IV.4. The variation of normalised PCE (a), J_{SC} (b), V_{OC} (c), and FF (d) as a function of time in the outdoor aging study of the PCE12:ITIC (blue squares) and PCE11:PCBM (red circles) OPV devices. Note that the dark shaded areas represent periods of the experiment when the devices were rested in the dark in an inert atmosphere and the light/yellow areas represent periods when the devices were aged under natural sunlight.

The most notable result of the outdoor testing is the presence of reversible degradation, i.e. degradation occurs when the device is illuminated, but after storing the device in the dark, the efficiency recovers. This effect appears to be primarily driven by V_{OC} and (to a lesser extent) J_{SC} (**Figure (c,b)**). While "dark recovery" is exhibited by both the NFA and PCBM based devices, it has a much stronger effect in the PCE12:ITIC devices due to the presence of an irreversible component of the degradation in the PCBM devices.

Degradation-recovery cycles are a well-documented phenomenon in perovskite solar cells [10,11]. The reversibility comes as a result of metastable defect formation and/or space-charge formation from mobile ions that move along grain boundaries in the active layer [11]. As this is a phenomenon that arises from mass-transport, once the photovoltage is removed, the mobile ions can return to their steady-state positions [11]. While an interesting parallel, this mechanism cannot explain the phenomenon observed in this study, as the morphology of the bulk heterojunction active layer of an OSC device would normally preclude the sort of long range mass transport on the timescales required for this dark recovery. There are some examples in the scientific literature of reversible degradation mechanisms in OSC devices, coming from studies carried on poly(3-hexylthiophene) (P3HT)-containing devices. Seemann *et al.* studied the effects of oxygen exposure on the performance of inverted devices [12]. They document that while there is a strong photooxidation effect, which is irreversible, there is also a reversible component of this degradation. They propose that this reversible component comes from p-doping of the active layer by absorbed oxygen, and that this effect can be reversed by heating the device in a nitrogen atmosphere [12]. This mechanism has also been documented by a number of other groups [23-27]. While the devices in this study were not heated, the recovery also takes place on a much longer timescale – consistent with the kinetics of an adsorption-desorption process. It should be noted as well that the devices in this study were fabricated in air before being encapsulated, whereas the devices in the study from Seemann *et al.* were exposed to oxygen throughout the aging process. Therefore the thermodynamic driving forces would be expected to be different in each case [12]. It is thus possible that the recovery behavior in this experiment arises from the absorption/desorption of oxygen that was trapped in the device during encapsulation.

Another possibility comes in a study from the groups of E. Katz and F. Krebs which worked with a similar device structure to Seemann *et al.* (inverted architecture, P3HT:PC_{60}BM active layer with a PEDOT:PSS HTL and a ZnO ETL), but instead were studying the effect of concentrated sunlight on the degradation behavior [13]. From their studies it is concluded that reversibility of the degradation is not necessarily an active layer mechanism, but can arise from a breakdown of the

diode character of the ZnO ETL, due to shunting effects, that is in fact also correlated with oxygen adsorption/desorption processes at the interface [13,28,29]. The devices used in their studies were fabricated using similar scalable techniques to those used in this study [13], making it a relevant comparison. This mechanism could explain the results seen in this study, as both the NFA and PCBM-containing devices have ZnO as an ETL, however, such asymmetry in charge extraction would be expected to have a larger effect on FF [30] than is currently seen. For now, the exact origin of the recovery mechanism observed in this study remains unclear.

IV.4.2 Indoor aging studies

Indoor aging studies were carried out in a typically employed laboratory setting using lab-scale device fabrication techniques and characterization under a solar simulator, i.e. ISOS-L conditions (specifically ISOS-L-2). In this case, two groups of PCE12:ITIC samples with the structure shown in **Figure IV.1(c)** were studied. One group was undergoing the same aging-recovering cycles as the outdoor samples (illuminated at 1 Sun), and the other group (control samples), were placed in identical conditions but shielded from radiation when under the solar simulator, so that they have similar temperature conditions.

From **Figure IV.5.(a)** (blue curves) it is immediately obvious that the degradation behavior of the PCE12:ITIC devices is completely different when tested in ISOS-L-2 conditions as compared to ISOS-O-1 conditions. Unlike in the outdoor experiments where the samples show strong recovery behavior in the dark, and exhibit no irreversible degradation, the degradation under the solar simulator is entirely irreversible, even with the same dark periods included. This degradation is predominantly FF-driven, with only minor contributions from V_{OC} and J_{SC} (**Figure IV.5.(b)**). Such a difference in degradation behavior must arise from the different sample geometry, the different stability experiment conditions, or both. The key differences in device structure (**Figure IV.1 (a & c)**) are top vs. bottom illumination of the device, and the materials used at the hole extraction interface. With respect to the degradation conditions, the main difference is the radiation intensity and the associated temperature difference during the illuminated periods.

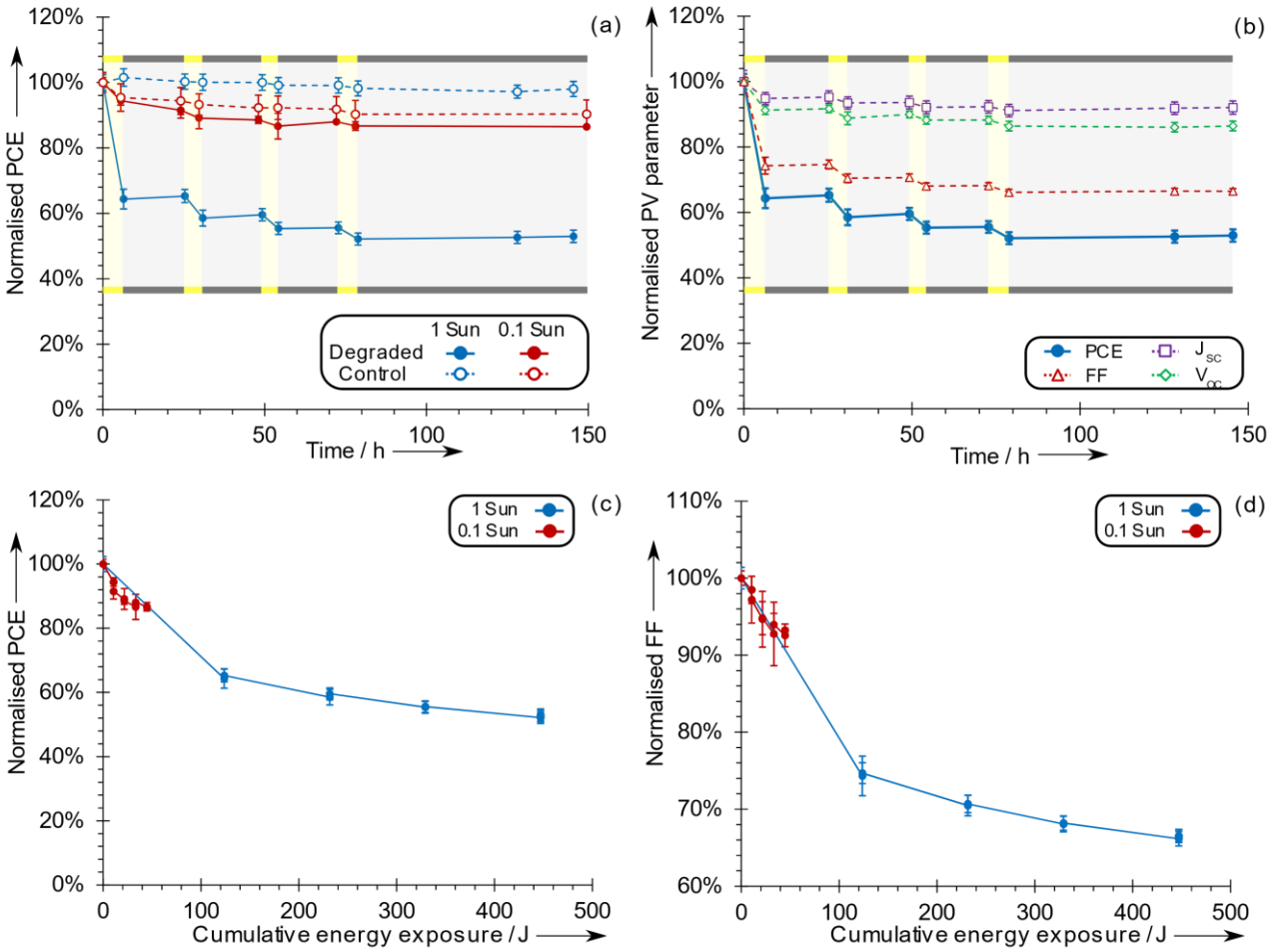

Figure IV.5. Results from the indoor ISOS-L-2 aging studies of the spin-coated PCE12:ITIC devices. In (a) the variation of PCE of the aged (solid circles, solid lines) and control devices (hollow circles with dashed lines) with time for the 1 Sun (blue) and 0.1 Sun (red) samples are shown. In (b) the normalised variation in the PV parameters PCE (solid, blue, circles), J_{SC} (dashed, purple, squares), V_{OC} (dashed, green, diamonds) and FF (dashed, red, triangles) of the 1 Sun aged samples with time are shown. In both plots the light/yellow shaded regions represent time that the samples were under the solar simulator (shaded in the case of the control samples) and the dark/grey shaded regions represent time that the samples were kept in the dark, to simulate the outdoor experiments' day/night cycles. In (c) and (d) the variation of normalised PCE and normalised FF (respectively) of the aged devices with cumulative energy exposure are shown for the samples aged at 1 Sun (blue circles) and at 0.1 Sun (red circles) All uncertainities represent one standard deviation across 6-8 devices.

In order to determine whether the sample architecture or light intensity were primarily responsible for the difference in degradation behavior, an additional indoor degradation experiment was carried out. The same experimental conditions were used with identical samples, but this time they were shielded with an OD1 neutral density filter, so that the radiation they received while illuminated (0.1 Sun) was similar to the levels absorbed in the outdoor experiments. The results of this experiment are shown in red in **Figure IV.5.(a)**. It is evident from the degradation behavior of these samples that the recovery effect is not present when the light intensity is reduced, and that the main difference causing recovery is the sample architecture, and not the testing conditions. Moreover, when the degradation data from the aged samples of the 1 Sun and 0.1 Sun experiments are plotted

as a function of cumulative energy exposure (**Figure IV.5. (c)**), it is evident that the degradation in the 0.1 Sun experiment is following the same trend as the 1 Sun experiment, suggesting that the same underlying mechanisms are operating, simply at one tenth of the rate. This is further reinforced when fill factor is plotted as a function of cumulative energy exposure, **Figure IV.5. (d)** shows that both experiments follow the same trend. It can be concluded from this that the dominating irreversible degradation mechanism in the ISOS-L-2 experiment that causes fill factor loss is photo-induced, depends linearly on light exposure, and is specific to the device design used for the indoor experiments (**Figure IV.1(a & c)**).

While discerning the precise mechanistic differences in the degradation mechanisms of the different architecture samples for the indoor and outdoor experiments goes beyond the scope of this work, it is possible to eliminate a few possibilities and speculate based on what remains. FF-driven degradation resulting from the use of silver and MoO_3 at the hole extraction interface of inverted OPV devices has been previously reported on, typically attributed to thermally-induced diffusion of electrode materials into the active layer [6,7,31,32]. It is unlikely that this is the origin of the irreversible degradation in the indoor samples as the control samples (which experienced the same temperature conditions as the aged samples in the indoor experiment) show minimal signs of degradation (**Figure IV.5. (a)**), the FF loss occurs at a proportional rate to the illumination intensity (**Figure IV.5. (d)**), and this type of degradation usually has a V_{OC} component too [31]. Given the lack of recovery in the 0.1 Sun indoor experiment, it is likely that the difference in degradation behavior between the indoor and outdoor experiments stems from the different device architectures used. One possibility is that the top-illuminated architecture of the outdoor samples (PET/PEDOT:PSS and glass/ITO have different transmission spectra [33]) suppresses a mechanism that would otherwise dominate the degradation of the device. Another is that the presence of MoO_3 as an HTL results in a chemical interaction with the active layer that is otherwise absent when PEDOT:PSS is used at the top contact. This could be photo-induced cleavage of functional groups in the active layer to form bulk charge traps that increase monomolecular recombination, and thereby decrease FF, or cause morphological changes to the polymer that change the asymmetry of charge carrier mobility in the active layer. [30,34-36]

Any mechanistic explanation of the decline in FF must both satisfy the observed pseudo-exponential nature of the decline with time, and the apparent linear dependence of the rate of loss on the illumination intensity. This eliminates many typical origins of FF loss that give rise to asymmetric charge extraction, such as energy level misalignment or charge-carrier mobility changes [30,37,38] as these mechanisms would not be expected to have such linearity. FF-driven,

rapid efficiency loss in photo-degraded MoO_3-containing devices is also something that has been previously observed in this laboratory, most recently by Ahmadpour *et al.*, [39,40] demonstrating that thermally deposited MoO_3, in contrast to sputtered MoO_3, (also in standard device architectures) can lead to accelerated device degradation resulting from chemical degradation at that interface. While the origin of this effect remains unclear, it could be similar to the irreversible degradation mechanisms observed in this work for the laboratory-scale cells, and thus also explain the difference in behavior of the different cell architectures used in the indoor and outdoor experiments.

IV.4.3 Transient photovoltage (TPV) measurements

In order to gain further information on the origin of the irreversible degradation in the 1 Sun laboratory aging experiment, TPV measurements were carried out throughout the 1 Sun ISOS-L-2 experiment. The TPV results are shown in **Figurre IV.6** and the experimental apparatus is shown in **Figure IV.2.** Note that the laser was calibrated to give a ΔV_{OC} of approximately 10 mV. An increase in the rate with which TPV lifetime drops with increasing backlight is consistent with an increase in the charge trap density near the interlayer-active layer interfaces [41]. This is because empty interfacial charge traps increase the TPV lifetime of laser pulse-generated free charges in the device. Since the device is in open circuit conditions and no charges are extracted, free charges are quickly captured by charge traps near the interfaces, which again take time to empty once the pulse is switched off. The higher the charge traps density near the interfaces, the longer the TPV lifetime. If the backlight is used, a portion of those traps are filled by charge carriers generated by the backlight, resulting in fewer trapped charge carriers originating from the laser pulse, and thus faster recombination when the pulse is switched off. The more traps there are, the more backlight is required to fill them to decrease the TPV lifetime from the laser pulse.

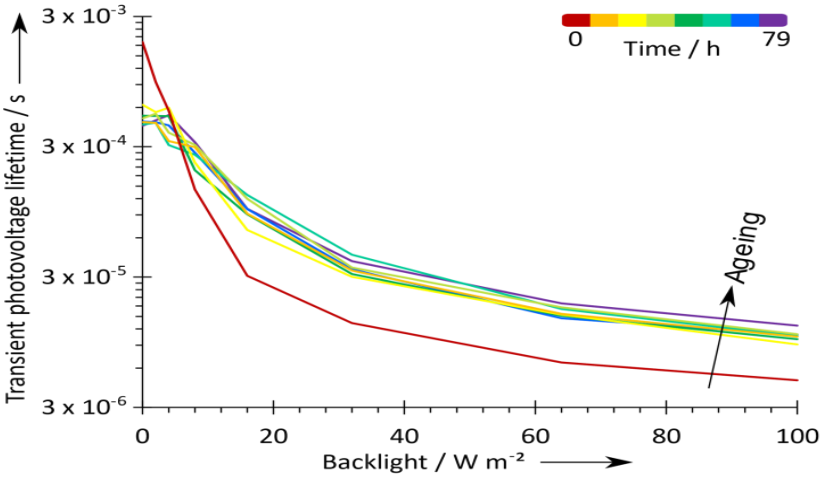

Figure IV.6.

TPV data measured throughout the indoor aging experiment from the aged PCE12:ITIC devices. Measurement was carried out using the apparatus described in the experimental section. Note that "time" in this figure refers to time since the start of the experiment and includes both illumination and dark-rest time.

In **Figure IV.6**, the TPV lifetime of the unaged device drops quickly with increasing backlight. This indicates relatively low trap density in the pristine devices, which is to be expected. Charge traps (monomolecular recombination) are typically thought to play a lesser role in non-geminate charge carrier recombination in organic semiconductors – which is typically dominated by bimolecular recombination from free charge carriers, so an efficient OSC device would be expected to have low charge trap densities at the on-set of degradation [34,42,43]. However, as the experiment progresses, the amount of backlight required to decrease TPV lifetime increases, in a similar fashion to the apparently exponential drop in FF occurring simultaneously (**Figure IV.5.(b)**). This is consistent with an increase in charge trap density near the interfaces as the experiment progresses. These traps could potentially come from impurities like cleaved side chains or processing additives [44,36,45-46], changes in the crystallinity/morphology of the donor or acceptor domains [47],or even changes in the polymer chain length [48,49]. Any or all of these are possible, although the latter would be expected to have a stronger effect on J_{SC} [50]. It should also be noted that other processes than interfacial trapping can give rise to these changes in the TPV lifetime – this is simply the most consistent with the trends in OSC statistics with device aging [51-53].

IV.4.4 Comparison of results from the indoor and outdoor tests and the role of the ISOS protocols

It is from the results evident that the same active layer can exhibit different degradation profiles when the device architecture and testing regime are altered. This is an important consideration with respect to the scale-up and commercialization of OSC technology. The vast majority of OSC degradation studies are carried out in very controlled ISOS-L-1 or L-2 conditions, using similar small-scale fabrication techniques and device architectures to the samples used in the indoor portion of this study. While these studies can be a useful way to study degradation mechanisms in devices with novel active layer materials, the results of this work show that they may not relate to the outdoor stability of these materials when employed in a scalable device design – which is more relevant to the eventual application of any commercialized product. A poor-performing material in an ISOS-L small-scale stability assessment may, in fact, perform well in an ISOS-O study at commercial-scale, as demonstrated here. This shows that OSC degradation studies that only use an ISOS-L protocol and laboratory-scale devices should not be used to eliminate potential candidates for materials for up-scaling/commercialization research. Such determinations can only be made via outdoor degradation experiments, carried out on devices fabricated with scalable architectures via scalable techniques, in addition to any other stability tests relevant for the application or industrial

processing conditions (e.g. thermal aging). This is not to say that an ISOS-O-1 study is inherently more useful than an ISOS-L-1 study, or that laboratory scale architectures are less useful than commercial-scale ones, simply that the results of each must be taken in the relevant context of the testing conditions and care must be taken before extrapolating to different degradation conditions and device architectures or forming general conclusions about particular materials' stability. Furthermore, correct application of a diverse range of ISOS protocols can reveal novel degradation behavior that generates opportunities for further research, as was the case with the dark recovery mechanism observed in the outdoor experiment in this study.

IV.5 Results of predication using ANN

In our application we have proposed RBFG neural network trained with Rondom Optimization Method (ROM) to predict the different parameters of organic solar cell and compared between their results. The purpose of the prediction task is to predict the effect of aging time on the electrical characteristics for two kinds of OSCs. The first type uses zinc oxide (ZnO) as active layer and the second use the titanium oxide (TiOx) as active layer. The presented characteristics in **Figure IV.7** show the prediction of TiOx aged under ISOS-L-1 protocol up to 150 hours. Different electrical characteristics have been used as: PCE, V_{oc}, FF, J_{sc}, R_s and R_{sh}. Also, **Figure IV.8** shows the results concerning the OSC based ZnO. The used RBFG model with two parameters first one is input: the value of aging time and the second it is the target (electrical parameters). From **Figures IV.7 and IV.8** the predicted values of electrical properties are in good agreement with the experimental values for all the studied characteristics.

The precision of prediction can be assessed by many statistical parameters such as Root Mean Square Error RMSE, Mean Absolute Relative Error (MARE) and determination coefficient R^2. The above parameters are given in equations (4) and (5):

$$\text{RMSE}=\sqrt{\frac{1}{n}\sum_{t=1}^{n}(A_t - F_t)^2} \quad (4)$$

$$MARE = \frac{1}{n}\sum_{t=1}^{n}\left|\frac{A_t - F_t}{A_t}\right| \times 100 \quad (5)$$

Where A_t is the actual value and F_t is the forecast value.

The obtained statistical parameters are listed in the Table IV.1 below.

Table IV.1 RBFG statistical parameters for the all cases

	ZnO aged						**Tiox aged**					
	PCE	Voc	FF	Jsc	Rs	Rsh	PCE	Voc	FF	Jsc	Rs	Rsh
MARE	2.53	1.04	0.8	0.41	0.81	8.8	1.2	1.3	1.5	1	1.4	3.2
RMSE	0.53	0.042	0.002	0.2	2.08	0.01	0.03	0.045	0.036	0.072	1.96	1.39

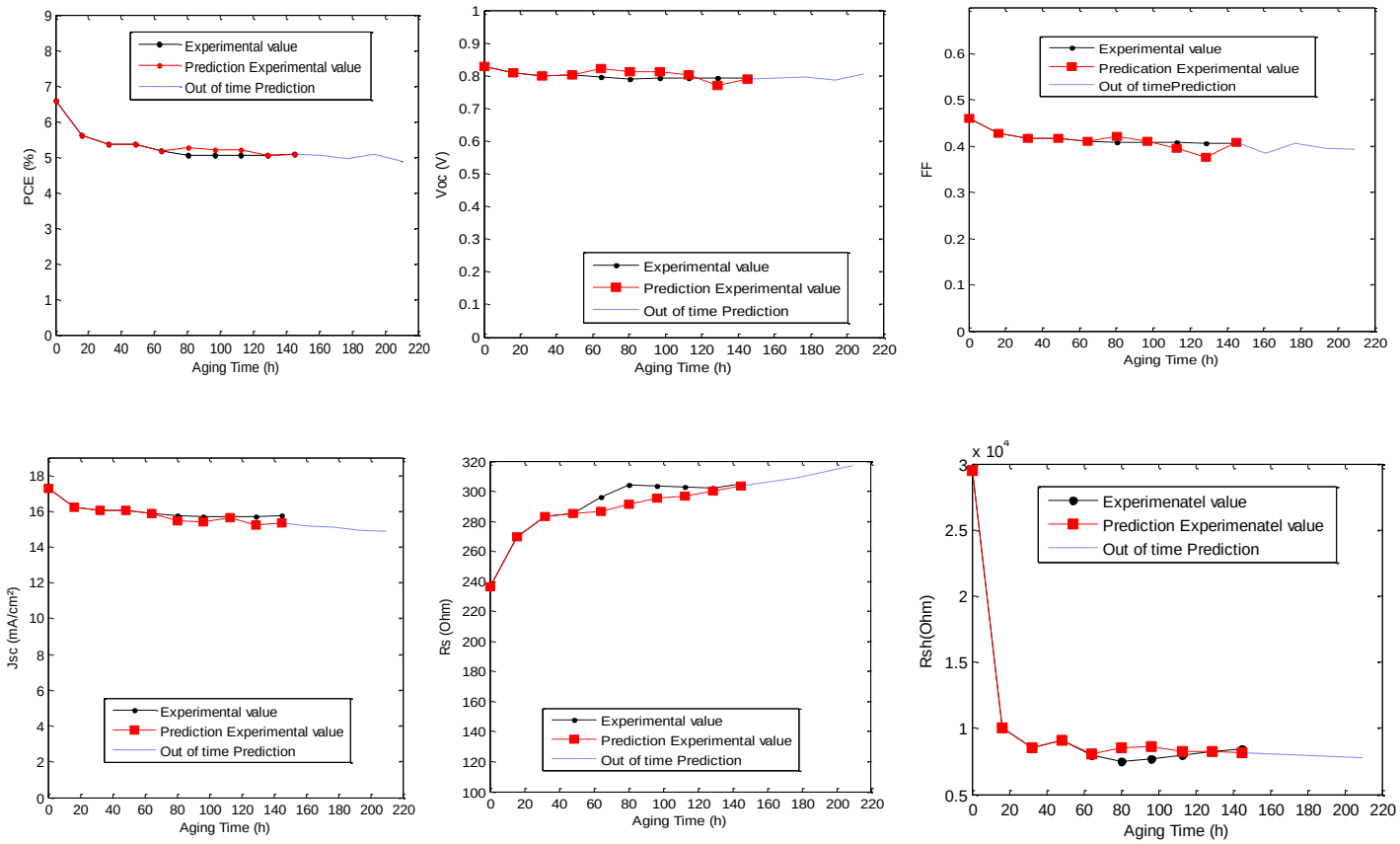

Figure IV.7: Electrical paramteres of Tiox aged

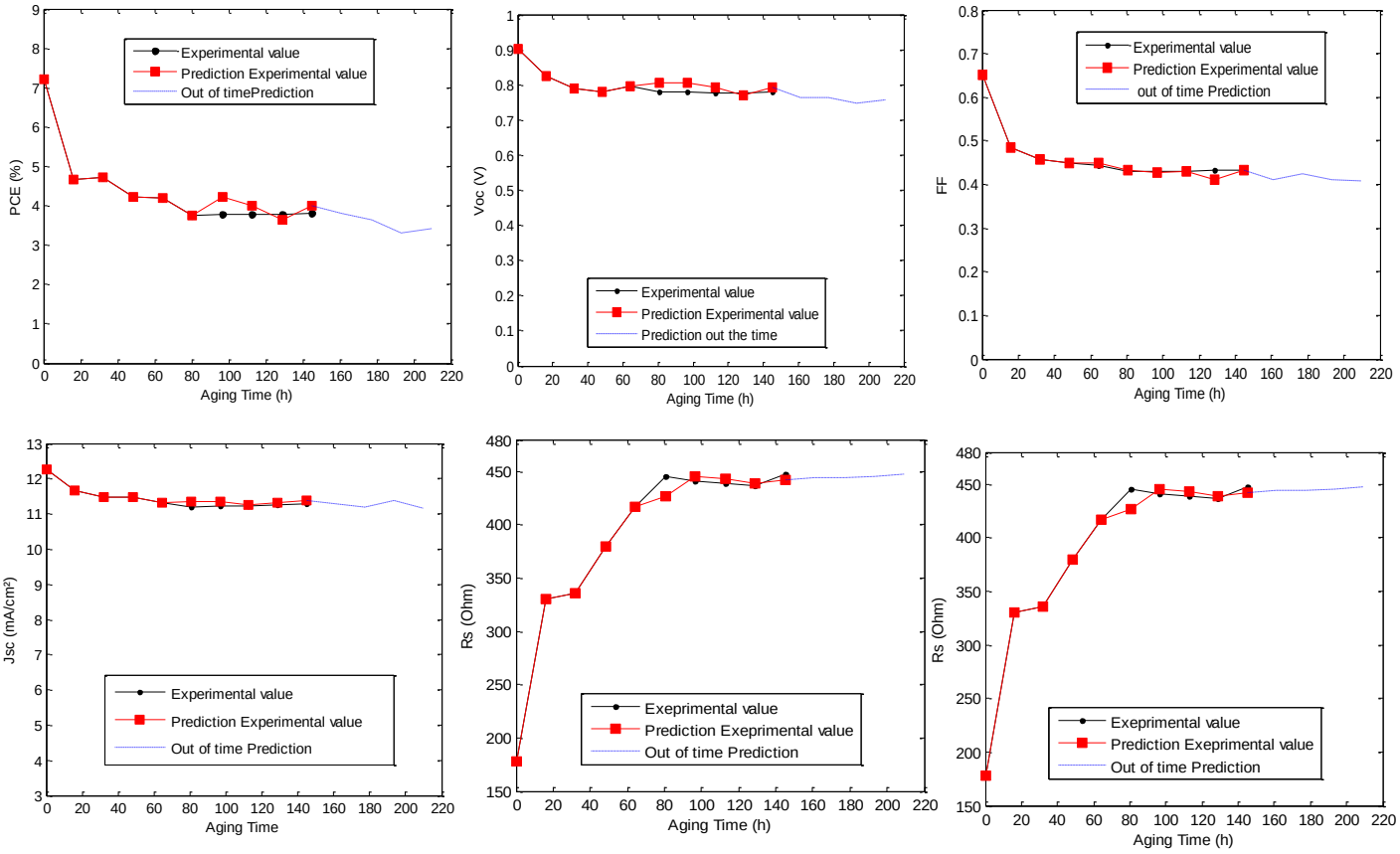

Figure IV.8: Electrical paramteres of ZnO aged

IV.6 Conclusion

This study has examined the difference in aging behavior of solar cells containing the high-efficiency polymer-NFA blend PCE12:ITIC when aged in a laboratory setting with small-scale device architecture, and in an outdoor setting with scalable device architecture. It was observed that in an outdoor setting, devices exhibited dark-recovery behavior and very little irreversible degradation – previously unreported behavior for this system that was not seen in PCE11:PCBM devices that were fabricated and investigated in the same settings. In contrast, small-scale spin coated PCE12:ITIC devices, when aged in a laboratory setting, exhibited rapid and completely irreversible degradation. This irreversible degradation was fill-factor-driven and showed linear dependency on light intensity. This is most likely due to the different device architectures used in laboratory-scale devices, compared to scalable devices. These results emphasize the risk in drawing general conclusions about the stability of active layer materials from laboratory scale devices and degradation studies, and the importance of using a diverse range of testing conditions and ISOS protocols in making such determinations.

In part of prediction we have used RBFG neural network trained with Random Optimization Method (ROM) to predict the electrical properties of OSCs. The quality of prediction was evaluated by many statistical parameters like RMSE and MARE and the obtained values pointed out that the used model give a good accuracy of prediction and can be used to predict a future state of the OSC device without undergoing the aging process experiments. This aspect of prediction leads to gain money and time.

IV.7 References

[1] Turkovic, Vida, Sebastian Engmann, Nikos Tsierkezos, Harald Hoppe, Morten Madsen, Horst-Günter Rubahn, Uwe Ritter, and Gerhard Gobsch. "Long-term stabilization of organic solar cells using hydroperoxide decomposers as additives." Applied Physics A 122, no. 3 (2016): 255.

[2] Turkovic, Vida, Sebastian Engmann, Nikos Tsierkezos, Harald Hoppe, Morten Madsen, Horst-Günter Rubahn, Uwe Ritter, and Gerhard Gobsch. "Long-term stabilization of organic solar cells using UV absorbers." Journal of Physics D: Applied Physics 49, no. 12 (2016): 125604.

[3] Turkovic, Vida, Michela Prete, Mikkel Bregnhøj, Liana Inasaridze, Dmytro Volyniuk, Filipp A. Obrezkov, Juozas Vidas Grazulevicius et al. "Biomimetic Approach to Inhibition of Photooxidation in Organic Solar Cells Using Beta-Carotene as an Additive." ACS applied materials & interfaces 11, no. 44 (2019): 41570-41579.

[4] Turkovic, Vida, Sebastian Engmann, Nikos Tsierkezos, Harald Hoppe, Uwe Ritter, and Gerhard Gobsch. "Long-term stabilization of organic solar cells using hindered phenols as additives." ACS applied materials & interfaces 6, no. 21 (2014): 18525-18537.

[5] Salvador, Michael, Nicola Gasparini, José Darío Perea, Sri Harish Paleti, Andreas Distler, Liana N. Inasaridze, Pavel A. Troshin, Larry Lüer, Hans-Joachim Egelhaaf, and Christoph Brabec. "Suppressing photooxidation of conjugated polymers and their blends with fullerenes through nickel chelates." Energy & Environmental Science 10, no. 9 (2017): 2005-2016.

[6] Greenbank, William, Lionel Hirsch, and Sylvain Chambon. "Electrode de-wetting as a failure mechanism in thermally-aged OPV devices." Solar Energy Materials and Solar Cells 178 (2018): 8-14.

[7] Greenbank, William, Nicholas Rolston, Elodie Destouesse, Guillaume Wantz, Lionel Hirsch, Reinhold Dauskardt, and Sylvain Chambon. "Improved mechanical adhesion and electronic stability of organic solar cells with thermal ageing: the role of diffusion at the hole extraction interface." Journal of Materials Chemistry A 5, no. 6 (2017): 2911-2919.

[8] Engmann, Sebastian, Chetan R. Singh, Vida Turkovic, Harald Hoppe, and Gerhard Gobsch. "Direct Correlation of the Organic Solar Cell Device Performance to the In-Depth Distribution of Highly Ordered Polymer Domains in Polymer/Fullerene Films." Advanced Energy Materials 3, no. 11 (2013): 1463-1472.

[9] Yu, Liyang, Deping Qian, Sara Marina, Ferry AA Nugroho, Anirudh Sharma, Sandra

Hultmark, Anna I. Hofmann et al. "Diffusion-Limited Crystallization: A Rationale for the Thermal Stability of Non-Fullerene Solar Cells." ACS applied materials & interfaces 11, no. 24 (2019): 21766-21774.

[10] Khenkin, Mark V., Anoop KM, Iris Visoly-Fisher, Sofiya Kolusheva, Yulia Galagan, Francesco Di Giacomo, Olivera Vukovic et al. "Dynamics of photoinduced degradation of perovskite photovoltaics: from reversible to irreversible processes." ACS Applied Energy Materials 1, no. 2 (2018): 799-806.

[11] Khenkin, Mark V., Anoop KM, Iris Visoly-Fisher, Sofiya Kolusheva, Yulia Galagan, Francesco Di Giacomo, Olivera Vukovic et al. "Dynamics of photoinduced degradation of perovskite photovoltaics: from reversible to irreversible processes." ACS Applied Energy Materials 1, no. 2 (2018): 799-806.

[12] Seemann, Andrea, Tobias Sauermann, Christoph Lungenschmied, Oskar Armbruster, Siegfried Bauer, H-J. Egelhaaf, and Jens Hauch. "Reversible and irreversible degradation of organic solar cell performance by oxygen." Solar Energy 85, no. 6 (2011): 1238-1249.

[13] Tromholt, Thomas, Assaf Manor, Eugene A. Katz, and Frederik C. Krebs. "Reversible degradation of inverted organic solar cells by concentrated sunlight." Nanotechnology 22, no. 22 (2011): 225401.

[14] Tessarolo, Marta, Antonio Guerrero, Desta Gedefaw, Margherita Bolognesi, Mario Prosa, Xiaofeng Xu, Mahdi Mansour et al. "Predicting thermal stability of organic solar cells through an easy and fast capacitance measurement." Solar Energy Materials and Solar Cells 141 (2015): 240-247.

[15] Deng, Dong, Lingzhi Yi, Zhenzhen Zhou, and Haicheng Peng. "Research of prediction and modeling about solar cells based on neural network." In 2011 Asia-Pacific Power and Energy Engineering Conference, pp. 1-4. IEEE, 2011.

[16] Destouesse, Elodie, Michiel Top, Jani Lamminaho, Horst-Günter Rubahn, John Fahlteich, and Morten Madsen. "Slot-die processing and encapsulation of non-fullerene based ITO-free organic solar cells and modules." Flexible and Printed Electronics 4, no. 4 (2019): 045004.

[17] Reese, Matthew O., Suren A. Gevorgyan, Mikkel Jørgensen, Eva Bundgaard, Sarah R. Kurtz, David S. Ginley, Dana C. Olson et al. "Consensus stability testing protocols for organic photovoltaic materials and devices." Solar Energy Materials and Solar Cells 95, no. 5 (2011): 1253-1267.

[18] Khemaissia, S., and M. S. Morris. "Review of networks and choice of radial basis function networks for system identification." Technologies avancées 6 (1994): 55-85.

[19] Mokhnache, L., and A. Boubakeur. "Use of neural networks in the monitoring of high voltage insulation thermal ageing." INTERNATIONAL JOURNAL OF COMADEM 6, no. 4 (2003): 18-23.

[20] Peters, Craig H., I. T. Sachs-Quintana, William R. Mateker, Thomas Heumueller, Jonathan Rivnay, Rodigo Noriega, Zach M. Beiley, Eric T. Hoke, Alberto Salleo, and Michael D. McGehee. "The mechanism of burn-in loss in a high efficiency polymer solar cell." Advanced Materials 24, no. 5 (2012): 663-668.

[21] Heumueller, Thomas, William R. Mateker, Andreas Distler, Urs F. Fritze, Rongrong Cheacharoen, William H. Nguyen, Markus Biele et al. "Morphological and electrical control of fullerene dimerization determines organic photovoltaic stability." Energy & Environmental Science 9, no. 1 (2016): 247-256.

[22] Heumueller, Thomas, Timothy M. Burke, William R. Mateker, Isaac T. Sachs-Quintana, Koen Vandewal, Christoph J. Brabec, and Michael D. McGehee. "Disorder-Induced Open-Circuit Voltage Losses in Organic Solar Cells During Photoinduced Burn-In." Advanced Energy Materials 5, no. 14 (2015): 1500111.

[23] Hintz, H., H. Peisert, H-J. Egelhaaf, and T. Chassé. "Reversible and irreversible light-induced p-doping of P3HT by oxygen studied by photoelectron spectroscopy (XPS/UPS)." The Journal of Physical Chemistry C 115, no. 27 (2011): 13373-13376.

[24] Liao, Hua-Hsien, Chia-Ming Yang, Chien-Cheng Liu, Sheng-Fu Horng, Hsin-Fei Meng, and Jow-Tsong Shy. "Dynamics and reversibility of oxygen doping and de-doping for conjugated polymer." Journal of applied physics 103, no. 10 (2008): 104506.

[25] Schafferhans, Julia, Andreas Baumann, Alexander Wagenpfahl, Carsten Deibel, and Vladimir Dyakonov. "Oxygen doping of P3HT: PCBM blends: Influence on trap states, charge carrier mobility and solar cell performance." Organic Electronics 11, no. 10 (2010): 1693-1700.

[26] Sperlich, Andreas, Hannes Kraus, Carsten Deibel, Hubert Blok, Jan Schmidt, and Vladimir Dyakonov. "Reversible and irreversible interactions of poly (3-hexylthiophene) with oxygen studied by spin-sensitive methods." The Journal of Physical Chemistry B 115, no. 46 (2011): 13513-13518.

[27] Weu, Andreas, Joshua A. Kress, Fabian Paulus, David Becker-Koch, Vincent Lami, Artem A. Bakulin, and Yana Vaynzof. "Oxygen-induced doping as a degradation mechanism in highly efficient organic solar cells." ACS Applied Energy Materials 2, no. 3 (2019): 1943-1950.

[28] Larsen-Olsen, Thue T., Roar R. Søndergaard, Kion Norrman, Mikkel Jørgensen, and

Frederik C. Krebs. "All printed transparent electrodes through an electrical switching mechanism: a convincing alternative to indium-tin-oxide, silver and vacuum." Energy & Environmental Science 5, no. 11 (2012): 9467-9471.

[29] Manor, Assaf, Eugene A. Katz, Thomas Tromholt, and Frederik C. Krebs. "Electrical and Photo-Induced Degradation of ZnO Layers in Organic Photovoltaics." Advanced Energy Materials 1, no. 5 (2011): 836-843.

[30] Zhang, Guichuan, Ruoxi Xia, Zhen Chen, Jingyang Xiao, Xuenan Zhao, Shiyuan Liu, Hin-Lap Yip, and Yong Cao. "Overcoming Space-Charge Effect for Efficient Thick-Film Non-Fullerene Organic Solar Cells." Advanced Energy Materials 8, no. 25 (2018): 1801609.

[31] Greenbank, William, Lionel Hirsch, Guillaume Wantz, and Sylvain Chambon. "Interfacial thermal degradation in inverted organic solar cells." Applied Physics Letters 107, no. 26 (2015): 115_1.

[32] Hermerschmidt, Felix, Achilleas Savva, Efthymios Georgiou, Sachetan M. Tuladhar, James R. Durrant, Iain McCulloch, Donal DC Bradley, Christoph J. Brabec, Jenny Nelson, and Stelios A. Choulis. "Influence of the hole transporting layer on the thermal stability of inverted organic photovoltaics using accelerated-heat lifetime protocols." ACS applied materials & interfaces 9, no. 16 (2017): 14136-14144.

[33] Gaynor, Whitney, George F. Burkhard, Michael D. McGehee, and Peter Peumans. "Smooth nanowire/polymer composite transparent electrodes." Advanced Materials 23, no. 26 (2011): 2905-2910.

[34] Proctor, Christopher M., Martijn Kuik, and Thuc-Quyen Nguyen. "Charge carrier recombination in organic solar cells." Progress in Polymer Science 38, no. 12 (2013): 1941-1960.

[35] Guo, Xugang, Nanjia Zhou, Sylvia J. Lou, Jeremy Smith, Daniel B. Tice, Jonathan W. Hennek, Rocío Ponce Ortiz et al. "Polymer solar cells with enhanced fill factors." Nature Photonics 7, no. 10 (2013): 825-833.

[36] Cha, Hyojung, Jiaying Wu, Andrew Wadsworth, Jade Nagitta, Saurav Limbu, Sebastian Pont, Zhe Li et al. "An efficient,“burn in” free organic solar cell employing a nonfullerene electron acceptor." Advanced Materials 29, no. 33 (2017): 1701156.

[37] Bartesaghi, Davide, Irene del Carmen Pérez, Juliane Kniepert, Steffen Roland, Mathieu Turbiez, Dieter Neher, and L. Jan Anton Koster. "Competition between recombination and extraction of free charges determines the fill factor of organic solar cells." Nature communications 6, no. 1 (2015): 1-10.

[38] Ray, Biswajit, and Muhammad Ashraful Alam. "Achieving fill factor above 80% in organic solar cells by charged interface." In 2012 IEEE 38th Photovoltaic Specialists Conference (PVSC) PART 2, pp. 1-8. IEEE, 2012.

[39] Ahmadpour, Mehrad, André L. Fernandes Cauduro, Christophe Méthivier, Birgit Kunert, Chiara Labanti, Roland Resel, Vida Turkovic et al. "Crystalline molybdenum oxide layers as efficient and stable hole contacts in organic photovoltaic devices." ACS Applied Energy Materials 2, no. 1 (2018): 420-427.

[40] Ahmadpour, Mehrad. "Metal-Oxide Based Interlayers for Organic and Perovskite Photovoltaics." PhD diss., University of Southern Denmark, 2017.

[41] Barnes, P. R. F., K. Miettunen, X. Li, and A. Y. Anderson. "480 T. Bessho, M. Gratzel, BC O'Regan, Interpretation of Opto-481 electronic Transient and Charge Extraction Measurements in Dye-482 Sensitized Solar Cells." Advanced Materials 25, no. 13 (2013): 1881-1922.

[42] Rauh, Daniel, Carsten Deibel, and Vladimir Dyakonov. "Charge density dependent nongeminate recombination in organic bulk heterojunction solar cells." Advanced Functional Materials 22, no. 16 (2012): 3371-3377.

[43] Göhler, Clemens, Alexander Wagenpfahl, and Carsten Deibel. "Nongeminate recombination in organic solar cells." Advanced Electronic Materials 4, no. 10 (2018): 1700505.

[44] De Villers, BJ Tremolet. "K. a. O'Hara, DP Ostrowski, PH Biddle, SE Shaheen, ML Chabinyc, DC Olson, N. Kopidakis." Chem. Mater 28 (2016): 876.

[45] Cowan, Sarah R., Wei Lin Leong, Natalie Banerji, Gilles Dennler, and Alan J. Heeger. "Identifying a threshold impurity level for organic solar cells: Enhanced first-order recombination via well-defined PC84BM traps in organic bulk heterojunction solar cells." Advanced Functional Materials 21, no. 16 (2011): 3083-3092.

[46] Pearson, Andrew J., Paul E. Hopkinson, Elsa Couderc, Konrad Domanski, Mojtaba Abdi-Jalebi, and Neil C. Greenham. "Critical light instability in CB/DIO processed PBDTTT-EFT: PC71BM organic photovoltaic devices." Organic Electronics 30 (2016): 225-236.

[47] Kim, Youngkyoo, Steffan Cook, Sachetan M. Tuladhar, Stelios A. Choulis, Jenny Nelson, James R. Durrant, Donal DC Bradley et al. "A strong regioregularity effect in self-organizing conjugated polymer films and high-efficiency polythiophene: fullerene solar cells." In Materials For Sustainable Energy: A Collection of Peer-Reviewed Research and Review Articles from Nature Publishing Group, pp. 63-69. 2011.

[48] Menon, Anoop, Hanpeng Dong, Zukhra I. Niazimbetova, Lewis J. Rothberg, and Mary E. Galvin. "Polydispersity effects on conjugated polymer light-emitting diodes." Chemistry of materials 14, no. 9 (2002): 3668-3675.

[49] Ballantyne, Amy M., Lichun Chen, Justin Dane, Thomas Hammant, Felix M. Braun, Martin Heeney, Warren Duffy, Iain McCulloch, Donal DC Bradley, and Jenny Nelson. "The effect of poly (3-hexylthiophene) molecular weight on charge transport and the performance of polymer: fullerene solar cells." Advanced Functional Materials 18, no. 16 (2008): 2373-2380.

[50] Greenbank, William, and Sylvain Chambon. "Degradation Mechanisms in Organic Photovoltaic Devices." In World Scientific Reference of Hybrid Materials: Volume 2: Devices from Hybrid and Organic Materials, pp. 331-336. 2019.

[51] Shuttle, C. G., B. O'regan, A. M. Ballantyne, J. Nelson, D. D. C. Bradley, J. De Mello, and J. R. Durrant. "Experimental determination of the rate law for charge carrier decay in a polythiophene: Fullerene solar cell." Applied Physics Letters 92, no. 9 (2008): 80.

[52] Clarke, Tracey M., Christoph Lungenschmied, Jeff Peet, Nicolas Drolet, and Attila J. Mozer. "A comparison of five experimental techniques to measure charge carrier lifetime in polymer/fullerene solar cells." Advanced Energy Materials 5, no. 4 (2015): 1401345.

[53] Haneef, Hamna F., Andrew M. Zeidell, and Oana D. Jurchescu. "Charge carrier traps in organic semiconductors: a review on the underlying physics and impact on electronic devices." Journal of Materials Chemistry C 8, no. 3 (2020): 759-787.

Conclusion

Conclusion

The interest of this study is the degradation and stability of organic solar cells under different climatic conditions, with take on consideration the different consensus stability testing protocols ISOS for organic photovoltaic materials. Furthermore, the lifetime prediction of organic solar cells using the Intelligence artificial was investigated.

The carried out research work is divided into two parts

First part

In this part we have investigated the QUV weathering test on the OSCs to simulate the effect of cyclic aging caused by the simultaneous appearance of different atmospheric conditions applied on the OSCs device. This cyclic aging applies different protocols ISOS simultaneously. The recovery phenomenon caused by the effect of dark/light exposure of OSCs was also investigated in this part by applying the outdoor ISOS-O-1 protocol. Many characteristics were used to study the degradation mechanisms of the OSCs under our QUV aging protocol such as the electrical properties (*J-V* characteristic, PCE, V_{oc}, FF, J_{sc}) and the optical properties (UV-VIS and PL measurement).

The results achieved in this part highlight that in the indoor test using the QUV tester we have observed that:

- The studied OSCs characteristics decrease with aging time for different aging conditions. The degradation is done in two steps : first step is done in the first 15 cycles of aging (360 h) and characterized by a fast degradation rate and the second steps (30 cycles of aging) represents the stabilization phase and characterized with the slow degradation rate, which is in agreement with the earlier finding in the literature.
- From the obtained results, it is highlighted that PCE evolution can be approximated by the sum of two decaying exponentials with time constants τ_1 and τ_2 having the same values. The deduced values show that environment conditions can have the same predominant degradation mechanism. Furthermore, J_{sc} has been fitted with linear model and degradation constant has been calculated for each aging step.
- After 360 h of aging under the carried out protocol, the OSCs lose more than 60%, and even more than 80% for some properties like PCE, of their initial performances. This result shows that the carried out protocol presents harsh aging conditions.

- The carried out cyclic aging process in the QUV chamber can be considered very harsh combining different protocols similar to commonly used ISOS protocols in the same time. In one cycle of aging, the samples were performed to a protocol similar to ISOS-L-2 (UV radiation (light), temperature and ambient humidity), followed by one similar to ISOS-D-3 (temperature and controlled humidity) and finally to the last one similar to ISOS-D-2 (temperature less than ISOS-D-3, ambient humidity).
- The formation of bubble defects was observed and their concentration and size increase with aging time. The probable cause of these bubbles is the expansion or contraction of gasses with exposure to the light and high temperature cycling.

For the outdoor test, partial recovery of performance during the dark is well observed in some studied properties and confirmed the existence of this phenomenon in OSCs as observed and confirmed in the case of the perovskite solar cells.

Second part

This investigation utilized small organic solar cells (Nano) for understand the behavior the aged of lab-scale and scalable non-fullerene (NFA) blend PCE12:ITIC OSCs in a laboratory and in an outdoor test with apply the ISOS protocols.

The results of this investigation using the NFA blend PCE12:ITIC have proved that there is a recovery in an outdoor test, when the OSC device is working under real outdoor setting, In other hand the PCE11:PCBM devices that were fabricated in the same settings show after the investigation a poor recovery reaction and very little irreversible degradation.

In the laboratory aged the small-scale spin coated PCE12:ITIC devices, it is showen that the OSCs device exhibits rapid and completely irreversible degradation.

ANN prediction part

Finally, the lifetime of samples having TiOx and ZnO as active layers after aging has been predicted using artificial neural network based on RBFG function and trained with Random Optimization Method (ROM). The preidected properties are PCE, Voc, Jsc, FF, Rs and Rsh. The results of prediction show a very good quality of fit with the experimental data, and it was confirmed these results using the Root Mean Square Error (RMSE) and Mean Absolute Relative Error (MARE). ANN can be considered a very helpful and power tool that leads to predict the

future behavior of the OSCs without carrying experimental tests which helps to gain more time and money.